Reactions between alkali rich melts and mafic upper mantle minerals with applications to alkali metasomatism

Dissertation zur Erlangung des Doktorgrades im Fachbereich Geowissenschaften an der Freien Universität Berlin

Vorgelegt von Thomas B. Grant

Berlin, January 2014.

PD Dr. Ralf Milke, FU Berlin (Erstgutachter)

Prof. Dr. Timm John, FU Berlin (Zweitgutachter)

Datum der Disputation 17.06.2014

Table of contents

Abstract 6
Zusammenfassung 7

1. Introduction 9
   1.1 What is metasomatism? 9
   1.2 Origin of phonolite magmas 10
   1.3 Evidence of phonolitic liquids in the upper mantle 11
   1.4 Case study – the Heldburg Phonolite, Central Germany 14
   1.5 Aims 16
   1.6 Author contributions 19

2. The Heldburg Phonolite, Central Germany: reactions between phonolite and xenocrysts from the upper mantle and lower crust.
   2.1 Abstract 21
   2.2 Introduction 21
   2.3 Geological background 22
   2.4 Petrography 22
   2.5 Analytical methods 29
   2.6 Results 31
   2.7 Discussion 35
   2.8 Conclusions 46

3. Experimental reactions between olivine and orthopyroxene with phonolite melt: implications for the origins of hydrous diopside + amphibole + phlogopite bearing metasomatic veins.
   3.1 Abstract 48
   3.2 Introduction 48
   3.3 Analytical methods 50
   3.4 Experimental methods 50
   3.5 Results 52
   3.6 Discussion 61
   3.7 Conclusions 66

4. Experimental study of phlogopite reaction rim formation on olivine in phonolite melts: the nature of hydrated interfaces and their effects on mantle metasomatism.
   4.1 Abstract 69
   4.2 Introduction 69

4.3 Experimental methods 71
4.4 Analytical methods 73
4.5 Results 74
4.6 Discussion 83
4.7 Implications 90

5. Conclusions and outlook 93

Bibliography 96

Acknowledgments 110

Erklärung der Eigenständigkeit 111

Abstract

The Earth's mantle cannot be viewed directly by geoscientists. To understand the chemistry and physical properties of the mantle we can use data from pieces of the mantle brought to the surface by volcanic eruptions, obducted mantle segments, experimentally reproducing the conditions of the deep earth, computational models and by seismology. It is widely accepted that the majority of the upper region of the mantle consists of olivine, orthopyroxene, clinopyroxene and an Al phase (plagioclase, spinel or garnet). Any loss or gain of chemical components mediated by a fluid, melt or diffusion is referred to as metasomatism. Investigating metasomatic processes that operate in the mantle is vital to understand the compositional and mineralogical variability of the mantle and the origins of mantle derived magmas. Much work has been conducted on this topic over the last decades but there are still many unanswered questions.

This thesis takes a detailed look at how extremely alkali enriched silicate melts react with mafic upper mantle minerals during metasomatism. Such extreme melt compositions are typically formed at much shallower pressures in the Earth's crust, however there is a large body of evidence to suggest that in some cases evolved alkali rich melts can be present at much higher pressures in the mantle. These melts may then metasomatise the mantle producing secondary mineral assemblages dominated by amphibole, phlogopite and diopside. Natural samples from the Heldburg Phonolite, Central Germany, where fragments (xenoliths) from the upper mantle that have been incorporated into an alkali rich evolved phonolite melt, are studied to observe how phonolite melts may react with mantle rocks. The mafic mantle minerals of olivine, orthopyroxene and spinel are consumed by the melt to form secondary polymineralic reaction rims.

In addition to this, experiments were conducted at upper mantle pressures and temperatures to reconstruct the textures, compositions and mineralogy of the naturally occurring reaction rims. Pressure, temperature, time and H_2O content of the melt were varied to provide constrains on the conditions of formation of the reaction rims observed in the Heldburg Phonolite. A range of analytical techniques and calculations were used to gain insights into how chemical components are exchanged between the mafic mantle phases within xenoliths and the host phonolite melt. Rates of reaction rim growth calculated from the experiments are then used to give quantitative estimates of the residence times of xenolithic material in the Heldburg Phonolite.

To understand the processes by which minerals react with melts, the experimental samples were viewed at the nano-scale using transmission electron microscopy. This technique was used to view the micro-structures the reaction rims and the role of intergranular fluid during mineral replacement reactions. These findings have implications beyond the specific system studied and provide a potential mechanism of chemical fractionation mediated by fluid along grain boundaries during metasomatism.

Zusammenfassung

Der Erdmantel ist für Geowissenschaftler nicht direkt zugänglich. Zum Verständis chemischer und physikalischer Eigenschaften des Mantels dient einerseits die Untersuchung von Mantelbruchstücken, die durch vulkanische Eruptionen oder durch Obduktion an die Oberfläche gebracht werden, oder man erhält Daten aus experimentell reproduzierten Bedingungen der tiefen Erde, von Computermodellen, oder aus seismologischen Untersuchungen. Es wird allgemein akzeptiert, dass der obere Erdmantel im wesentlichen aus Olivin, Orthopyroxen, Klinopyroxen und einer Al-reichen Phase (Plagioklas, Spinell oder Granat) besteht. Jedwede Ab- oder Zunahme chemischer Komponenten transportiert durch ein Fluid, eine Schmelze oder durch Diffusion wird als Metasomatose bezeichnet. Die Untersuchung metasomatischer Prozesse bei Mantelbedingungen ist grundlegend für das Verständnis kompositioneller und mineralogischer Variabilität des Mantels und des Ursprungs von im Mantel entstandenen Magmen. Zu dieser Thematik wurde in den letzten Jahren viel erarbeitet, jedoch gibt es immer noch viele unbeantwortete Fragen.

In dieser Arbeit wird detailiert die Reaktion von extrem alkali-reichen silikatischen Schmelzen mit mafischen Mineralen des oberen Mantels während der Metasomatose untersucht. Solche Schmelzen extremer Zusammensetzung bilden sich typischerweise durch Differentiation bei geringeren Drücken in der Erdkruste, jedoch gibt es viele Hinweise darauf, das sich alkali-reiche Schmelzen auch bei höheren Drücken im Mantel bilden können. Solche Schmelzen können dann im Mantel metasomatische Reaktionen bewirken, wobei es zur Bildung sekundärer Mineralvergesellschaftungen mit Amphibol, Phlogopit und Diopsid als dominierende Phasen kommt. Um zu untersuchen, wie phonolithische Schmelzen mit Mantelgesteinen reagieren, wurden natürliche Proben des Heldburg Phonoliths, Thüringen, untersucht, in dem alkali-reiche Schmelze im Kontakt mit Fragmenten (Xenolithen) des oberen Mantels vorliegt. Dabei reagierten die mafischen Mantelminerale Olivin, Orthopyroxen und Spinell mit der Schmelze unter Bildung von sekundären polymineralischen Reaktionssäumen.

Es wurden zusätzlich Experimente unter Druck- und Temperaturbedingungen des oberen Mantels durchgeführt, um die Texturen, Zusammensetzungen und die Mineralogie der natürlich auftretenden Reaktionssäume zu rekonstruieren. Dabei wurden Druck, Temperatur, Versuchszeit und Wassergehalt der Schmelze variiert, um die Bildungsbedingungen der Reaktionssäume beim Heldburg Phonolith zu bestimmen. Es wurden verschiedene analytische Techniken und Berechnungen verwendet, um Einblicke darüber zu gewinnen, wie der Austausch der chemischen Komponenten zwischen den mafischen Phasen des Xenoliths und der vorliegende Schmelze erfolgte. Die aus der Experimenten ermittelten Raten des Reaktionssaumwachstums wurden verwendet um quantitative Abschätzungen von Aufenthaltszeiten der Xenolithe beim Heldburg Phonolith zu ermitteln.

Zum Prozessverständnis der Mineral-Schmelze Reaktion wurden Untersuchungen der experimentellen Proben mit dem Transmissionselektronenmikroskop im Nanobereich durchgeführt. Diese Technik diente zur Aufklärung der Mikrostrukturen der Reaktionssäume und zur Bestimmung der Rolle intergranularer Fluide bei den Austauschreaktionen. Die Beobachtungen haben

weiterführende Implikationen auch für andere Systeme und liefern Hinweise auf Mechanismen, fluid-bedingter chemischer Fraktionierung entlang von Korngrenzen während der Metasomatose.

Chapter 1

Introduction

1.1 WHAT IS METASOMATISM?

Metasomatism involves the addition or removal of chemical components either by fluids or melts, or by diffusion (Green and Wallace, 1988). This can be simply expressed by equation 1.11, whereby a solid phase reacts with a melt (or fluid). Both the original solid and melt are modified. A metasomatic reaction that results in a change in mineralogy is referred to as modal or patent metasomatism. If there are no visible changes in mineralogy or textures but there is a change in composition, this is referred to as cryptic metasomatism (see review e.g. Roden and Murthy, 1985).

(1.1) $Solid_1 + Melt_1 = Solid_2 + Melt_2$

Metasomatism is a common process in the Earth's mantle and has been identified in xenolith fragments brought to the surface in their host magmas (e.g. Wulff-Pedersen et al., 1999; Franz et al., 2002; Grégoire et al., 2008; Liu et al., 2010; Miller et al., 2012) and in peridotite complexes (e.g. Zanetti et al., 1999; Morishita et al., 2003a; Morishita et al., 2003b; Bodinier et al., 2004). Numerous experimental studies of peridotite-melt/fluid reactions have also been conducted (for example - Rapp et al., 1999; Shaw and Dingwell, 2008; Rapp et al., 2010). The composition of metasomatic liquids (or agents) can be extremely varied but they can be subdivided into several broad categories;

1. Primary basaltic melts that result from direct melting of the mantle by decompression, heating by thermal anomalies such as mantle plumes, or by lowering of the peridotite solidus by volatiles (H_2O or CO_2). The interaction of basaltic melts with mantle peridotites predominantly leads to the formation of olivine at the expense of orthopyroxene (see Zhang, 2005 for some discussion) and can result in the formation of dunites (Kelemen, 1990; Morgan and Liang, 2003).
2. Si-rich melts or fluids are common in the mantle wedge and originate from dehydration or melting of subducted oceanic crust (Manning, 2004; Spandler and Priard, 2013). This commonly results in the consumption of olivine and the formation of secondary orthopyroxene (Smith and Riter; 1997; Kelemen et al., 1998; Smith et al., 1999; Morishita et al., 2003a; Arai et al., 2004; Manning, 2004; Downes et al., 2004). Reactions between mantle peridotite and Si –rich melts are linked to the formation of harzburgites (Kelemen et al., 1992).
3. Carbonatitic liquidus can be formed by partial melting of pargasitic lherzolite (Wallace and Green, 1988), carbonated garnet lherzolite (Dalton and Presnall, 1998), carbonated eclogite (Yaxley and Brey, 2004) or by immiscibility between silicate and carbonatitic melts (for example, Baker and Wyllie, 1990). These can then metasomatize the mantle by forming

olivine and jadeitic clinopyroxene at the expense of primary orthopyroxene (Yaxley et al., 1991) producing wherlites and lherzolites. Carbonatitic metasomatism has been documented in many locations (for example - Frezzotti et al., 2002; Neumann et al., 2002; Liu et al., 2010).

4. The generation of alkali rich and silica undersaturated melts at intraplate settings is often linked to partial melting of garnet pyroxenite (Hirose, 1997; Hirschmann et al., 2003) or perhaps even deeply subducted oceanic crust (Spandler et al, 2010) and that these melts then metasomatise the upper mantle. However, the generation of alkali magmas is strongly linked to melting of previously metasomatised mantle (Pilet et al, 2011). Reactions between alkali melts and peridotite result in vein assemblages in a continuum between anhydrous (clinopyroxene + garnet + olivine + orthopyroxene) to hydrous (amphibole + clinopyroxene + phlogopite + orthopyroxene) veins (Pilet et al, 2011). As alkali metasomatism is the main focus of this thesis, these concepts are discussed in more detail later on along with more examples.

In some cases several forms of metasomatism may have affected the mantle. This case arises either from several events separated by a time interval (for example, Downes et al., 2004) or by percolation and modification of the metasomatic agent as it reacts with the wall rock (Bodinier et al, 2004). The latter may also be referred to as percolative fractional crystallization (PFC). "Metasomatism" of mantle xenoliths can also be induced by reaction with host melts during eruption or residence within a magma chamber prior to eruption (Shaw et al, 2006).

This thesis concentrates on the reactions between phonolite and mafic upper mantle minerals with applications to metasomatism involving highly alkaline melts and peridotite wall rocks. The origins of most normal phonolite magmas are summarized before discussing the possible processes that may form rarer "high pressure phonolites". The main features of one such 'high-pressure" phonolite, including the regional geology, are reviewed before highlighting the main aims of the thesis.

1.2 ORIGIN OF PHONOLITE MAGMAS

Low-pressure fractionation of basanites-phonolites

Phonolites are highly evolved silica undersaturated rocks with high alkali contents. The vast majority of phonolite magmas originate by fractional crystallization of basanite or nephelinite melts. This typically involves the extraction of olivine, clinopyroxene, amphibole, plagioclase and feldspar as well as other minor phases such as titano-magnetite, apatite, zircon and haüyne. For detailed studies of the origins of phonolites from a range of locations worldwide see: Kyle et al., 1992; Ablay et al., 1998; Berndt et al., 2001; Freise et al., 2003; Harms et al., 2004; Holm et al., 2006; Melluso et al., 2007; Andújar et al., 2008; Scaillet et al., 2008; Henderson et al., 2012; Jung et al., 2013; Moussallam et al., 2013). The parent basanites and nephelinites form by low degree (<5%) partial melting of the upper mantle (Kyle et al., 1992; Panter et al., 1997; Holm et al., 2006) and much of their differentiation occurs within the crust. Therefore most phonolites are formed at shallow pressures of around 100-200 MPa corresponding to depths of 5-10 km. The contribution of crustal contamination by assimilation

fractionation processes (AFC), observed in $^{87}Sr/^{86}Sr$ abundances, can be significant (Baker et al., 1994) or nearly absent (Kyle et al., 1992; Holm et al., 2006; Jung et al., 2013) in the generation of phonolite magmas. Some phonolites, such as the Wehr volcano (East Eifel) may also contain crustal xenoliths including low-grade metamorphic schists, higher-grade mica schists, metaquartzites and rare granulites (Wörner et al., 1982; Wörner and Schmincke, 1984). The fractionation of feldspars is limited to lower, crustal pressures and results in negative anomalies in Ba, Eu, Sr, and Sm, however this can potentially be balanced by fractionation of clinopyroxene and apatite for example (Kyle et al., 1992). These are all strong indicators of the low pressures that most phonolites form at.

1.3 EVIDENCE OF PHONOLITIC LIQUIDS IN THE UPPER MANTLE

Although the majority of phonolites are formed at shallow crustal pressures there are several lines of evidence to suggest that similarly evolved alkali enriched melts can form at much higher pressures, even in the upper mantle. Data from partial melting experiments of peridotites, glasses and glass inclusions within upper mantle xenoliths, high-pressure fractionation models, percolative fractionation crystallization (PFC) models, and mantle xenolith bearing phonolites are summarized in the following sections. This provides some compelling evidence that melts with phonolitic compositions can be produced at high pressures by several different processes but that the volumes of phonolite melt produced may vary significantly. Many of these concepts are further explored in Chapter 3.

Glasses observed in xenoliths

Interstitial glass within xenoliths is extremely common but the compositions of these glasses are highly variable spanning large ranges in all major element components. Glasses preserved in xenoliths brought to the surface in their host magmas can occur as inclusions within primary and secondary mineral phases (e.g. Schiano et al., 1998), as interstitial glasses (e.g. Neumann and Wulff-Pedersen, 1997) or along grain boundaries (Drury and Fitzgerald, 1996; Wirth, 1996; Franz and Wirth, 1997; Neumann and Wulff-Pedersen, 1997), or within reaction zones and metasomatic veins (Wulff-Pedersen et al., 1996; Xu et al., 1996; Wullf-Pedersen et al., 1999; Zajacz et al., 2007). Models of the origins of glasses include; trapping of partial melts (Schiano et al., 1998), decompression melting of phases such as amphibole (Shaw and Klügel, 2002; Ban et al., 2005) or orthopyroxene (Shaw et al., 1998; Shaw, 1999) and these melts may then react with the primary assemblage of the xenolith (Yaxley et al., 1997), infiltration and reaction with the host melt (Klügel, 1998; Klügel, 2001; Miller et al., 2012) or the remnants of a metasomatic agents at mantle depths (Schiano et al., 1995; Neumann and Wulff-Pedersen, 1997; Coltorti et al., 2000).

Due to the huge variability in composition, textural associations and origins of glasses in xenoliths, only extreme compositions with SiO_2; >60 wt.%, Al_2O_3; 18-20 wt.%, alkalis; 4-10 wt. % with low concentrations of MgO, FeO and CaO (Draper and Green, 1997) that plot within or close to the phonolite phase field are considered. As Draper and Green (1997) discuss, these more extreme melt compositions are most likely to be the remnants of metasomatic agents within the mantle. However, the glasses themselves may not represent the initial composition of the metasomatic agent but are likely to

be the products of reactions with the wall rock peridotite phases (Coltorti et al., 2000). The complexities of this are further explored later on in the introduction.

Partial melting of peridotite

Experimental studies of very low degree partial melts of peridotite have been shown to produce evolved silica and alkali enriched melts (Kinzler and Grove, 1992; Baker et al., 1995; Kushiro, 1996; Falloon et al., 1997; Hirschmann et al., 1998; Robinson et al., 1998; Chalot-Prat et al., 2010). The melt compositions are mostly primitive basalts but can have much more evolved compositions such as trachytes, and tephri-phonolites that form in the most extreme cases (see Figure 1.1). Alkali and silica contents of melt in equilibrium with olivine and orthopyroxene increase with decreasing melt fraction (also temperature), and are higher at lower pressures of around 0.7-1.5 GPa (Hirschmann et al., 1998). The concentrations of P_2O_5, TiO_2 and H_2O tend to reduce the silica content of the melt (Hirschmann et al., 1998). Therefore the production of highly alkaline, silica rich melts occurs over a limited set of conditions. Furthermore, many of the melts in these studies are not silica undersaturated enough to then fractionate towards phonolitic compositions. Recent unpublished work by Didier Laporte (at Clermont Ferrand, France, through a personal communication, 2013) has shown that low degree melts (<1.6 wt.%) of K-doped lherzolite at 1.3 GPa and 1200ºC can have phonolitic compositions. Draper and Green (1997) also found that some extreme melt compositions (DG-1 – that is a phonolite) could be in near equilibrium with harzburgite or lherzolite rocks. However, in order to form such a K-rich melt by partial melting, the peridotite source must be previously enriched in K, i.e. phlogopite bearing (Draper and Green, 1997). Partial melting of peridotite may therefore in some extreme cases form melts with phonolitic compositions but more data are required in this field of research.

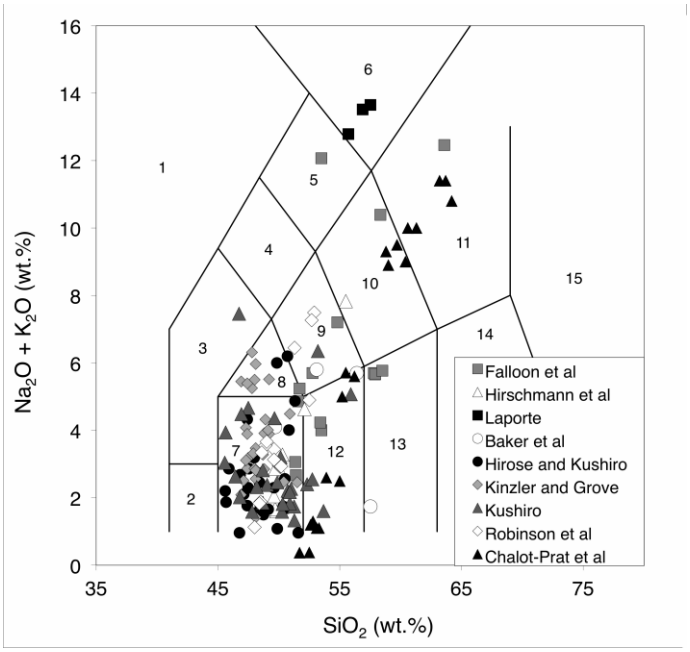

Figure 1.1. TAS diagram (LeBas et al., 1986) of melt compositions formed by experimental partial melting of peridotite rocks. References; Kinzler and Grove (1992), Hirose and Kushiro (1993), Baker et al. (1995), Kushiro (1996), Falloon et al. (1997), Hirschmann et al. (1998), Chalot-Prat et al. (2010) and a personal communication with Didier Laporte (2013). 1; foidite, 2; picro-basalt, 3; tephrite / basanite, 4; phonotephrites, 5; tephriphonolite, 6; phonolite, 7; basalt, 8; trachy-basalt, 9; basaltic trachy-andesite, 10; trachy-andesite, 11; trachyte / trachy-dacite, 12; basaltic andesite, 13; andesite, 14; dacite, 15; rhyolite.

High-pressure fractionation models

Irving and Green (2008) showed that fractionation of nepheline normative asthenospheric melts in the upper mantle can lead to phonolitic liquids by the removal of olivine, clinopyroxene and amphibole. Pilet et al. (2010) also modeled the high-pressure liquid line of descent of basanite. Fractional crystallization predominantly of olivine, clinopyroxene and amphibole leads to increasingly alkali enriched residual melts, however the SiO_2 contents were not high enough for the most evolved melts to be classified as phonolites.

The high-pressure phase relationships of phonolite melts have also been investigated (Hay and Wendlandt, 1995; Draper and Green, 1997), although to a far lesser extent than at low pressures. It appears that the precipitating phases from phonolite melt at pressures between 0.8 – 1.5 GPa vary largely depending on temperature and the water content of the melt. For dry phonolite melts at low temperatures (<900°C), alkali feldspar and clinopyroxene are the dominant phases. Between 900-1000°C amphibole, clinopyroxene, and phlogopite will crystallize. The experiments of Draper and Green (1997) showed that above 1000°C olivine (1-1.5 GPa) and orthopyroxene (>1.5 GPa) can both be stable phases, meaning that phonolites can be in near equilibrium with upper mantle peridotite wall rocks at high temperatures.

Percolation of asthenosperic melts through shallower, cooler lithospheric mantle results in the precipitation of liquidus phases, forming secondary metasomatic veins (Pilet et al., 2010; Pilet et al., 2011). This process is referred to as percolative fractional crystallization (PFC) or reactive percolative fractional crystallization (RPFC) if there is a contribution of reactions or chemical exchange with wall rock peridotite. Both processes lead to fractionation of the melt towards more evolved compositions (Wulff-Pedersen et al., 1996; Xu et al., 1996; Wulff-Pedersen et al., 1999; Zajacz et al., 2007; Miller et al., 2012). Therefore PFC of a basanite should, much like normal fractionation processes, eventually culminate in phonolite residual liquids (Irving and Green, 2008), even if only locally. This is indeed the case (see Figure 1.2), where glass inclusions formed by PFC range from primitive silica undersaturated basalts up to phonolite compositions. The compositions of residual melts from the percolation of cabonatites are markedly more SiO_2 rich and range from basalts to trachytes (see Frezzotti et al., 2002; Neumann et al., 2002).

Mantle xenolith bearing phonolites and trachytes

There are numerous examples of spinel lherzolite xenolith bearing phonolites (Wright, 1966; Price and Green, 1972; Irving and Price, 1981; Downes, 1989; Huckenholz and Werner, 1990) and trachytes (Wright, 1969; Dautria et al., 1983). The presence of xenolith fragments from the upper mantle in these phonolites, the lack of physical (phenocrysts) and chemical (Eu or Sr anomalies) signs of feldspar fractionation and primitive Sr/Nd trace element ratios (Wedepohl et al., 1994) suggest that these phonolites could have originated from much higher pressures than most other phonolites. Irving and Price (1981) suggested that these high-pressure phonolites originate from pressures of 10-15kbar.

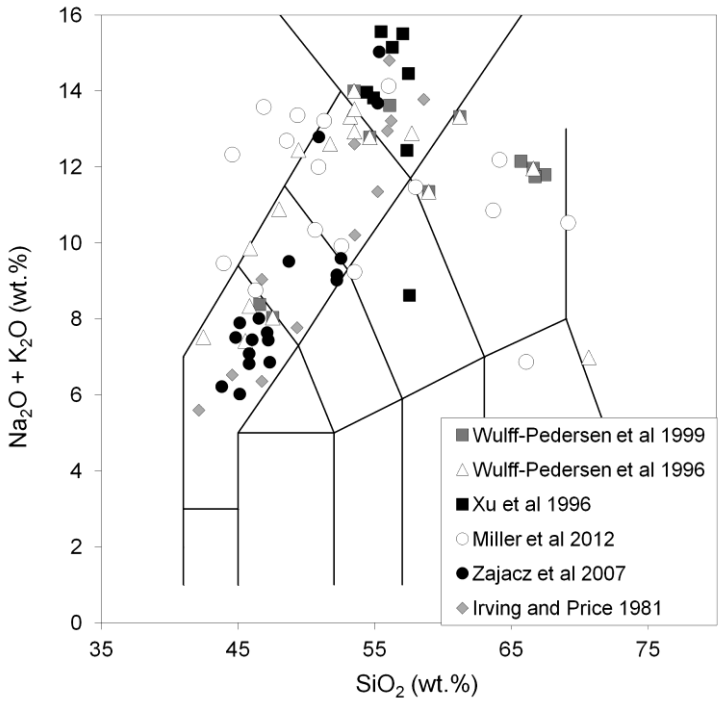

Figure 1.2. TAS diagram (LeBas et al., 1986) of glasses compositions from xenoliths that were formed by percolative fractional crystallization (PFC) of silica undersaturated basalts (Wulff-Pedersen et al., 1996; Xu et al., 1996; Wullf-Pedersen et al., 1999; Zajacz et al., 2007; Miller et al., 2012). This data is also compared to phonolites and their parent melts from Irving and Price (1981) that show typical fractionation trends from basanite to phonolite.

However, there are several examples from Cantal, Massif Central (Downes, 1989) where basic (tephrite) melts containing upper mantle xenoliths have mixed with more evolved melts such as phonolites. This may result in a xenolith bearing phonolite at crustal conditions. The presence of xenocrysts is therefore not a clear indicator of high-pressure origins. Although feldspar fractionation is limited to lower pressures; its absence does not necessarily require high pressures. The experimental results (Hay and Wendlandt, 1995; Draper and Green, 1997) show that high temperatures and high bulk water contents are also effective at suppressing feldspar fractionation. It is unclear whether the spinel lherzolite bearing phonolite eruptions discussed by Irving and Price (1981) did originate from the mantle or if they formed in the crust under high-temperature and hydrous conditions. It is also uncertain how the xenolithic material was incorporated into these phonolites; whether they were directly sampled from upper mantle wall rocks during eruption / intrusion (Irving and Price, 1981) or were incorporated during a mixing event with a xenolith bearing magma in the crust

Lack of an Eu anomaly is also a potentially weak line of evidence for suggesting high pressures. Fractionation of clinopyroxene and apatite, for example, could balance the depletion of Eu by feldspar precipitation (Kyle et al., 1992).

1.4 CASE STUDY – THE HELDBURG PHONOLITE, CENTRAL GERMANY

In this thesis we concentrate on one of the high –pressure, spinel lherzolite xenolith bearing phonolites described by Irving and Price (1981). This is the Heldburg Phonolite, Central Germany, which lies beneath the Veste Heldburg Castle overlooking the town of Bad-Colberg Heldburg, Thuringia. The

intrusion is a phonolite plug cut by olivine tephritic dykes (Irving and Price, 1981). Ages of 13.3-11 Ma for the Heldburg Phonolite (Huckenholz and Werner, 1990) and 16-14 Ma for basaltic rocks in the region (Abratis et al., 2007) have been determined. It has been known to contain spinel lherzolite, hypersthene rich gabbro-norite and other mafic cumulate xenoliths since the 19th century (Pröschold and Thürach, 1895; Irving and Price, 1981; Huckenholz and Werner, 1990).

The Heldburg Phonolite is located in the Heldburg volcanic region that is part of the Central European Volcanic Province extending right across Germany including Eifel, Westerwald, Vogelsberg, Rhön and Heldburg volcanic centers (see Figure 1.3). Alkaline volcanism across Central Europe formed as result of extensional tectonics and continental rifting during the Miocene and Pliocene, and is contemporaneous with the latter stages of the alpine orogeny (Wilson and Downes, 1991; Ziegler, 1992; Franz et al., 1997; Abratis et al., 2007). Minor plume activity is also likely in some areas such as Vogelsberg and Cantal due to high volumes of melt production and because rift faults of Tertiary ages cross-cut older structures of Variscian ages (Jung et al., 2013). Lithospheric thicknesses of around 50 km are reported by Wedepohl et al. (1994) and Franz et al. (1997) with a crust thickness as low as around 30 km (Prodehl et al., 1992). The mantle source region for the parent basanites and nephelinites is thought to be a mixture of HIMU, depleted and enriched peridotites from a variably metasomatised asthenopheric mantle (Wedepohl et al., 1994; Witt-Eickschen and Kramm, 1997; Jung et al., 2013).

Jung et al. (2005) and Mayer et al. (2013) suggest that the asthenospheric melts precipitated veins at the lithosphere-asthenosphere boundary (50 km depth). These were then partially melted shortly afterwards giving strong phlogopite and amphibole trace element signatures (depleted Ba, Rb and K) of the primary melts in the Rhön region (see also Wedepohl et al., 1994). The formation of veins by ascending primary mantle melts and their subsequent melting and compositional characteristics have been modeled well by Pilet et al. (2011). Assimilation of lower crust mafic wall rocks is also likely (Jung et al., 2013; Mayer et al., 2013).

The Heldburg and Rhön regions largely consist of basanite and nephelinite eruptions with a seyenitic dyke swarm in the Heldburg region. Many of these contain ultra mafic xenoliths, including spinel lherzolites (Franz et al., 1997; Schmidt and Snow, 2002). These are often angular, large and are not surrounded by visible selvages, indicating that the host magmas originate from upper mantle depths and reached the surface relatively rapidly. This information was collected during field-work in the Heldburg and Rhön regions in 2011. Fractionation of basanite and nephelinite magmas towards more evolved compositions was dominated by early olivine, clinopyroxene and amphibole as well as plagioclase, K-feldspar, apatite and magnetite (Jung et al., 2013). Note that the Heldburg phonolite is different to other phonolites in the region as it appears to have formed without significant fractionation of feldspar (Irving and Price, 1981).

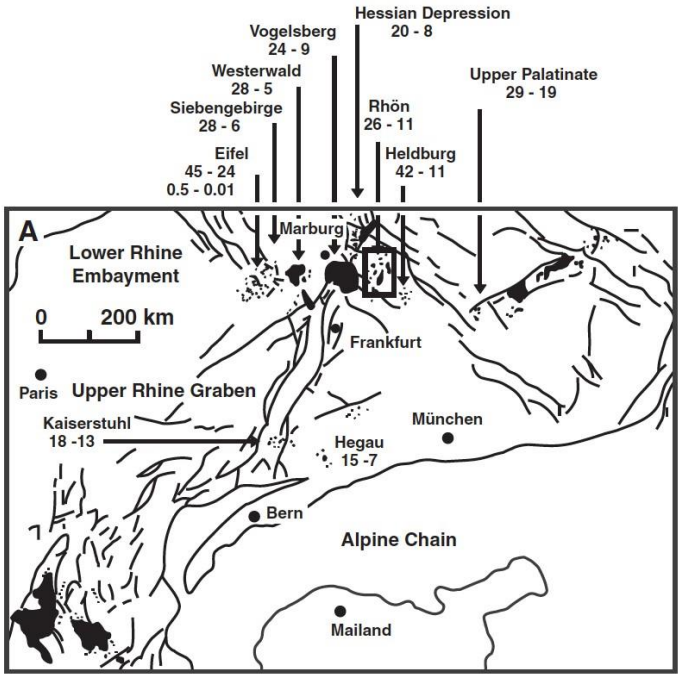

Figure 1.3. Locations of the main volcanic centers across Central and Southern Germany that are part of the Central European Volcanic Province (CEVP). Image was taken from Jung et al. (2013), which is a modified figure originally from Wedepohl et al. (1994).

In summary, there is a large amount of evidence from glass inclusions, partial melting of peridotite experiments, high pressure fractionation models and mantle xenolith bearing phonolites to suggest that phonolite melts can form in the upper mantle. The most likely method of their production is either high-pressure fractionation of basanites or by percolative fractional crystallization (PFC) models. This thesis looks at how phonolite melts may then react with mafic upper mantle phases and what implications this may have for metasomatic models involving highly alkaline melts. The main project aims are discussed in a little more detail below with an outline of how each chapter attempts to answer the main goals of the research project.

1.5 AIMS

The thesis includes five main aims that are investigated across the three chapters. These are discussed in the following paragraphs.

Did the Heldburg Phonolite originate from the upper mantle?

From the literature is seems possible that the Heldburg Phonolite and other spinel lherzolite bearing phonolites originated from upper mantle pressures of 10-15 kbar (Irving and Price, 1981). However, this interpretation is based on circumstantial evidence of the presence of high-pressure xenoliths and the lack of feldspar fraction that is typically indicative of higher pressures. It is possible that high temperatures (>900°C) and high water contents in the melt are able to suppress feldspar fractionation at low pressures within the crust (Hay and Wendlandt, 1995). Secondly, the xenoliths could have been incorporated into the phonolite by mixing processes in the crust between a xenolith free phonolite and a

xenolith bearing basaltic melt from the mantle (which are commonly observed throughout the region). In order to obtain a better understanding and provide constraints on the origins of the Heldburg Phonolite, further data must be collected and alternative models to Irving and Price (1981) must be discussed. This is the primary aim of Chapter 2. A detailed examination of the petrography, textures and compositions of phenocrysts as well as xenolith / xenocryst phases is conducted along with thermo-barometeric calculations. Due to high levels of fragmentation of the xenolithic material into single xenocrysts and micro-xenoliths, careful comparisons are made to establish the original xenolith phase assemblages. This data, along with more recent literature data is used to constrain the likely origin of the Heldburg Phonolite.

How do mafic upper mantle xenocryst phases react with phonolite melts?

Draper and Green (1997) showed that both olivine and orthopyroxene can be stable liquidus phases crystallizing from a phonolite melt (DG-1) at upper mantle conditions of 10-15 kbar and >1000°C. However, at lower pressures and temperatures both phases may well be out of equilibrium with a phonolite melt, with clinopyroxene, phlogopite and alkali feldspar as liquidus phases (Hay and Wendlandt, 1995; Draper and Green, 1997). Chapter 2 records and discusses the range of reaction rims formed between xenocryst phases of olivine, orthopyroxene, spinel, clinopyroxene, plagioclase and magnetite with the host phonolite melt. The textures, mineralogy and chemistry of the reaction rims formed on the xenocrysts are used to explore how a phonolite melt could metasomatise the upper mantle. In addition to this, calculations are made to determine the amounts and rates of exchanges of elements between xenocrysts and melt. The aim of this is to produce some estimates of the rates of reactions and therefore place some constraints on the residence times of the xenocrysts in the phonolite. Diffusion profiles in reaction zones have been used to determine residence times of xenoliths in their host melts in other studies (e.g. Klügel, 1998).

In conjunction with the natural data, a series of experiments are designed to replicate the reaction rims under controlled experimental conditions. This is done by placing single crystals of olivine and orthopyroxene (both natural and synthetic) in contact with synthetic phonolite melt. Chapter 3 documents these reactions and aims to determine how pressure, temperature and melt water contents affect the reaction rim mineralogy, growth rates and compositions of reaction rim phases.

What are the implications of these reactions for metasomatism in the upper mantle by highly evolved alkali rich melts?

Both natural and experimental samples show that olivine reacts with phonolite melt to form a phlogopite rim with a halo of diopside, whereas orthopyroxene reacts to form a rim of amphibole and a halo of either diopside or phlogopite. This occurs at conditions of 900-1000°C, melt water contents >3.5-4 wt.% H_2O and at pressures between 10-15 kbar. Therefore, a metasomatic assemblage of phlogopite + amphibole + diopside will be formed by a reaction between phonolite and peridotite at these conditions. Such a reaction assemblage is similar in mineralogy to widely observed hydrous metasomatic veins of phlogopite + amphibole + diopside (Dawson and Smith, 1988; Bodinier et al., 1990; Wulff-Pedersen et al., 1999; Zanetti et al., 1999; McInnes et al., 2001; Shaw et al., 2005; Szabó

et al., 2009; Pilet et al., 2011). The major element composition of the metasomatic agents that forms these veins is poorly constrained (Witt-Eickschen et al., 1998; Szabó et al., 2009; Pilet et al., 2010; Pilet et al., 2011). It is the aim of the latter part of Chapter 3 to investigate if phonolite or near phonolite melts could be the metasomatic agents responsible for the formation of hydrous metasomatic veins. These veins are often associated with highly Si, Al and alkali enriched glasses that can cross into the phonolite phase field (Wulff-Pedersen et al., 1999). This part of the thesis aims to see if phonolites can form these veins by reaction with peridotite, if similar residual glasses are formed and if the trace element compositions of high-pressure phonolites are similar to those of Si-Al-alkali rich glasses and from metasomatic models such as Pilet et al. (2011).

Kinetics of reactions between olivine and phonolite and the calculation of residence times

Reactions between xenocrysts / xenoliths and phenocrysts with their host melt can be used as tools to constrain estimates of residence times (Rutherford, 2008; Klügel, 2001). To do this accurately the rates of the reactions must be known for different parameters such as temperature etc. By plotting the rim growth rates against time, the rate limiting process can potentially be determined. Rim growth rates that are linear with time indicate that the reaction is interface controlled. This means that interfacial process such as dissolution and precipitation are rate limiting. Rim growth rates that are linear with the square root of time (parabolic) are considered to be controlled by diffusion. The slowest diffusing component is therefore the rate limiting species. Chapter 4 aims to determine whether phlogopite rim growth on olivine is interface or diffusion controlled and what the diffusion rates of components are during these reactions. It is also important to consider that the diffusion rate of a single component will vary depending on what it is diffusing through; volume diffusion through mineral lattices (slow), melts or fluids (fast) and along grain boundaries (intermediate) in the reaction rim (Dohmen and Milke, 2010). Once these processes are well constrained over a range of conditions, quantitative estimates of the residence times of olivine xenocryst can be made.

Effects of intergranular fluid during metasomatic reactions.

There is a large amount of data that shows how intergranular fluids significantly increase the rates of mineral replacement reactions (Liu et al., 1997; Yund, 1997; Harlov and Milke, 2002; Putnis, 2002; Keller et al., 2008; Putnis, 2009; Carlson, 2010; Gardés et al., 2012; Milke et al., 2013). This is because fluid increases the solubility of components, reduces the activation energies for diffusion, and acts as a medium for rapid chemical exchange at dissolution and precipitation interfaces (Rubie, 1986). Chapter 4 also aims to investigate the textures and properties of phlogopite-phlogopite grain boundaries and phlogopite-olivine interphase boundaries during reaction rim formation using transmission electron microscopy (TEM). This will be the first (to our knowledge) detailed experimental study of grain and interphase boundaries during a metasomatic reaction.

1.6 AUTHOR CONTRIBUTIONS

Chapters 2, 3 and 4 include contributions from other authors. Electron probe micro analyses (EPMA) data for some of the phenocrysts and xenocrysts was taken by Sanjay Pandey and amphibole phenocrysts by Sarah Incel. Ralf Milke made the mass balance calculations. Natural sample collection and selection was undertaken by Ralf Milke.

In Chapter 3 the experimental design and initial experiments were conducted by Bernd Wunder. Bernd also contributed to the ideas and early revisions during writing of the paper. Ralf Milke contributed also contributed to the revising of the paper and formed the initial idea for conducting these experiments.

TEM analyses in Chapter 4 were taken by Richard Wirth who also contributed to the interpretation of this data and the writing of the TEM methods section. Dieter Rhede collected the EPMA analyses in the glass line scans and helped with the writing of the EPMA methods section. Ralf Milke and Bernd Wunder contributed to the revising of the paper, the experimental design and ideas included in the discussion section.

Chapter 2

The Heldburg Phonolite, Central Germany: reactions between phonolite and xenocrysts from the upper mantle and lower crust.

Published as;

Grant, T.B., Milke, R., Pandey, S., Jahnke, H. (2013). The Heldburg Phonolite, Central Germany: reactions between phonolite and xenocrysts from the upper mantle and lower crust. *Lithos*, **182-183**, 86-101. http://dx.doi.org/10.1016/j.lithos.2013.09.012

2.1 ABSTRACT

The Heldburg Phonolite, Central Germany contains abundant fragments of xenolithic material most commonly seen as single xenocrysts of olivine and orthopyroxene as well as larger poly-mineralic micro-xenoliths. The xenocryst and micro-xenolith compositions indicate two cumulate source rocks; a spinel-bearing lherzolite and a pyroxene rich gabbro-norite. Disequilibrium between the host melt and xenocrysts lead to the formation of phlogopite – diopside double rims on olivine and either amphibole-phlogopite or amphibole-diopside double rims on orthopyroxene. The rim assemblages and infiltration of melt into some micro-xenoliths suggest that the xenolithic material was sampled by the phonolite directly from their source rocks. The idea that the phonolite originated from the upper mantle is supported by thermobarometry of amphibole and clinopyroxene phenocrysts. The reaction rims therefore provide small-scale analogues of a metasomatic event involving an evolved alkali enriched melt and upper mantle and lower crust wall rocks. Chemical zoning within the rims and the inheritance compositional features from their hosts indicates rapid rim growth rates with slow diffusion rates of components through the rims. Residence times for the xenocrysts in the melt are in the order of several months to a year.

2.2 INTRODUCTION

During eruption, magmas can bring with them fragments of the wall rock through which they have passed. Such material provides information about the structure and composition of the crust and upper mantle. Due to compositional differences between the host magma and the xenolithic material, diffusional exchange, dissolution, recrystallization and reaction rim / vein formation can occur. The features and rates of these processes can then be used to determine estimates of parameters such as the residence times, storage conditions and ascent rates of magmas.

Most phonolites reside in crustal magma chambers, commonly at around <10km (2kbar) depth (Berndt et al., 2001; Freise et al., 2003; Harms et al., 2004; Scaillet et al., 2008; Moussallam et al., 2013, for review of some data) and originate from the fractionation of more mafic alkaline parent melts. However, some phonolites and trachytes contain spinel-lherzolite xenoliths (Wright, 1966; Wright, 1969; Price and Green, 1972; Green et al., 1974; Irving and Price, 1981; Dautria et al., 1983; Huckenholz and Werner, 1990) and this observation together with the fact that these rocks lack evidence for feldspar fractionation (e.g. absence of Eu anomalies), led Irving and Price (1981) to suggest that some phonolites could have originated from the upper mantle. This paper is concerned with one of these phonolites, the Heldburg Phonolite from Central Germany. This has been known for a long time to contain spinel bearing peridotite xenoliths and hypersthene rich norite xenoliths (Pröschold and Thürach, 1895; Irving and Price 1981, Huckenholz and Werner, 1990). We provide petrographic descriptions of the phonolite, its phenocrysts and the xenolithic material that it contains but focus particularly on the reaction rims formed between xenocrysts and melt. The rim reaction processes provide insights into the origins of the phonolite and the kinetics of reactions between mafic minerals and highly evolved alkali melt. These reactions have not been described before and could provide small-scale analogues for metasomatic reactions between the upper mantle / lower crust and phonolite melt.

2.3 GEOLOGICAL BACKGROUND

Alkaline magmatism across Central Europe in the Miocene and Pliocene, which was related to extensional tectonics were contemporaneous with the later stages of the alpine orogeny, is collectively referred to as the Central European Volcanic Complex (Abratis et al., 2007; Wilson and Downes, 1991; Franz et al., 1997). The majority of these eruptions were basaltic in character but a number of more evolved melts such as phonolites and trachytes also occur (Abratis et al., 2007; Meyer et al., 2009). One such example is the Heldburg Phonolite from Central Germany. This is a phonolitic plug cut by olivine tephritic dykes (Irving and Price, 1981), and ages of 16-14 Ma for basaltic rocks in the Heldburg area (Abratis et al., 2007) and 13.3-11 Ma for the phonolite by Huckenholz and Werner (1990) have been recorded. Mantle nodules are common in the less evolved basaltic rocks in the region but the Heldburg Phonolite is the only evolved magma in the immediate area, making this outcrop one of the rare examples globally of a mantle xenolith-bearing phonolite.

The Heldburg Phonolite is situated beneath the Veste Heldburg castle, which overlooks the town of Bad Colberg-Heldburg (50°17’21.28’’N, 10°43’58.83’’E). The samples were taken from an outcrop in a former quarry at the road 250m northeast of the castle, which represents the central part of the phonolite plug. We found no large and complete xenoliths at the sample location. It is not indicated in the literature where the complete xenoliths were collected.

2.4 PRETOGRAPHY

Host phonolite

The groundmass constitutes around 90-95% of the bulk rock and consists predominantly of alkali feldspar and nepheline with minor clinopyroxene, analcite, nosean, apatite, titanomagnetite, zircon, titanite and ilmenite with accessory phases of allanite or rare niobium phases such as microlite, aeschynite and columbite. Groundmass grain sizes are generally between <30microns, but are mostly <10. Glass is also present in the groundmass. Bulk rock compositions from Irving and Price (1981) are given in Table 2.1.

The phenocryst population is dominated by phlogopite, amphibole and diopside. There is a distinct lack of alkali feldspar phenocrysts present at Heldburg. Phenocrysts are typically several hundred microns in size but can be larger, with some amphiboles exceeding 1000 microns.

Amphiboles are light brown, sometimes with a slight greenish tinge. They are also variably zoned, typically with Fe-rich rims that are spongy or cellular in texture (Figure 2.1A-B). Some have more Fe-rich cores that are rounded to subhedral in shape (see Figure 2.1B) but these are rare. Melt inclusions are common and can be present in the cores as well as nearer to the rims of amphiboles (Figure 2.1A-B). These melt inclusions tend to have subhedral shapes. Small, <20micron, inclusions of apatite and magnetite are also common in phenocryst amphibole. Amphiboles can also have rounded clinopyroxene in their core regions. Phlogopite forms very light to dark brown plates with no significant ampunts of zoning. They tend to show some signs of resorption with spongy cellular rims of smaller grained phlogopite (Figure 2.1C). Euhedral but irregular shaped melt inclusions up to 20 microns in size are sometimes present. Small inclusions of magnetite are also observed as well as

apatite, which can be as large as 30 microns (Figure 2.1C). Darker brown phlogopite grains are often densely interspersed with magnetite. Diopsides have subhedral crystal shapes with spongy-form rim regions consisting of finer grained diopside-augite with higher Fe contents. They are generally colourless but at their margins they have a more pale greenish hue. Small euhedral melt inclusions (<20 microns) and magnetite inclusions (<10 microns) are common (Figure 2.1D) in diopside.

Sanidine, nepheline and albite rich feldspar are extremely rare (except for in the groundmass) and are therefore not considered to have played a significant role in the evolution of the Heldburg Phonolite. These rare phenocrysts could represent small amounts of crustal rocks sampled during intrusion.

Bulk rock analyses		
SiO_2	56.04	55.91
TiO_2	0.33	0.60
Al_2O_3	20.61	21.58
FeO	1.05	2.19
MnO	0.98	0.43
NiO	0.12	-
MgO	1.16	1.22
CaO	1.42	3.18
Na_2O	10.17	9.93
K_2O	4.64	3.03
Total	96.52	98.07
xMg	67.8	83.5

Table 2.1. Bulk rock analyses from Irving and Price (1981) and references within.

Crystal clots

The phonolite contains many large (up to 1-2cm) glomerocrysts or crystal clots (see Figure 2.1E-F). The mineralogy of these clots is similar to the phenocryst assemblage but they have distinctive textures and therefore may not necessarily have the same origins. The clots themselves can be up to several mm in diameter, and are predominantly composed of amphibole (70-80%) and clinopyroxene (15-25%) with minor phlogopite and magnetite (<10%). In contrast to the isometric habits of single amphibole phenocrysts, the amphibole in the crystal clots is elongate with typical aspect ratios between 2 and 6. Amphibole, clinopyroxene and phlogopite grains have thin Fe-rich rim zones. Grain sizes of amphiboles, clinopyroxenes and phlogopite within the clots vary significantly from several hundred microns down to tens of microns. Magnetite always occurs as small <10 microns grains. All crystal clots have large volumes (up to 40%) of interstitial glass that is very crystal poor to crystal free. Most clots are ellipsoid in shape, but some have elongated shapes or occur as trails of crystals aligned in the flow direction of the ground mass phases.

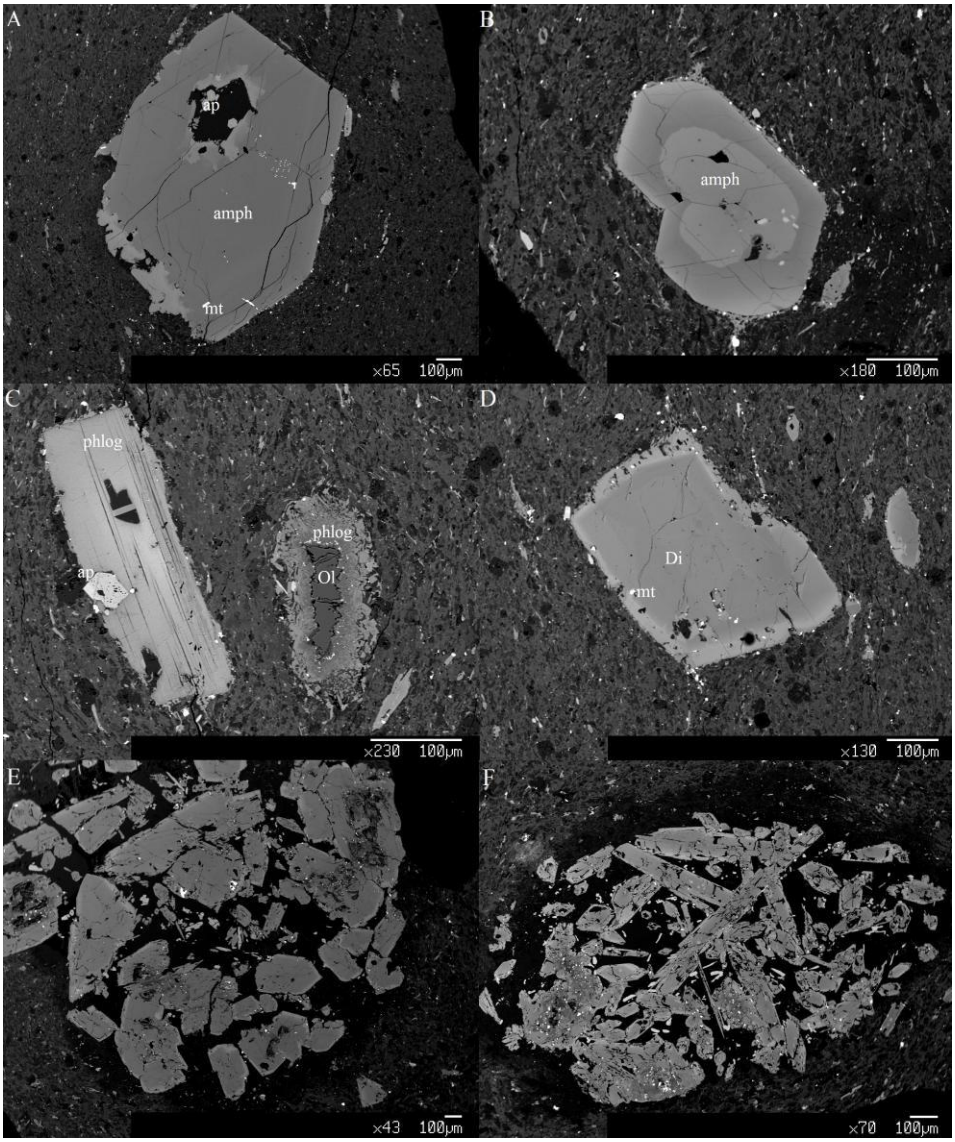

Figure 2.1. BSE (back scattered electron) images of phenocrysts and crystal clots. Abbreviations; ap = apatite, amph = amphibole, Di = diopside, mt = magnetite, ol = olivine, phlog = phlogopite. **A** – amphibole phenocryst with large subhedral glass inclusion that has crystallized apatite crystals. Also some smaller glass inclusions occur in the rims. Some small magnetite inclusions are observed. The outer edges of the amphibole show partial re-sorption and re-growth or more Fe rich rims. **B** – amphibole phenocryst with a rounded Fe-rich core zone that includes several anhedral glass inclusions and magnetite inclusions. Outer zone is more Mg-rich becoming gradually more Fe-rich towards the rims, which are surrounded by small amphibole crystals. **C** – Phlogopite phenocryst with large glass inclusions in the core and at the rims. These are spongy and cellular in texture with growth of fine-grained phlogopite crystals. The phenocryst also has large apatite inclusions surrounded by a thin glass zone. This is image also includes a reacted xenocryst of olivine with a phlogopite dominated rim. **D** – diopside phenocryst with a spongy and cellular rim zone that is more Fe-rich than the core, which is largely homogenous. Some glass inclusions are seen near the rims along with some small magnetite inclusions. **E** – crystal clot consisting predominantly of amphibole and diopside with minor phlogopite and magnetite. All crystals contain glass inclusions and have skeletal and more Fe-rich rim zones. Interstitial crystal poor to crystal free glass separates the phases in the clots. **F** – crystal clot with an ellipsoid shape. This consists predominantly of amphibole and phlogopite with some diopside and minor magnetite. Skeletal crystal forms and glass inclusions are common

as well as Fe-rich rims. Again there is abundant interstitial, crystal poor glass, which forms a halo around the crystal clot.

Xenocrysts and micro-xenoliths

The Heldburg Phonolite contains around 1-3% xenolithic material. Isolated single grains are referred to here as xenocrysts and fragments consisting of more than one phase will be referred to as micro-xenoliths. Some xenocrysts and large sections of the micro-xenoliths have been altered and their original phases have been pseudomorphed by carbonates. Most xenocrystic material is, however, unaltered and predominantly observed as single crystals of olivine, orthopyroxene, clinopyroxene, chromian spinel, magnetite or anorthitic plagioclase. Olivine and orthopyroxene are the most commonly observed xenocryst phases making up around 70-80% of the total xenocryst population, with clinopyroxene constituting most of the remainder. Plagioclase, magnetite, and chrome spinel are much less common.

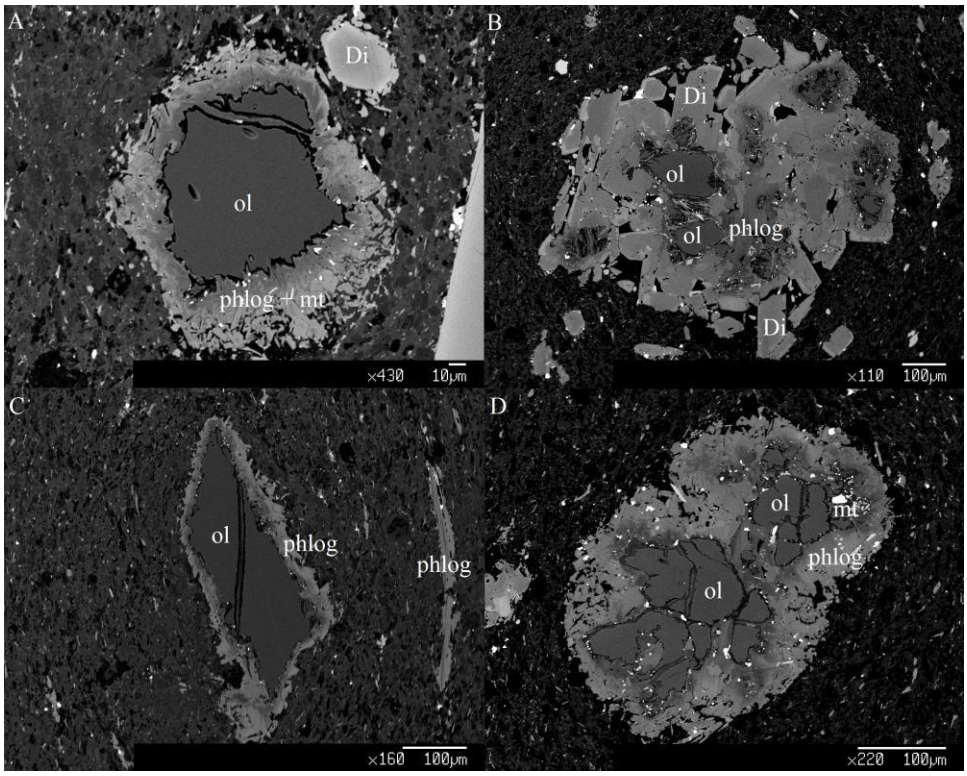

Figure 2.2. BSE image of olivine xenocrysts and reaction rims. Abbreviations are the same as in Figure 2.1. **A** – xenocryst of olivine from olivine group I, with a rim dominated by phlogopite with minor magnetite, which is concentrated in the inner regions of the rim. The interface between olivine and the rim is convoluted and highly irregular. Rim crystal sizes get larger away from the olivine interface. No internal zoning of the olivine is visible from this image or from any other observed olivines. **B** – olivine xenocryst from group II olivine, with a small inner rim zone of phlogopite and minor magnetite and a thicker outer rim dominated by diopside. Rim diopside has thin Fe-rich rims and between diopside rim grains there are glass pools. Olivine cores have rounded and irregular shapes. **C** – olivine xenocryst from olivine group I with a phlogopite dominated reaction rim. **D** – Olivine xenocryst from olivine group II with a phlogopite dominated rim. The olivine rim interface is highly irregular.

Due to high levels of fragmentation it is difficult to reconstruct the original phase assemblages and to relate one xenocryst to the next. Less common micro-xenoliths provide the links between isolated xenocrysts and the potential source rocks and reveal the original phase assemblages. Two distinct assemblages are present in the micro-xenoliths; an orthopyroxene ± plagioclase ± clinopyroxene ± magnetite (Figure 2.5 C-D) assemblage and an olivine ± orthopyroxene ± spinel ± clinopyroxene assemblage (Figure 2.5 E-F). This observation is consistent with xenoliths at Heldburg being described previously as spinel lherzolite and norite-gabbro respectively. These assemblage classifications are used herein and are supported by the major element chemistry.

Reaction rims on xenocrysts and micro-xenoliths

Most xenolithic material has reacted with the melt to form reaction rims. The xenocryst cores are rounded and anhedral. No examples were observed where the host xenocrysts had been completely replaced by rim phases. Olivine, orthopyroxene, and spinel xenocrysts are enclosed in reaction rims consisting of varying combinations of amphibole, phlogopite, diopside and magnetite. Plagioclase and clinopyroxene xenocrysts have rims of compositionally slightly different plagioclase and clinopyroxene respectively or are just partially resorbed. We have focused on reaction rim formation around olivine and orthopyroxene for three reasons. Firstly, these are the most abundant xenocryst phases and they are therefore likely to have been the major constituents of the original xenoliths. Secondly, the more common occurrence of reaction rims involving these phases means that it is easier to characterize the reactions. This contrasts with, for example spinel where only a handful of examples of reaction rims are observed. Thirdly, olivine and orthopyroxene appear to be much more reactive to phonolite melt compared, for example with clinopyroxene or plagioclase. This means that a potential metasomatic reaction will be dominated by the exchange of elements between olivine and orthopyroxene with melt.

Reaction rims around Olivine

Reaction rims on olivine consist of diopsidic clinopyroxene, phlogopite, minor magnetite and very rare amphibole. Reaction rims on olivine are displayed in Figure 2.2. The inner parts of the reaction rims are dominated by phlogopite and the outer by diopside. Magnetite occurs nearly exclusively in the inner phlogopite rim zones. In some cases diopside is present in the inner rim zones and phlogopite in the outer rim zones, and the relative proportions of inner phlogopite to diopside can vary significantly. However, the sequence of a phlogopite + magnetite inner zone and a diopside outer zone is very consistent across all observed reaction rims on olivine. The interface between olivine and the phlogopite inner rims is always highly convoluted and irregular (see figure 2.2A). This is a common feature observed during dissolution and replacement reactions (Coombs and Gardner, 2004 for example). Similar reaction rims have been observed on olivine from a variety of K-rich melts (Carmichael 1967, Neal and Taylor 1989, Davis and Smith 1993), including phonolite (Henderson et al., 2012). These too had an inner rim of phlogopite with minor and sometimes absent diopside.

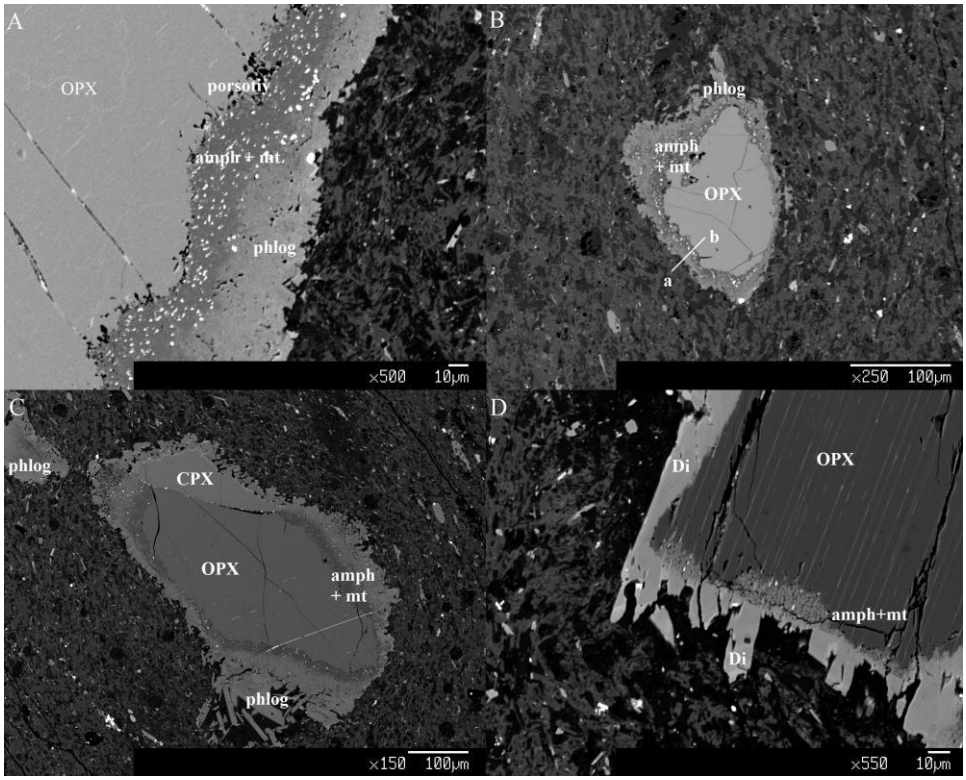

Figure 2.3. BSE image of orthopyroxene xenocrysts. Abbreviations are the same as in Figure 1, with OPX = orthopyroxene. **A** – orthopyroxene from group II, with an inner rim zone consisting of amphibole and magnetite with an outer rim consisting of phlogopite. The orthopyroxene – rim contact is highly irregular and small pockets of porosity are visible. Some porosity is also seen throughout the rim. **B** – orthopyroxene from group II with an inner rim of amphibole and magnetite and an outer rim of phlogopite. **C** – micro-xenolith of group I orthopyroxene and group I clinopyroxene. Clinopyroxene has a rim of finer grained clinopyroxene and orthopyroxene has an inner rim of amphibole + magnetite and an outer rim of phlogopite. The contact between orthopyroxene and clinopyroxene is sharp but has a thin band of glass and some crystallization of magnetite. Augite lamella visible in orthopyroxene is preserved in the amphibole inner rim but ends abruptly at the start of the phlogopite outer zone. **D** – orthopyroxene from group II with inconsistent discontinuous single rim of diopside punctuated by amphibole + magnetite inner rim zones located at the orthopyroxene surface perpendicular to augite lamellae. Contacts between diopside and orthopyroxene are more regular but show some signs of dissolution of the host. Saw tooth texture of diopside rims is seen only on surfaces perpendicular to the augite lamellae.

Orthopyroxene

Orthopyroxenes show much more varied reaction assemblages than olivine. The most common assemblage is an inner rim zone of amphibole and minor magnetite surrounded by an outer rim zone of phlogopite with minor to absent diopside (Figure 2.3A-C). The interface between the host orthopyroxene and the amphibole inner rim zone is always highly convoluted and in some cases porosity is visible at the interface (see Figure 2.3A). Porosity can also be seen throughout the reaction rims in both the inner and outer rim zones. Pore fillings are generally too small to be accurately analyzed using the microprobe without contamination by rim phases. Grain sizes of amphibole in the rims are typically <1 micron. Magnetite is larger at 1-2 microns, and outer rim phlogopite is larger again (mostly 10-20 microns) with phlogopite grain-size increasing towards the outer rim. Some outer

rim phlogopite can be several 10s of microns in size or greater. Augite lamellae formed in the host orthopyroxene are preserved as ghost lamellae in the inner amphibole zones (Figure 2.3D and Figure 2.4). These ghost lamellae stop abruptly at the amphibole – phlogopite interface.

A variation is the development of nearly pure rims of diopside on orthopyroxene. This type of reaction is much less common than the formation of amphibole – phlogopite double rims. Tarney (1969) described similar epitaxial rim growth of clinopyroxene on orthopyroxene, where rim and host have the same crystallographic orientation. The diopside rims on Heldburg orthopyroxene xenocrysts are in some cases punctuated by amphibole growth at the diopside orthopyroxene interface forming localized double rims (Figure 2.3D). The inner rim zones are primarily composed of amphibole with some minor magnetite. Where this occurs, the amphibole – orthopyroxene interface is convoluted as with the amphibole – phlogopite rims described above. However the amphibole – diopside interface is more regular and linear, whether amphibole inner rims are present or not. Augite lamellae form parallel to the c-axis of the orthopyroxene and therefore permit an approximate estimation of the orientation of the host orthopyroxene. The localized patches of amphibole growth in this rim variety are restricted to diopside – orthopyroxene interfaces that are perpendicular to the augite lamellae. This is a strong indication that amphibole growth is preferentially located at the (001) surfaces of the orthopyroxene. Diopside rims also have a saw-toothed texture (Figure 2.3D) on surfaces where amphibole inner rim growth develops.

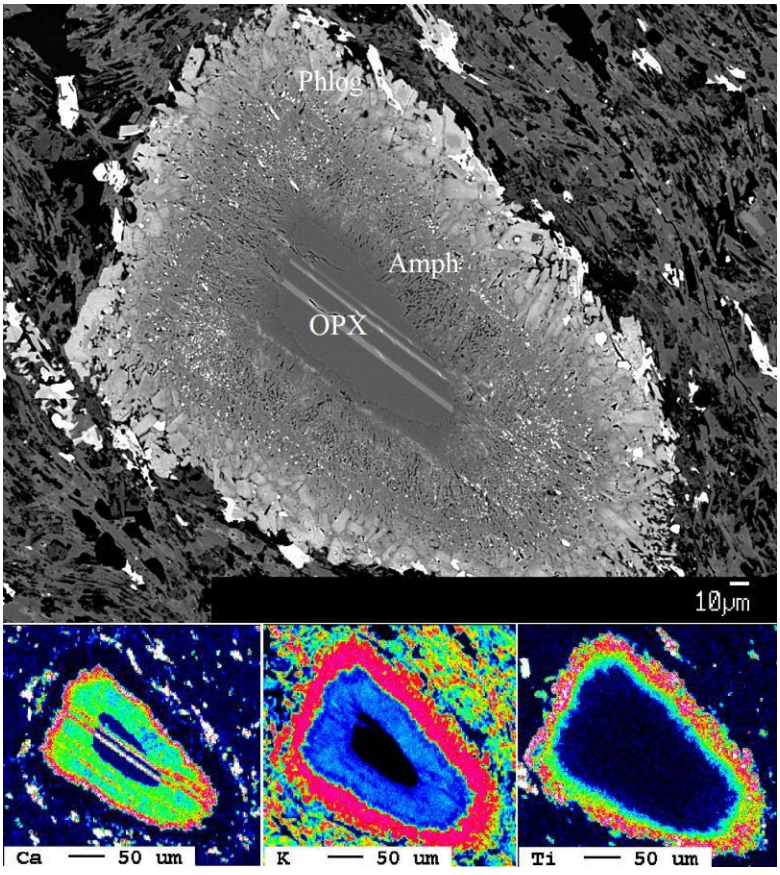

Figure 2.4. BSE image and element maps of a reaction rim around orthopyroxene. Ca element map shows the location of ghost lamellae in the inner amphibole rim, which end abruptly at the phlogopite outer rim zone.

Spinel, magnetite, clinopyroxene and plagioclase

Spinel typically forms single rims of phlogopite mica (Figure 2.5A). The interfaces between spinel and mica are regular and typically straight with small embayments into the spinel on a scale of several microns. Phlogopite rim grains are several microns in size. In some cases, large titanomagnetites also have phlogopite rims with features similar to those observed in spinel rims, but these are only rarely observed as isolated xenocrysts. Clinopyroxene xenocrysts form spongy or cellular rims of fine-grained diopside (Figure 2.5B). Plagioclase is often resorbed and dissolved giving irregular rim edges, in some cases with a minor amount of alkali feldspar growth.

In summary, four main types of reaction rim assemblages on xenocrysts are distinguished;

(1) Olivine + melt = phlogopite + magnetite | diopside

(2) Orthopyroxene + melt = amphibole + magnetite | phlogopite ± minor diopside

(3) Orthopyroxene + melt = ± amphibole + magnetite | diopside

(4) Spinel + melt = phlogopite

Micro-xenoliths

Where in contact with the host phonolite, constituent mineral phases of micro-xenoliths always show the same rim growth patterns as their xenocryst counterparts, i.e. olivine in micro xenoliths forms inner rims of phlogopite and magnetite with outer rims of diopside. In some cases, interior grain-to-grain contacts in micro-xenoliths show signs of reaction and infiltration of melt (see Figure 2.5D). Clinopyroxene and plagioclase do not form rims with different mineralogy, but they have irregular grain to grain contacts and manifest resorption and re-growth similar to that observed when they are in direct contact with the host phonolite (see Figure 2.5C). Orthopyroxene interfaces within the interiors of micro-xenoliths have reacted to form amphibole and magnetite but phlogopite is absent or is a minor phase. However there are several examples where the internal interfaces of micro-xenoliths are linear and show little to no signs of reaction (Figure 2.5E), have small amounts of glass present (Figure 2.3C) or are too altered for this to be accurately determined (Figure 2.5F).

2.5 ANALYTICAL METHODS

All electron microprobe analyses and back-scattered electron images were collected using the JEOL JXA-8200 superprobe at the Geocampus Lankwitz, Freie Universität Berlin. Accelerating voltages of 15KV and beam currents of 20nA were used for all data points and fully focused beams were used for all results except some glass analyses that had defocused 15µm beams. Natural silicate and oxide standards were used. Maps and line scans are non-standardized WDS measurements.

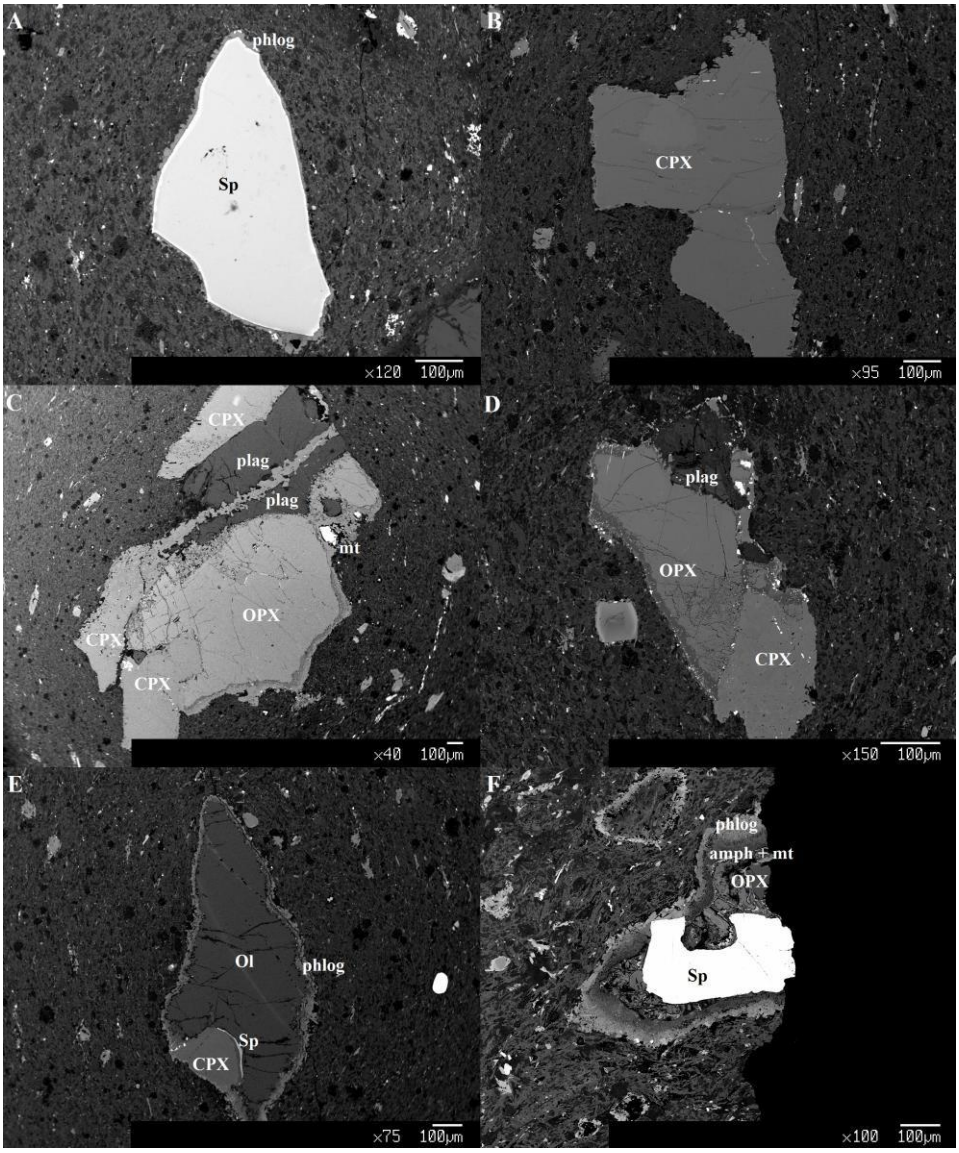

Figure 2.5 – BSE images of other xenocrysts and some examples of micro-xenoliths. Abbreviations are the same as in previous figures, with sp = spinel, plag = plagioclase, CPX = clinopyroxene. **A** – spinel xenocryst with a reaction rim of phlogopite. The contact between rim and host are generally regular and linear. **B** – xenocryst of clinopyroxene that shows signs of partial dissolution and formation of fine-grained rim of more clinopyroxene. **C** – Micro-xenolith (MX002) consisting of clinopyroxene, plagioclase, small magnetite grains and orthopyroxene. Clinopyroxene and plagioclase in contact with the host phonolite are partially resorbed and have fine rims of clinopyroxene and plagioclase respectively. Similar textures are also observed at the contacts between the two phases within the micro-xenolith. Orthopyroxene in contact with the phonolite host has an inner rim of amphibole and magnetite with an outer rim zone of phlogopite. The rims of orthopyroxene in contact with other phases within the xenolith have also been partially replaced by amphibole and magnetite. **D** – Micro-xenolith (MX005) that consists of plagioclase, orthopyroxene and clinopyroxene. Interior grain contacts show signs of reaction or resorbtion similae to those formed along the contact with the host phonolite and have the same reaction rim formation observed in MX002. **E** – micro-xenolith (MX008) consisting of olivine, clinopyroxene and spinel. Olivine has reacted to form a rim dominated by phlogopite and clinopyroxene forms a thin rim on diopside. Internal contacts between phases are sharp and show no signs of reaction. **F** – micro-xenolith (MX008) consisting of spinel and orthopyroxene which have rims of amphibole + magnetite and phlogopite outer rim zones. Much of the xenolith has been altered.

2.6 RESULTS

A summary of representative chemical data is given in Table 2.2. Some further data is also available in the supplementary data online.

Host phonolite

The compositions of the groundmass phases were not studied in detail and are therefore not reported. Some measurements of glass were taken but all had very low totals of around 90%. The difference to 100% is mainly attributed to high volatile contents in the glass, as the Na_2O contents are high indicating little to no loss of alkalis. All glasses observed within the groundmass, interstitially within crystal clots or as melt inclusions were very similar, having enriched contents of SiO_2; 53-58wt.%, Al_2O_3; 22-25wt.%, Na_2O; 8.7-12 Wt.% relative to the bulk rock composition. All other major components are depleted relative to the bulk composition and are <1 wt.%. Regardless of local association with solid phases, glass compositions are generally uniform indicating that this glass represents the final residual melt of the phonolite. The glasses are generally tephri-phonolites but this is likely due to loss of K_2O relative to the bulk rock by the crystallization of groundmass alkali feldspar.

Phenocryst amphibole is Ca-rich hornblende to pargasite (Leake et al., 1997). It has a limited range in CaO; 10-12 wt.% and alkalis; 4-5 wt.% $Na_2O + K_2O$ (Figure 2.6). The xMg ($Mg/(Mg + Fe_{tot})$ numbers vary significantly from 0.5-0.85. They are rich in TiO_2 with >2wt.% of this component. Clinopyroxene within amphibole is Ti rich diopside / augite with xMg ($Mg/Mg+Fe^{2+}$) of 0.77-0.91 and Ti concentration increases with Fe content. These inclusions are compositionally different from phenocryst clinopyroxenes, which have much lower Ti contents (Figure 2.7). Phenocryst clinopyroxene rims are richer in Fe, Al and Na than the cores and are more similar to smaller phenocrysts in the groundmass. Phlogopite phenocrysts have a very wide range of xMg ($Mg / Mg+ Fe^{2+}$) from 0.90 (cores) down to 0.41 (rims) and show increasing Ti with increasing Fe content (Figure 2.6).

The compositions of phases in the crystal clots are the same as the phenocrysts of the same mineral (Figure 2.6). Amphibole in crystal clots has limited ranges in CaO; 9-11.5 wt.%, low total alkalis; 4.5-5.5 wt.%, high TiO_2; >2 wt.% and xMg varying from 0.45-0.88. The high Fe contents are observed at the rims of amphibole grains with the cores being more magnesian. The amphiboles are classified as hornblende to pargasite. Diopside in the crystal clots is Ti-enriched and is comparable in major element composition to the diopside seen as cores in amphibole phenocrysts. They also become increasingly Ti-enriched with increasing Fe content.

Xenocrysts and micro-xenoliths

The xenocrysts can be connected more strongly to their occurrences in micro-xenoliths by their major element chemistry. By comparing the xenocryst compositions with the mineral components of micro-xenoliths, it is possible to identify the source rocks of the xenolithic material. For olivine, orthopyroxene and clinopyroxene xenocrysts, more than one compositional population is identified in each case.

Olivine xenocryst compositions can be separated into two populations. The first has very high Fo contents of 0.91-0.93, low CaO of around 0.02wt.% and high NiO of 0.38 wt.%. This population

will be referred to as olivine group I. The second population of olivine has distinctly lower Fo of 0.83-0.85, lower NiO; 0.19 wt.% and much higher CaO; 0.186 wt.%. This population of olivines will be referred to as olivine group II. Compositionally olivine group 1 matches well with olivine in micro-xenoliths of olivine-orthopyroxene-clinopyroxene-spinel (spinel lherzolite). This olivine composition is also similar to that of olivine from spinel-lherzolite found as xenoliths in the nearby Rhön area of Central Germany (Witt-Eickschen and Kramm, 1997) (Figure 2.8). No olivine from group II was found in textural association with any other phase in a micro-xenolith and olivines of this group only occur as single xenocrysts.

Two separate populations of orthopyroxene xenocrysts can also be identified. Orthopyroxene group I has a narrow range in compositions with xMg ($Mg/Mg+Fe^{2+}$) of 0.92-0.96 and high Cr_2O_3 of 0.4 wt.%, whereas orthopyroxene group II has lower and more varied xMg of 0.83-0.65, lower Cr and systematically decreasing Al_2O_3 with increasing xMg. Orthopyroxenes of group I have compositions that match those found in micro-xenoliths of spinel lherzolite (olivine-orthopyroxene-clinopyroxene-spinel). These compositions are also similar to orthopyroxenes from spinel lherzolite xenoliths described by Witt-Eickschen and Kramm, (1997) (see Figure 2.8). Orthopyroxenes of group II are found within orthopyroxene-plagioclase-clinopyroxene-magnetite or norite-gabbro micro-xenoliths.

Two varieties of clinopyroxene compositions can be identified on the basis of chemical composition. A Cr-diopside (clinopyroxene group I) that is highly magnesian (0.94-0.93) is found within spinel lherzolite micro-xenoliths, whereas a more Fe rich and Cr-poor clinopyroxene (group II) is found in gabbro-norite xenocrysts. Spinel is Cr-rich and has xMg of 0.66-0.74 and within the group, Cr and Al decrease with increasing Fe content. Plagioclase within the micro-xenoliths varies from An99 down to An29.5.

To further emphasize the relationships between different xenocrysts and the minerals in micro-xenoliths the compositions of phases in a selection of micro-xenoliths and xenocrysts are compared in Table 2.3. This shows clearly that there is a refractory (group I) olivine + orthopyroxene + Cr-diopside + spinel assemblage consistent with a spinel lherzolite. A second (group II) assemblage of orthopyroxene + plagioclase + clinopyroxene + and magnetite is consistent with a gabbro-norite.

Reaction rims

All rim amphibole is enriched in alkalis compared to the phenocrysts (6-10 wt.%). They are relatively low in CaO (<8 wt.%) and TiO_2 (<2 wt.%) and are sodic-calcic amphiboles, typically K-richterite in composition but sometimes with higher Al taking them into the katophorite field (Leake et al., 1997). There are no large differences in composition between amphiboles in rims on group I compared to group II orthopyroxene but there are in some cases large differences within a single rim. Phlogopite in reaction rims do not show great compositional variations, regardless of reaction rim type and phlogopite reaction rim and phenocryst compositions are very similar except the latter have narrower ranges in xMg and Ti content. Diopsides in rims and phenocrysts are compositionally similar. The details of compositional variations within reaction rims are best seen in the rim profile.

	Amphiboles				Clinopyroxenes				Phlogopite		Olivines		Orthopyroxenes		Glass
	Pheno	Clots	Rims		Xeno		Clots	Rims	Pheno	Rims	OlI	OlII	OPXI	OPXII	
			OPXI	OPXII	MX011	MX001		OPXI		OPXI					Ave.
SiO_2	39.37	39.73	53.10	41.13	53.51	52.28	51.28	54.34	40.53	40.45	42.23	39.89	55.41	51.89	55.57
TiO_2	4.54	3.74	1.96	2.08	-	0.21	0.89	0.25	2.44	3.27	-	0.07	0.05	0.10	0.06
Cr_2O_3	-	-	0.08	-	1.04	0.02	-	-	0.17	0.11	-	0.03	0.48	0.14	0.01
Al_2O_3	15.25	13.59	2.60	13.35	3.05	5.49	4.10	0.80	13.43	13.70	0.03	0.04	3.45	3.72	24.86
FeO	10.78	12.82	8.84	14.21	2.11	13.99	5.27	5.22	6.24	8.60	8.44	13.44	5.75	15.98	0.69
MnO	0.09	0.20	-	-	-	-	008	0.09	-	-	-	0.17	0.02	0.41	-
NiO	-	-	-	-	0.09	0.05	-	0.07	-	-	-	0.20	0.03	0.09	-
MgO	13.27	12.54	16.68	11.53	17.66	23.63	15.98	16.52	21.68	18.98	50.12	46.12	34.85	26.34	0.35
CaO	10.78	11.15	5.66	10.44	20.89	2.82	21.31	21.15	0.58	0.68	0.03	0.22	0.30	0.40	0.51
Na_2O	2.67	2.80	6.93	3.42	0.52	0.14	0.65	0.91	0.69	1.15	-	-	0.02	0.04	11.79
K_2O	1.85	1.71	1.38	1.48	0.01	0.01	0.01	0.06	9.91	9.18	-	0.01	-	0.01	0.25
F	-	-	-	-	-	-	-	-	4.36	3.26	-	-	-	-	0.01
Cl	-	-	-	-	-	-	-	-	0.01	0.01	-	-	-	-	0.01
Total	98.60	98.27	98.42	97.83	98.88	98.64	99.57	99.39	98.20	98.01	100.84	100.2	100.37	99.11	94.09
Si	5.71	5.86	7.68	6.11	1.96	1.92	1.88	1.95	2.94	2.96	1.02	0.99	1.89	1.89	-
Ti	0.50	0.41	0.21	0.23	-	0.01	0.02	0.01	0.13	0.18	-	-	-	-	-
Al	2.61	2.36	0.44	2.34	0.13	0.24	0.18	0.14	1.15	1.18	-	-	0.14	0.16	-
Fe3+	0.54	0.44	-	0.39	-	-	0.06	0.09	0.38	0.53	-	-	0.06	0.06	-
Fe2+	0.77	1.14	1.07	1.38	0.06	0.43	0.10	0.13	-	-	0.17	0.28	0.10	0.42	-
Mg	2.87	2.76	3.59	2.55	0.96	1.29	0.87	0.76	2.34	2.07	1.81	1.71	1.78	1.43	-
Ca	1.68	1.76	0.88	1.66	0.82	0.11	0.84	0.77	0.04	0.05	-	0.01	0.01	0.02	-
Na	0.75	0.8	1.94	0.98	0.04	0.01	0.05	0.14	0.10	0.16	-	-	-	-	-
K	0.34	0.32	0.25	0.28	-	-	-	-	0.92	0.86	-	-	-	-	-
xMg	0.69	0.64	0.77	0.65	0.94	0.75	0.90	0.85	0.86	0.80	0.91	0.85	0.94	0.77	0.48

Table 2.2. A selection of representative chemical data for the most important mineral groups. xMg = (Mg / Mg + Fe^{2+}) except for amphiboles which use Fe_{tot}. A hyphen indicates that the element was not measured in the data point of that the value was 0.00 to within 2 decimal places. Amphiboles were calculated based upon 22 oxygens and 15 cations, clinopyroxenes: 4 cations and 4 oxygens, orthopyroxene: 4 cations and 4 oxygens, olivine calculated with 3 cations, spinel with 3 cations and 4 oxygens. Glass average was calculated from 15 different analyses.

Line scan on orthopyroxene

Figure 2.9 shows a line scan across an amphibole-phlogopite double rim (rim type 2) on an orthopyroxene (group II). The location of the scan is indicated by the white a-b line in Figure 2.3B. Several line scans were taken on other amphibole-phlogopite double rims, however in many cases porosity or small grains of magnetite produced profiles complicated by many contaminated data points. The line scan displayed in Figure 2.8 was chosen because it had not been affected by contamination as much as others. It must be emphasised that, despite the contamination effects all the line scans show similar patterns and the displayed scan is representative of the trends observed in other reaction rims.

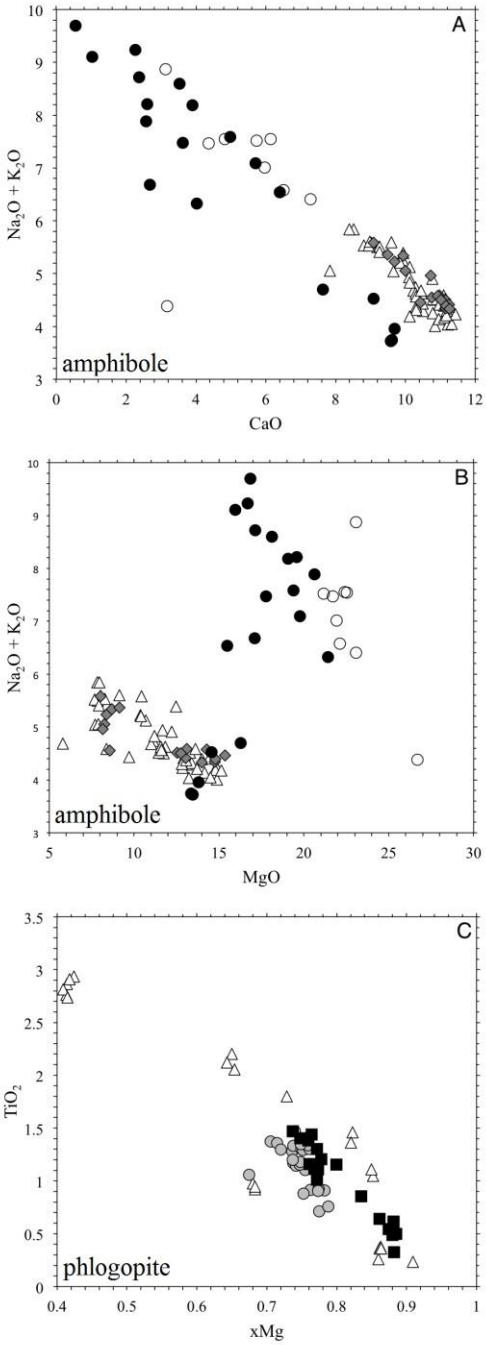

Figure 2.6. Symbols; for amphiboles; **A** and **B,** white triangles – phenocrysts, grey diamonds = amphiboles in crystal clots, white circles = amphibole in rims on group I orthopyroxene, black circles = amphibole in rims on group II orthopyroxene. For phlogopites; **C**, white triangles = phenocrysts, black squares = rims on olivine I and II, grey circles = rims on group I and group II orthopyroxene.

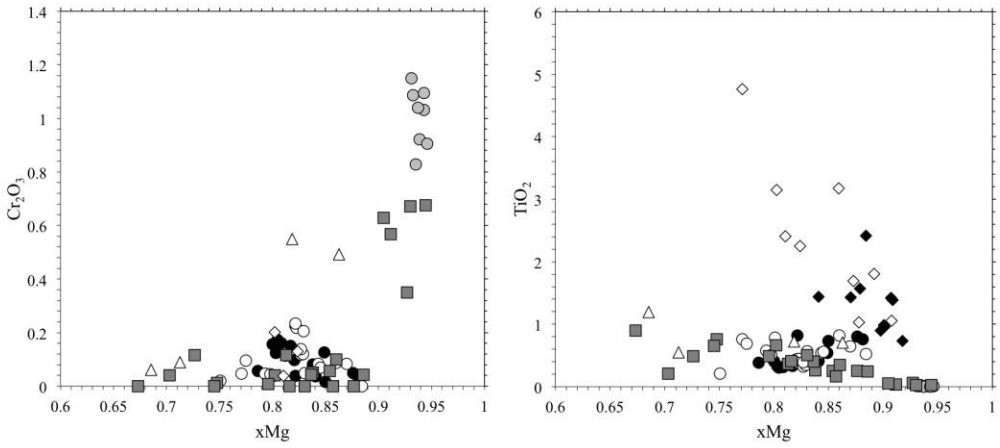

Figure 2.7. Clinopyroxenes. Symbols; white triangle = phenocrysts, grey circle = clinopyroxene I, white circles = group II clinopyroxene, grey squares = reaction rim diopside, white diamonds = cores in amphiboles, black diamonds = in crystal clots.

In the representative scan, the host orthopyroxene has very consistent major element abundances right up to the interface with amphibole. There are no signs of Mg-Fe interdiffusion within the orthopyroxene. This makes it possible to accurately determine the location of the interface between orthopyroxene and amphibole. The interface between amphibole and phlogopite is more difficult to define, but can be approximated using the Na_2O concentrations. Rim phlogopite is relatively depleted in this component (<1wt.%) whereas rim amphibole tends to have a much higher Na_2O concentration (3-5wt.%). The interface between the reaction rim and the host phonolite is marked by an abrupt increase in SiO_2 abundance and very low MgO content. As a focused beam was used for the line scan, glass and matrix analyses show significant Na loss and are therefore not reliable. These data have therefore been removed from the line scan images. Data points close to or at the interfaces are likely to be mixed analyses due to the excitation volume of the microprobe. This should only affect data points 1-2 microns either side each interface.

2.7 DISCUSSION

Xenoliths

Two pyroxene thermobarometry using the equations from Brey and Kohler (1990) and Putirka (2008) was used to calculate P-T for gabbro-norite and spinel lherzolite micro-xenoliths. Only cases where there was data for both phases coexisting within a single micro-xenolith were used. This gave estimates of 870ºC ±40 and 9.8kbar ± 2.9 for gabbro norite and 1065°C ±10 and 14.7kbar ± 1.4 for spinel lherzolite. For the spinel lherzolite this is within the range given by Franz et al. (1997) and Witt-Eickschen and Kramm (1997) for similar xenoliths in the Rhön region. The presence of gabbro-norite is close to the likely base of the crust, which is generally approximated at around 9-10kbar in the region (Franz et al., 1997).

Clinopyroxene

The new clinopyroxene thermobarometric calculations for phonolite and trachyte melts by Masotta et al. (2013) were used for clinopyroxenes from crystal clots, cores in amphibole phenocrysts and phenocryst clinopyroxene cores. Liquid compositions were the bulk rock compositon from Irving and Price (1981). Temperatures were calculated using the recommended Talk model from Masotta et al. (2013) and pressures were calculated using equation 32c from Putirka (2008). This barometer was used instead of the recommended Palk from Masotta et al. (2013) because it appears to be more accurate (although less precise) for higher pressures. The Palk equation underestimates pressure by several kbar beyond around 6kbar. The results of these calculations gave temperature estimates that ranged between 920-980°C ±15 and pressures of 7.7-16kbar ±2 for clinopyroxene as cores in amphibole. These were close but not in equilibrium with the bulk rock composition in terms of $K_D(Fe\text{-}Mg)^{cpx\text{-}liq}$, which averages at 0.25. This indicates slightly higher Mg/Fe contents of the melt than the bulk rock. The phenocryst clinopyroxene had similar pressures of around 9kbar and temperatures of around 950°C for their core compositions, although we report limited data for this.

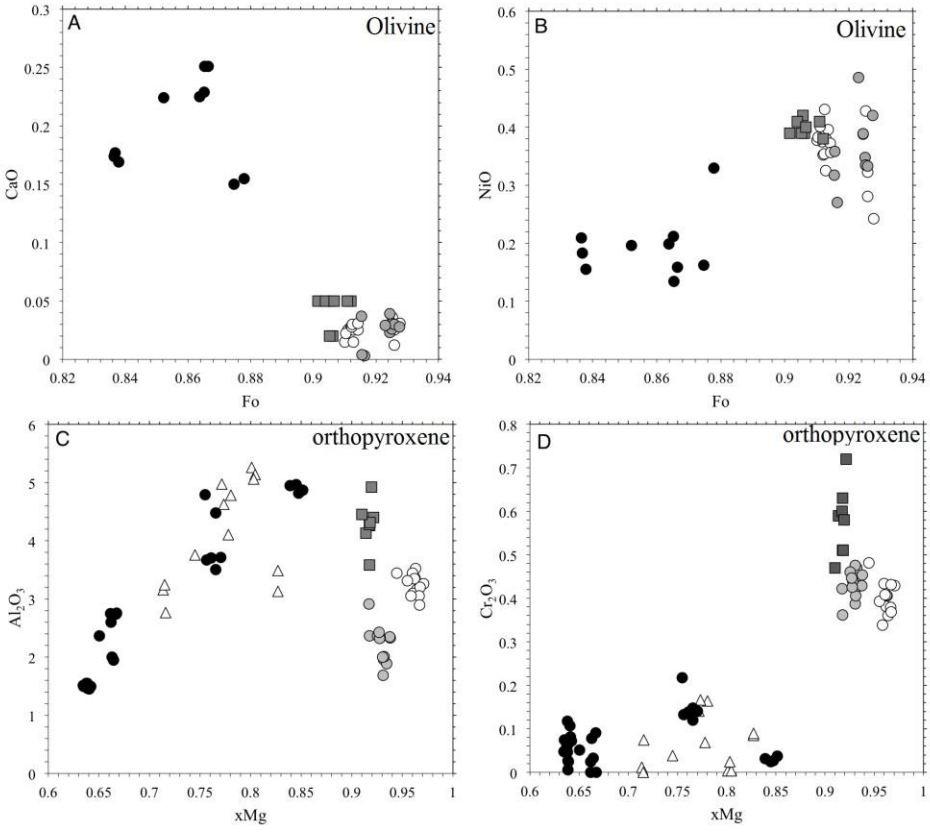

Figure 2.8. Comparison of olivines and orthopyroxenes from xenocrysts, micro-xenoliths with spinel lherzolite xenoliths described by Witt-Eickschen and Kramm (1997). A – B are olivines with symbols; black circles = group II xenocryst olivine, white circles = group I xenocryst olivine, grey circles = micro-xenolith olivine I, grey squares = olivine from Witt-Eickschen and Kramm (1997). C –D are orthopyroxenes with symbols; black circles = xenocryst orthopyroxene group II, white circles = xenocryst orthopyroxene group I, grey circles = micro-xenolith orthopyroxene group I, white triangles = micro-xenolith orthopyroxene group II, grey squares = olivine from Witt-Eickschen and Kramm (1997).

Amphibole

We used the theromobarometers presented in Ridolfi and Renzulli (2012). No combination of thermometers or barometers from their results produced P-T estimates that plotted within the amphibole stability field that they provide. By following their criteria for which equation to use, equation 1E should be the most accurate. This would give P-T estimates for phenocryst amphibole and amphibole in crystal clots between 850-950°C and pressures of 10-25kbar. However, it is important for the amphibole to fit with the textural observations and crystallization sequence that would imply that amphibole formed after clinopyroxene. There must therefore be a consistent P-T trajectory between clinopyroxene and amphibole. The model of temperature calculated by equation 2 with pressure calculated using equation 1b gives temperatures of 940-840°C and pressures of 8.5-3.9Kbar.

Petrogenesis

Phenocrysts

The results of the thermobarometric calculations indicate that the phenocrysts of clinopyroxene and amphibole originated from temperatures between 850-960°C and pressures between 4-10kbar. It is necessary to try to relate these findings to existing experimental studies on the phase relationships of phonolites. Although most of studies concentrate on low-pressure phase relationships of phonolites (~2kbar) (Berndt et al., 2001; Freise et al., 2003; Harms et al., 2004; Scaillet et al., 2008; Moussallam et al., 2013), there are a few studies that look into the phase relationships of phonolites at higher pressures (Hay and Wendlandt, 1995; Draper and Green, 1997). There is also the high-pressure fractionation model from Irving and Green (2008).

Early crystallization was probably dominated by clinopyroxene at lower crust to upper mantle conditions. Clinopyroxene in the amphibole cores originate from higher pressures and temperatures and could come from a more mafic melt that mixed with the phonolite at the crust mantle boundary leading to their partial consumption. If so, the melt composition used in the P-T calculations would not be appropriate and the conditions of formation for this type of clinopyroxene are uncertain. Rims of clinopyroxene phenocrysts that are more Fe-rich and jadeite rich probably formed during groundmass crystallization as the melt increased in both Al_2O_3 and Na_2O.

Amphibole was the dominant phenocryst phase from lower to mid crustal conditions. Inclusions of magnetite and apatite in amphibole imply that both these phases were also saturated in the melt at this time. The occurrence of magnetite and apatite inclusions in phlogopite phenocrysts indicates that both phlogopite and amphibole formed at similar conditions. It is not clear exactly why there was a change from clinopyroxene dominated crystallization to amphibole + phlogopite. This is inconsistent with the expected crystallization sequence in the fractionation model proposed by Irving and Green (2008) that predicts amphibole before clinopyroxene. It is also inconsistent with the phase relationships of Hay and Wendlandt (1995). These models, however, do not include the effects of changing pressure, temperature and H_2O during crystallization.

A distinct feature of the Heldburg Phonolite is the lack of feldspar phenocrysts, and that the chondrite normalized rare earth element patterns do not have Eu anomalies (Irving and Price 1981).

Therefore, it is very unlikely that feldspar was a liquidus phase with a role in the crystallization history of the Heldburg Phonolite. This has been used to suggest a high pressure origin, however, feldspar can form at upper mantle pressures from phonolite melts with low H_2O (<3.4-4 wt.%) in the melt and at temperatures below ~900°C (Hay and Wendlandt, 1995) or below ~1100°C at completely anhydrous conditions (Draper and Green, 1997). The lack of feldspar is therefore not necessarily an indicator of high pressure but suggests high water contents in the melt and potentially high temperatures that are consistent with the thermometry results (850-950°C).

At shallow pressures cooling and degassing would have stabilized alkali feldspar leading to crystallization of the groundmass phases that also include nepheline and diopside. The changes in temperature, volatile abundances and melt composition induced by groundmass crystallization made the pre-existing phenocrysts of amphibole, phlogopite and diopside less stable, resulting in spongy and partially resorbed rims.

Crystal clots

The crystal clots have compositions and mineralogy that are similar to those of the phenocryst assemblages, except that Ti abundance is higher than in diopside phenocrysts. The clots are most likely to have originated from the phonolite as aggregates of phenocryst phases. Large crystal clots or glomerocrysts have been interpreted as indications of the initial stages of a crystal mush or cumulate forming process (Jerram et al., 2003). Loose packing and high melt porosity in the clots arises from a mixed population of crystals with different shapes (Jerram et al., 2003). The absence of feldspar and phases similar to the groundmass and the close similarity between the clots and the phenocryst assemblage suggests that the clots formed prior to intrusion. Hydrous phases within the clots could have buffered the interstitial melt with respect to H_2O and other volatiles, keeping the melt above the liquidus, and thereby preserving a crystal poor glass.

Xenocrysts and micro-xenoliths

We have shown that individual xenocrysts are compositionally and textural linked to one of two types of micro-xenolith assemblages of spinel lherzolite or gabbro-norite. This is in accordance with previous descriptions of xenoliths from the Heldburg Phonolite by Irving and Price (1981, and references within). Gabbro-norite xenocrysts have also been observed in Vogtland / NW Bohemia (Giessler et al., 2007) and are typically of mid-lower crustal origin. Xenocrysts and micro-xenoliths most likely have lower crust to upper mantle origins.

Group II olivines could not be related to any micro-xenoliths and were not observed to be in a local association with another xenocryst phase. These olivines are different to the spinel lherzolite olivines and texturally they do not appear to be related to the norite assemblage. These olivines could be derived from one of the less common olivine-gabbro or olivine-melilite xenoliths described by Huckenholz and Werner (1990) but these were not found as micro-xenoliths within our investigated samples. It is also possible that olivine group II and clinopyroxene in the cores of amphiboles both originated from a more mafic melt that was mixed into the phonolite. Alternatively this olivine type could be a cognate phenocryst. Using the Rhodes diagram from Rhodes et al. (1979)

olivine group II appear to be in equilibrium with the bulk phonolite rock values given in Irving and Price (1981). Phase relations from Draper and Green (1997) suggest that olivine would be on the liquidus at >1000°C. Olivine could also be involved in fractionation trends from a possible basanite parent melt (Irving and Green, 2008). These studies also suggest that upon cooling olivine would then be unstable with the phlogopite being a major liquidus phase.

	Olivine I	OPX I	CPX I	Spinel	Olivine II	OPX I	CPX II	Magnetite	Plagioclase
MX001						74.5	82.5	x	
MX002						71.5	79.5	x	23.2
MX003						80.3	85.3		
MX005						77.5	82.4		99.5
MX006						77.8	82.0		
MX010							77.3		40.2
MX012						82.3	87.5		29.5
MX004	92.5	93.2							
MX007		93.8		x					
MX008	91.6		94.3	x					
MX009		91.7	93.3	x					
MX011		92.7	93.7	x					
MX013	92.5	92.7							

Table 2.3. Distribution of different xenocryst populations in a selection of micro-xenoliths. This shows the co-variance of different compositions and difference phases in larger fragments of xenolithic material in order to link the xenocrysts to micro-xenoliths.

Reaction rim formation

Rate limiting processes

The reaction rims are the product of disequilibrium between the xenocrysts and the phonolite. This leads to dissolution of the xenocrysts and the instantaneous precipitation of rim phases. The rim phases are dependent on the fluxes of components between melt and xenocryst. Hence, only localized instantaneous equilibrium is achieved in the growing rim. This is how the rims can inherit compositional features of the host xenocrysts, such as ghost lamella from orthopyroxene or rim amphiboles that are different to phenocryst amphiboles.

During rim formation, diffusion, dissolution and re-precipitation processes all operate simultaneously. The slowest process is referred to as the rate limiting process (Berner 1978, Dohmen and Chakraborty 2003 for some discussion) and determines the rates of reaction. The rates of dissolution and re-precipitation are difficult to quantify, however, and due to the preservation of compositional heterogeneities within the rims it is likely that diffusional mass transport is the slowest process. The rim reaction rates are therefore diffusion controlled and the diffusion rates of components through the rims or into the rims from the melt are rate limiting. Due to the extensive groundmass crystallization the near field melt composition cannot be studied. This makes it impossible to assess whether a depleted / enriched boundary layer in the melt developed as a response to slow diffusion in the melt, as is seen in other reaction rim studies (Coombs and Gardner, 2004; Klügel, 2001 for example). If diffusion in the melt was limiting, it would be expected that the internal compositions of

the rims were able to equilibrate. Therefore diffusion within the reaction rims via grain boundary diffusion or even fluid / melt filled grain contacts is most likely to be rate limiting.

Replacement of olivine by phlogopite and orthopyroxene by amphibole and phlogopite leads to an increase in molar volume and yet porosity is still formed in both reaction rim types. This is often the case for mineral replacement reactions (Putnis 2002, Putnis and Putnis 2007) and can be the result of dissolution being greater than precipitation, leading to a loss of mass to the melt. Some porosity could also be formed by the over-saturation of fluid along grain or inter-phase boundaries (Gardés et al., 2012). Fluid filled pores at the interfaces between the anhydrous xenocrysts and reaction rims have been shown to locally increase the rates of dissolution and form self-propagating reaction fronts (Milke et al., 2012). Instabilities and localized disturbances in the interfacial – dissolution process such as these, coupled with heterogeneities in the host xenocryst such as dislocations and the tortuosity of rim grain boundaries could explain the highly convoluted and irregular rim interfaces. The interfacial process is still faster than diffusional transport, but the rates of dissolution vary at the micron to submicron scale.

From the line scans, element maps and BSE images for all reaction rim types, it is clear that the internal compositions of the xenocrysts are in all cases homogenous right up to the rim interface. This means that the rates of dissolution and reaction rim growth significantly exceed the rate at which major elements can diffuse within olivine or orthopyroxene. Fast rim growth rates and short residence times for the xenocrysts are therefore likely. Quantifying this is problematic as several parameters are unknown. A semi-quantitative estimate for olivine, for which Fe-Mg interdiffusion is well characterized, can be made based upon some simple assumptions. This approach gives a maximum residence time.

Using the equations from Dohmen and Chakraborty (2007), and, of P = 5kbar, xFe = 0.1, fO_2 = 4 $x10^{-6}$ Pa, and using the fastest diffusion direction in just the c direction, the diffusion rate can be estimated over a temperature range of 800-1000ºC. This approach gives a diffusion rate of between 4.7 $x10^{-18}$ to 1.3 $x10^{-19}$ m/s^{-2} for 1000ºC and 800ºC respectively. Most phlogopite rims on olivine are typically under 100µm in thickness. In order to grow a rim of this size, at growth rates equal to or faster than the diffusion rates of Fe-Mg in olivine, the residence time would have to be less than around 320 days at 800ºC or around 50 days at 1000ºC. This is a poorly constrained estimate but it gives some indication of the time scales involved.

Element mobilities

Using the line scan given in Figure 2.8 some information can be gained on the relative mobilities of elements during xenocryst-melt reactions. The orthopyroxene-amphibole interface is unstable and migrates inwards towards the core of the xenocryst by dissolution. During this process SiO_2, MgO, FeO and Al_2O_3 are released and incorporated into growing amphibole. The amphibole-phlogopite interface is static but there is an exchange of cations across it, allowing K, Al, Ti, Na, Ca, and Fe from the melt to pass into the amphibole inner rim, and Mg and Si pass from the amphibole to the outer rim. Within most of the amphibole rim Al and Ti concentrations are constant and the same as those in the host amphibole, implying that their diffusion rates are particularly slow or that the exchange with Si is

slow. For Mg, Fe, K and Ca some equilibration has taken place but this is only partial. Partitioning of Ca and K between amphibole and phlogopite has led to enrichments of the former and depletions in the latter at the outer regions of the amphibole rim as seen in Figures 2.4 and 2.9. Sodium concentrations are constant within amphibole but are higher than in orthopyroxene and phlogopite. The mobilities of elements are therefore likely to have been in the order of Na > Ca, K > Mg, Fe, Si ≥ Al > Ti. It has been shown that in many metamorphic reactions diffusion of Al is slow and rate limiting (Carlson 2010).

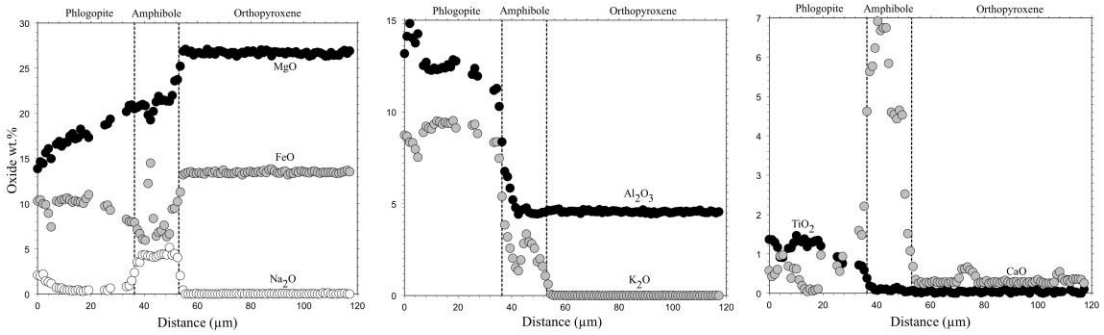

Figure 2.9. Line scan across a amphibole-phlogopite reaction rim on orthopyroxene. Location of the line scan is given as A-B line in Figure 2.3B.

Mass Balance

Mass balance calculations for the reaction rims can give an indication of the way in which elements have been exchanged between the melt and xenocrysts. This allows us to estimate how melt will fractionate during metasomatic reactions where the wall rock: melt ratio is high. Secondly the relative fluxes of elements can be calculated if the original interface between xenocryst and melt can be approximated. It should therefore be possible to draw some conclusions about the relative mobilities of different components during the reaction in which the rims were formed. The location of the original interface can be difficult to determine but in this particular case there is some indication that this was at the boundary between amphibole and phlogopite inner / outer rims. This is because compositional features of the orthopyroxene, such as ghost lamellae and Al and Ti concentrations are inherited and preserved in the amphibole inner rim but not in the phlogopite outer rim.. We assume that this boundary is static during reaction. In other words, neither amphibole nor phlogopite is consumed once formed. If the assumption is correct then the inner rim involves isovolumetric replacement of orthopyroxene by amphibole. As amphibole has a greater molar volume than orthopyroxene and porosity is present, there must be a loss of mass from the inner rim (Putnis 2002, Putnis and Putnis 2007). The location of the interface here also suggests that amphibole grows directly at the expense of orthopyroxene, whereas phlogopite grows from the melt and from the outward flux of components from the dissolving orthopyroxene. A further assumption is that the two rim zones grow simultaneously.

For this calculation, the bulk melt during reaction must be known. This can be best approximated by the bulk rock composition given by Irving and Price (1981). Although some contamination of the bulk rock analyses by xenocrysts is possible, this should not significantly affect

the major element budget of the melt although the trace element compositions could be effected. We can therefore only model the major element exchange during reaction.

A Oxide component	B mass balance amph-OPX replacement ($mmol/cm^3$ opx)	C uptake of the entire rim from the melt ($mmol/cm^3$ opx)	D molar uptake of the entire rim from the melt (sum = 100)	E molar% in the melt	F fractionation factor: uptake / mol% in melt (1 = no fractionation)
SiO_2	-105.3	126.5	25.7	65.0	0.4
TiO_2	10.2	12.8	2.6	0.3	9.0
Al_2O_3	-1.6	86.3	17.5	14.1	1.2
FeO	39.8	60.4	12.3	1.9	6.5
MnO	3.7	4.5	0.9	0.1	7.7
MgO	-181.3	0.0	0.0	2.0	0.0
CaO	25.3	26.0	5.3	1.8	3.0
Na_2O	80.1	86.1	17.5	11.4	1.5
K_2O	26.7	90.3	18.3	3.4	5.3

Table 2.4. Mass balance for amphibole + phlogopite double rim around orthopyroxene. See supplementary data for further information. Column B – average compositions for the grain are taken and converted in per formula unit values, which are then divided by the standard molar volume for either orthopyroxene or amphibole and then renormalized to 1. The values for orthopyroxene are then deducted from amphibole + magnetite (in area fractions). A minus value in Column B indicates that the component is released during reaction. Column C – takes the fluxes from Column B as well as the amount of each component required to form phlogopite to give a total uptake of the rim from the melt. Column D – re-normalized values from Column C. Column E – Molar values of each component in the bulk melt. Column F – fractionation factor calculated from Column D divided by Column E. Values of 1 indicate no fractionation, minus values indicate release of a component and positive values indicate influx of a component into the rim. The greater the departure from 1, the higher the flux. A value of 0.0 for MgO is because it is assumed to be fixed within the phlogopite rim.

The mass balance calculations, which are given in Table 2.4, are based on intermediate compositions between the extremes of mineral zonation documented from the rims. Isovolumetric replacement of orthopyroxene by amphibole releases MgO and SiO_2 (negative numbers in column B of Table 2.4). If all MgO becomes fixed in the outer rim, then the calculated molar amount of MgO released by the reaction is consistent with an outer phlogopite rim with a thickness similar to that of the inner amphibole rim. This appears to fit closely to the observed layer thicknesses, particularly for Figure 2.4 and is also appropriate considering the low MgO contents of the melt.

The results of the mass balance calculation indicate that there is a flux of all major chemical components, except MgO, towards the reaction rims. These fluxes differ greatly in size, with SiO_2, Al_2O_3, and Na_2O having very small fluxes. This modelling indicates that the reaction would enrich residual melt in Si, Al, and Na. Metasomatism of an orthopyroxene bearing rock such as the gabbro norite will result in residual interstitial melts enirched in Si, Al and Na. Such a melt could be very similar to the Na-rich glass phase found in association with SCHARM (sulphate, carbonate, H_2O, alkali-rich aluminosilicate melt), which is similar in composition to a phonolite (McInnes and

Cameron, 1994). McInnes and Cameron, (1994) document reactions between alkaline melt and olivine that form titanomagnetite, titanian phlogopite and sodian diopside. Reactions involving olivine and phonolite (alkali rich melts) are therefore likely to result in depletion and enrichment patterns similar to those calculated for orthopyroxene.

Orientation effects: amphibole – diopside double rims on orthopyroxene

Clinopyroxene rims can grow epitaxially on orthopyroxene (Tarney 1969), so that the outer rim diopside has the same crystallographic orientation as the host. An epitaxial growth process may not necessarily require the dissolution of orthopyroxene but rim growth is intiated because of low nucleation energies on the surface of the pre-existing crystal. This could explain why the diopside-orthopyroxene interfaces are more regular, partially preserving the original surface of orthopyroxene that came into contact with the melt before rim formation.

Amphibole growth is localized predominantly on orthopyroxene surfaces that are perpendicular to the augite lamellae, which are parallel to the c-axis. This is a strong indication that there is a crystallographic orientation control on amphibole rim growth. To our knowledge there are no reported examples of anisotropic dissolution rates for orthopyroxene. A simpler mechanism is perhaps more likely. If the diopside outer rims form first, a partially protective barrier will be formed between the orthopyroxene and the melt. Exchange of elements can only therefore occur through the diopside rim via grain boundaries. Along orthopyroxene surfaces parallel to the c-axis, clinopyroxene is elongated in the same direction giving a low incidence of diopside-diopside grain boundaries. At surfaces perpendicular to the c-axis a saw tooth texture (Figure 2.3D) develops, creating a higher density of rim grain boundaries. This might enhance the overall diffusion rates through the rims allowing amphibole rims to form locally.

The reasons for different outer rim assemblages, whether phlogopite or diopside dominated, do not appear to be related to the composition of the host orthopyroxene. In both types of reaction it is likely that orthopyroxene is resorbed to form amphibole and is overgrown by either phlogopite or diopside from the melt. Minor differences in the melt composition could therefore have had an influence on the outer rim mineralogy. This could also explain the variable amounts of diopside in the rims around olivine. As the melt is low in CaO, which is essential for diopside to form, perhaps small variations in this component in the melt could cause different amounts of diopside to form in the outer rims.

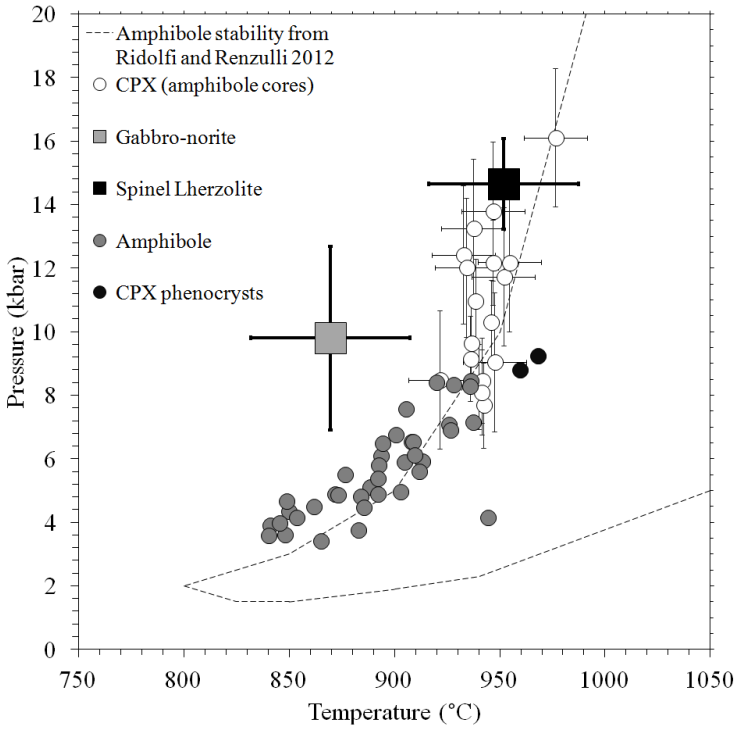

Figure 2.10. Thermometry and barometery of phenocryst amphibole and clinopyroxene as well as spinel lherzolite and gabbro-norite xenoliths.

Incorporation of xenocrysts

The occurrence of upper mantle and lower crustal xenocrysts and xenoliths in the Heldburg phonolite requires some explanation and several models are possible. The phonolite could have originated in the upper mantle and picked up spinel lherzolite and gabbro-norite xenoliths by fragmenting wall rocks it passed through as it moved towards the surface (Irving and Price, 1981). The phonolite may have formed by fractionation of a basanite in the upper mantle or lower crust and then mixed with a xenolith bearing melt at similar pressures, as was thought to be the case for phonolites in Cantal, Massif Central France (Downes, 1989). Alternatively the phonolite formed by fractionation in the crust and then mixed with a xenolith bearing melt or crustal rocks prior to or after emplacement. We summarize the data presented here and from previous studies and review these potential models for the incorporation of xenocrysts / xenoliths into the Heldburg Phonolite and its likely origin.

1. If the xenoliths resided within another type of magma before being incorporated into the phonolite, we would expect to see some evidence of this. Our observations clearly show no evidence of previous melt interactions. The reaction rims formed between olivine and orthopyroxene with phonolite melt are inconsistent with reaction rims formed in other types of magmas recorded in the literature; such as basanites (Shaw et al., 1998; Shaw, 1999; Klügel, 2001) mugearites and phonotephrites (Shaw et al., 1998) and alkali basalts (Brearly and Scarfe, 1986). In most of these studies clinopyroxene formed in the reaction rims. As clinopyroxene is a stable phase in the phonolite, it is unlikely that rims of clinopyroxene could have been destroyed during mixing. Evidence of melt infiltration and reaction into the micro-

xenoliths suggests that the phonolite played an important role in the break-up of xenolithic material.

2. There is some trace element and isotopic data for the Heldburg phonolite available in the literature. First of all the Heldburg phonolite shows no geochemical (lack of phenocrysts as well) signs of feldspar fractionation by a lack of a Eu anomaly (Irving and Price, 1981). This is usually associated with high pressures but can also be formed by high melt H_2O contents (Hay and Wendlandt, 1995). Wedepohl et al. (1994) provide some isotopic data of low $^{87}Sr/^{86}Sr$ (0.70394) and high $^{143}Nd/^{144}Nd$ (0.512839) compared to other phonolites in the Rhön region. This is generally consistent with very little crustal contamination and plots closer to mafic alkaline rocks in the Central European Volcanic Province (Jung et al., 2013). The Heldburg Phonolite is also not as enriched in trace elements compared to other phonolites and trachytes in the Rhön area (Jung et al., 2013). Additionally the lack of lithic clasts and the small number of albite, nepheline and sanidine xenocrysts further support the idea that crustal contamination was minimal. Mixing and assimilation with mafic lower crustal rock is possible and likely considering the presence of gabbro-norite xenoliths. Therefore, the phonolite most likely originated from depths of the lower crust or upper mantle.
3. Thermobarometry indicates that the phenocrysts of amphibole and clinopyroxene predominantly formed at lower crust and upper mantle conditions.
4. Mixing models with a more mafic melt that contained xenoliths also seem unlikely. Xenolithic material constitutes around 1-3% of the phonolite, which would require any mixing melt to be unrealistically xenolithic rich in order to preserve a phonolite bulk composition. Although the presence of partially reacted Ti rich clinopyroxene in amphibole cores, olivine group II and some reverse zoning in amphibole phenocrysts suggest that some mixing might have happened at the crust mantle boundary, but the xenoliths may not necessarily have been introduced by the same mixing event. This would still imply a very deep origin of the phonolite. Mixing at shallow pressures seems less likely as a small volume of phonolite residing at low pressure would cool significantly, meaning that any mixing of mafic magma would chill upon contact rather than mix.

From the data presented here it seems likely that the phonolite originated depths corresponding to the crust-mantle boundary. The xenocrysts and micro-xenoliths could have been incorporated during a mixing event at these depths but it seems more likely that they were sampled directly from mantle and lower crust wall rocks. In either case the crucial point is that the reaction rims provide small-scale analogues of a potential metasomatic interaction between a highly evolved, alkali enriched melt and mafic upper mantle –lower crustal wall rocks. If phonolites or other similar melts can exist at such high pressures then olivine and orthopyroxene incorporated into them will be replaced by a metasomatic assemblage amphibole, phlogopite and diopside with minor magnetite. Glasses in a number of mantle xenoliths have a wide variety of compositions, with many examples having phonolite compositions (McInnes and Cameron, 1994, Draper and Green, 1997, Coltorti et al., 1999,

Coltorti et al., 2000). Many of these authors attribute these glasses to be the remnants of a metasomatic agent in the mantle.

2.8 CONCLUSIONS

The Heldburg Phonolite contains a phenocryst assemblage of amphibole, clinopyroxene and phlogopite indicating high temperature and bulk water contents and relatively high pressures; physical and compositional conditions that are likely to inhibit feldspar crystallization. The phonolite also contains a wide variety of xenolithic material of two predominant varieties; an upper mantle spinel lherzolite and a lower crust gabbro-norite rich in orthopyroxene. All xenolithic material has reacted with the host magma represented by the phonolite to form zoned coronae or reaction rims. The most common reaction rims are: (a) phlogopite inner and diopside outer rims around surrounding olivine; and (b) either phlogopite or diopside outer rims on amphibole inner rims surrounding orthopyroxene. The reactions are the result of disequilibrium between the original xenocrysts and the phonolite melt. Preservation of chemical inhomogeneities in the rims suggests that diffusive re-equilibration was slow and probably rate limiting, however, the rates of rim growth were still sufficiently fast to out pace internal diffusion of major elements in olivine and orthopyroxene. Residence times of xenocrysts in the phonolite must therefore have been short and in the order of months to a year.

The reaction rims could not have been produced by interaction of the xenocrysts with a melt other than one with a composition similar to that of the host phonolite and they must have been incorporated in the upper mantle or lower crust. The implication is that the host phonolite evolved at depths much greater than is normal for most other phonolites. The reaction rims formed over a range of pressures and a relatively short time as the host phonolite moved towards the surface. The spinel lherzolite fragments are samples of the upper mantle. The reaction rims are small-scale analogues showing how a phonolite melt could metasomatise the upper mantle.

Chapter 3

Experimental reactions between olivine and orthopyroxene with phonolite melt: implications for the origins of hydrous diopside + amphibole + phlogopite bearing metasomatic veins.

Submitted as;

Grant, T.B, Milke, R., Wunder, B. Experimental reactions between olivine and orthopyroxene with phonolite melt: implications for the origins of hydrous diopside + amphibole + phlogopite bearing metasomatic veins. Submitted to Contributions to Mineralogy and Petrology.

3.1 ABSTRACT

Experimental reactions between single crystals of olivine and orthopyroxene with phonolite melt were conducted at upper mantle conditions of 1.0-1.5 GPa, 900-1000ºC. Melt water content were varied between anhydrous to >12 wt. H_2O. Olivine reacts to form phlogopite reaction rims with a halo of diopside <1000ºC or rims of secondary olivine >1000ºC. Orthopyroxene reacts to form amphibole with epitaxial diopside overgrowths <1000ºC. No reaction rims form when the bulk melt H_2O is lower than ~3.8 wt.% and are unlikely to form below 900ºC. Pressure has little effect over the small range tested. These experiments recreate reaction rims on olivine and orthopyroxene observed in the Heldburg Phonolite, Central Germany and suggest that a relatively narrow range of temperatures and melt water contents are required for rim formation, consistent with previous estimates. The reaction of phonolite with upper mantle peridotite will form hydrous metasomatic vein assemblages of diopside + amphibole + phlogopite. Such vein assemblages are common in metasomatised peridotites but the major element compositions of the metasomatic agents are often poorly constrained. There is sufficient evidence from melt / glass inclusions, partial melting experiments and fractional crystallization of basanites to suggest that phonolite melts can form in the upper mantle and therefore form hydrous metasomatic veins. Subsequent melting events involving hydrous vein assemblages may have significant implications for the generation of alkali rich continental lavas.

3.2 INTRODUCTION

There are a handful of observations of spinel lherzolite bearing phonolites and trachytes (Wright, 1966; Wright, 1969; Price and Green, 1972; Irving and Price, 1981; Dautria et al., 1983; Huckenholz and Werner, 1990; Grant et al., 2013). It is thought that these originate from relatively high pressures compared to most phonolites and trachytes due to the presence of the mafic xenoliths and a complete lack of feldspar fractionation. Recent data by Grant et al. (2013) show that the Heldburg Phonolite, Central Germany most likely originated from at least lower crustal depths of around 0.9 GPa. This is on the basis of phenocryst thermo-barometery and reaction rim mineralogy formed on the mafic xenocrysts and xenoliths. The lack of crustal contamination and more primitive trace element signatures ($^{87}Sr/^{86}Sr$ = 0.70394; $^{143}Nd/^{144}Nd$ = 0.512839) from Wedepohl et al. (1994) further support this. There are signs of a potential mixing event at lower crust – upper mantle depths that brought the xenolith material into the phonolite, consistent with the model suggested by Downes (1989) for phonolites from Cantal, Massif Central France. The mixing relationships are however still difficult to reconcile for the Heldburg Phonolite (Grant et al., 2013) and sampling of the mantle by the phonolite is likely. Most importantly, the xenolithic material has reacted with the phonolite host melt, forming rims of phlogopite + diopside around olivine, and either amphibole + diopside or amphibole + phlogopite around orthopyroxene (Grant et al., 2013). Regardless of the incorporation mechanism, these reaction rims provide potentially insightful analogues for how a phonolite or an evolved alkalic melt could metasomatise the upper mantle. The modal mineralogy of the reaction rims is also similar to hydrous metasomatic veins that mainly consist of amphibole + phlogopite + diopside within xenoliths (Dawson and Smith, 1988; Wulff-Pederesen et al., 1999; McInnes et al., 2001; Shaw et al., 2005; Szabó et al., 2009) and peridotites (Bodinier et al., 1990; Zanetti et al., 1999). The compositions of the melts that

form these veins are generally poorly constrained, but they must be relatively enriched in alkalis, H_2O and trace elements (Witt-Eickschen et al., 1998; Szabó et al., 2009; Pilet et al., 2010).

This paper presents results of simple experiments designed to recreate the reaction rim mineralogy observed in the Heldburg Phonolite by placing olivine and orthopyroxene single crystals in contact with phonolite melt. The primary aim is to see if these reaction rims can be formed at upper mantle pressures of 1.0-1.5 GPa and how rim formation is affected by both temperature and the H_2O content of the melt. The results are then discussed in the context of alkali metasomatism in the upper mantle and the formation of hydrous metasomatic veins. Several models of phonolite melt formation at these conditions are evaluated along with the potential for phonolite melts to produce the modal, cryptic and trace element signatures required for models of intraplate alkali melt generation by melting of hydrous veins (Pilet et al., 2011).

The Heldurg Phonolite, Central Germany

It is necessary to review some of the main features of the Heldburg Phonolite documented in the literature (Irving and Price, 1981; Huckenholz and Werner, 1990; Grant et al., 2013). The Heldburg Phonolite is a phonolite plug dated at 13.3-11 Ma and is located in the Heldburg region, Central Germany. It is part of the regional alkaline volcanism across central Europe during the Miocene and Pliocene, collectively known as the Central European Volcanic Province (CEVP).

The Heldburg Phonolite contains phenocrysts of amphibole, clinopyroxene and phlogopite and is lacking any evidence of feldspar fractionation. This implies that the conditions under which the phonolite fractionated must have suppressed feldspar fractionation. Irving and Price (1981) suggested that this could be a sign of high pressure fractionation, however it is also possible to suppress feldspar at lower pressures if the temperatures and melt water contents are high enough; >900ºC and >3-4 wt.% H_2O (Hay and Wendlandt, 1995). High water contents, and high aH_2O, are likely considering the large number of amphibole and phlogopite phenocrysts. Pressure and temperature estimates for amphibole and clinopyroxene phenocrysts range from 0.9-0.4 GPa and 850-950ºC (Grant et al., 2013).

The Heldburg Phonolite also contains significant amounts of xenolithic material broken up into single xenocrysts and polymineralic micro-xenoliths. These originate from two cumulate sources: spinel lherzolite consisting of olivine + orthopyroxene + clinopyroxene + spinel, and a gabbro-norite assemblage of orthopyroxene + clinopyroxene + plagioclase + magnetite. Olivine reacts to form inner rims of phlogopite + magnetite and outer rims of diopside. Orthopyroxene forms inner rims of amphibole + magnetite with outer rims of diopside or phlogopite. Inner rims are formed by partial replacement of olivine or orthopyroxene, and the outer rims appear to be a halo (Or “overgrowth” but not a direct reaction rim) formed by the melt. The rates of reaction rim growth are likely to be limited by diffusion through growing rims and the estimated residence times are in the order of several months to a year (Grant et al., 2013; Grant et al. - Chapter 4.).

3.3 ANALYTICAL METHODS

Electron probe microanalysis (EMPA)

EMP analysis and BSE images were collected using the JEOL JXA-8200 at the Freie Universität Berlin. For all data points accelerating voltages of 15 kv and beam currents of 20 nA were used. Glass measurements were taken using a defocused beam of 12-15 µm to minimize loss of alkalis, whereas a focused beam of <1 µm was used for the analysis of mineral phases. Natural standards were used for all elements with counting times of 10s on peak and background for all elements except Na, which had 5s on peak and background.

3.4 EXPERIMENTAL METHODS

Starting Materials

An anhydrous, Fe and Ti-free synthetic phonolite glass was synthesized based on the proportions of phonolite from Whittington et al. (2001). The different oxides and carbonates were weighed accurately to within around 50µg and the excess weight for carbonates was accounted for. The mixture was then ground in acetone in an agate pestle and mortar, dried, then placed in a platinum crucible to be de-carbonated at 800-1200°C for 20 hrs, then melted at 1600°C for a further 24 hrs. Following this, the glass was quenched in de-ionized water and then crushed. The powder was placed back into the furnace in the same Pt crucible at 1600°C for a further 48 hrs. Once this was completed the final anhydrous melt was quenched and removed from the platinum crucible to be stored. A small sample of the glass product was crushed and looked at under a petrographic microscope to see if any microcrystals had formed during the quench. None were observed. Several large fragments of glass were then prepared in a grain mount and analysed by electron microprobe to determine the starting composition. The results of this are given in Table 3.1.

	Heldburg	**PHG2 glass**	**San Carlos olivine**	**Enstatite**	**Kilosa**
SiO_2	56.04	60.5	41.31	59.71	58.42
TiO_2	0.33	-	-	-	0.05
Cr2O3	-	-	0.03	-	-
Al_2O_3	20.61	19.41	0.04	-	0.17
FeOtot	2.03	-	8.71	-	5.78
NiO	-	-	-	-	-
MgO	1.16	1.96	49.81	39.23	35.45
CaO	1.42	2.51	0.12	-	0.24
Na_2O	10.17	8.43	-	-	0.06
K_2O	4.64	7.13	-	-	0.05
Total	96.40	99.94	100.16	99.02	100.25

Table 3.1. Starting material compositions. Heldburg bulk rock data from Irving and Price (1981). For glass PHG2 see also Grant et al. (submitted: see Chapter 4).

Xenocryst analogues included; a synthetic end-member forsterite crystal, San Carlos olivine, enstatite crystals synthesised at Freie Universität Berlin, and a single natural enstatite crystal from Kilosa, Tanzania. These were initially crushed dry in a metal pestle and mortar and then were separated into size groupings of <250µm, 250-500 µm and >500 µm. The median size interval was used. Analyses of pre-experiment xenocrysts are given in Table 3.1.

Run name	Duration (hr)	Pressure (Kbar)	Temperature (°C)	Bulk H_2O	Rim (+ halo) Mineralogy	Matrix mineralogy
En40	5	10.7	900	5.0	Di	Di + Fsp
En41	5	14.7	900	9.7	Di + Amph	Di + Phlog
En43	5	10.7	950	4.8	Di + Amph	Di
En46	48	10.7	950	5.7	Amph + Di	Di
Ki39	5	10.7	900	12.4	Amph + Di	Di + Phlog
Ki42	5	14.7	900	6.5	Di + Amph	Di
Ki44	5	10.7	950	6.6	Di + Amph	Di
Ki47	168	10.7	950	6.5	Amph + Di	Di + Phlog
Ki49	#	10.7	1000	5.1	Di	Di
Fo1*	5	10	900	0.0	-	Fsp
Fo4*	5	10	900	3.3	-	Fsp + Di
Fo5*	20	10	900	6.2	Phlog + Di	Di
Fo9*	2	14	900	4.7	Phlog + Di	Fsp + Di
Fo10	2	14.7	900	4.2	-	Fsp + Di
Fo25	3	14.7	950	9.1	Phlog + Di	Di
Fo30	3	10.7	950	7.7	Phlog + Di	Di
Fo32	3.75	14.7	1000	4.7	Phlog + Di	Di
SC22	3	14.7	950	8.1	Phlog + Di	Di
SC28	3	10.7	950	8.6	Phlog + Di	Di
SC31	3.75	14.7	1000	4.2	Phlog + Di	Di
SC31	3.75	14.7	1000	4.2	Ol ± Di	± Di
SC33	24	10.7	950	3.8	Phlog + Di	Di
SC48	#	10.7	1000	2.2	-	Fsp + Di

Table 3.2. Run conditions. Run names indicate the xenocryst used where En = synthetic enstatite, Ki = Kilosa orthopyroxene, Fo = synthetic forsterite and SC = San Carlos olivine. Bulk H_2O calculated as H_2O added / glass + xenocryst mixture. Due to some potential variation in glass : xenocryst ratios this may vary by up to 5%. Mineral abbreviations; Di = diopside, Fsp = alkali feldspar, amph = amphibole, phlog = phlogopite, ol = olivine. # denotes an experiment where the run duration is unknown due to failure overnight, and * indicates an experiment that may have experienced some water loss at peak run conditions, in these cases the bulk H_2O values refers to the added amounts but not the actual amounts during the experiments.

Mixtures of phonolite glass and xenocrysts were made for each type of olivine and orthopyroxene. The mixtures always had a ratio of 84 wt.% glass to 16 wt.% xenocrysts to replicate the high melt to xenocryst ratio seen at Heldburg. This also simplifies the experiments as the distances between

different xenocrysts should be large and the melt should be abundant enough for large-scale differentiation to be limited. Platinum capsules were used in all experiments with a length of 6-8 mm, width of 3 mm and wall thickness of 0.3 mm. Double distilled water was added to the capsule via micro-syringe and then the sample mixture was added.

Piston Cylinder apparatus

All experimental run conditions are detailed in Table 3.2. An initial set of experiments was conducted in an end loaded piston cylinder (Boyd and England, 1960) press using graphite ovens, crushable alumina pressure medium and Pt/Pt-Rh thermocouples (for further details see Gardés et al., 2011). Capsules dimensions were 4 mm high, 3 mm wide and 0.25 mm thick. In this set of experiments the capsules were cold sealed. Unfortunately some water loss was observed in these experiments. Experiments that used this method are noted with a * in Table 3.2.

To minimise loss of water in the rest of the experiments a second method was used. These experiments were conducted using a non-endloaded Johannes type piston cylinder press, as described by Johannes et al. (1971) and Johannes (1973). Platinum capsules were used in all experiments with a length of 6-8 mm, width of 3 mm and wall thickness of 0.3 mm. Double distilled water was added to the capsule via micro-syringe and then the sample mixture was added. Platinum capsules were welded using a PUK3 arc welder and were then put in a 100°C oven for several hours and then weighed to check the quality of the seal. If they passed this test they were then used in the experiments. The second method used CaF_2 pressure medium, graphite ovens and a Ni/Ni-Cr thermocouple. Pressure was calibrated using the quartz + corundum – kyanite transition (Harlov and Milke, 2002). All capsules were then cleaned and weighed after the experiment to check for any water loss. No capsules experienced any weight loss using the second method.

3.5 RESULTS

Liquidus phases

All experiments included phases grown directly from the melt. These included; diopside, phlogopite and alkali feldspar. They rarely exhibit signs of rapid growth i.e. only a small minority have skeletal growth habits or contain melt pools. Their abundances consistently vary depending on the peak P-T-H_2O conditions. With quench rates being greater than 20ºC/s it is unlikely that these phases formed during quenching and are most likely to be the stable phases at peak conditions. Table 3.2 contains information regarding all run conditions and phenocryst phases present.

Feldspar formed as small, <30 µm tabular crystals within the melt. As water contents and temperatures increase, diopside becomes stable within the melt, forming small <20 µm crystals along with feldspar. Above 5 wt.% H_2O at 900°C and 2.2 wt.% at 1000°C feldspar becomes unstable and only diopside forms in the melt. Phlogopite forms in some experiments with only orthopyroxene present and never when olivine is present. In one sample (SC32) at 1000°C, diopside became nearly absent and the glass was free of crystals at one end of the capsule.

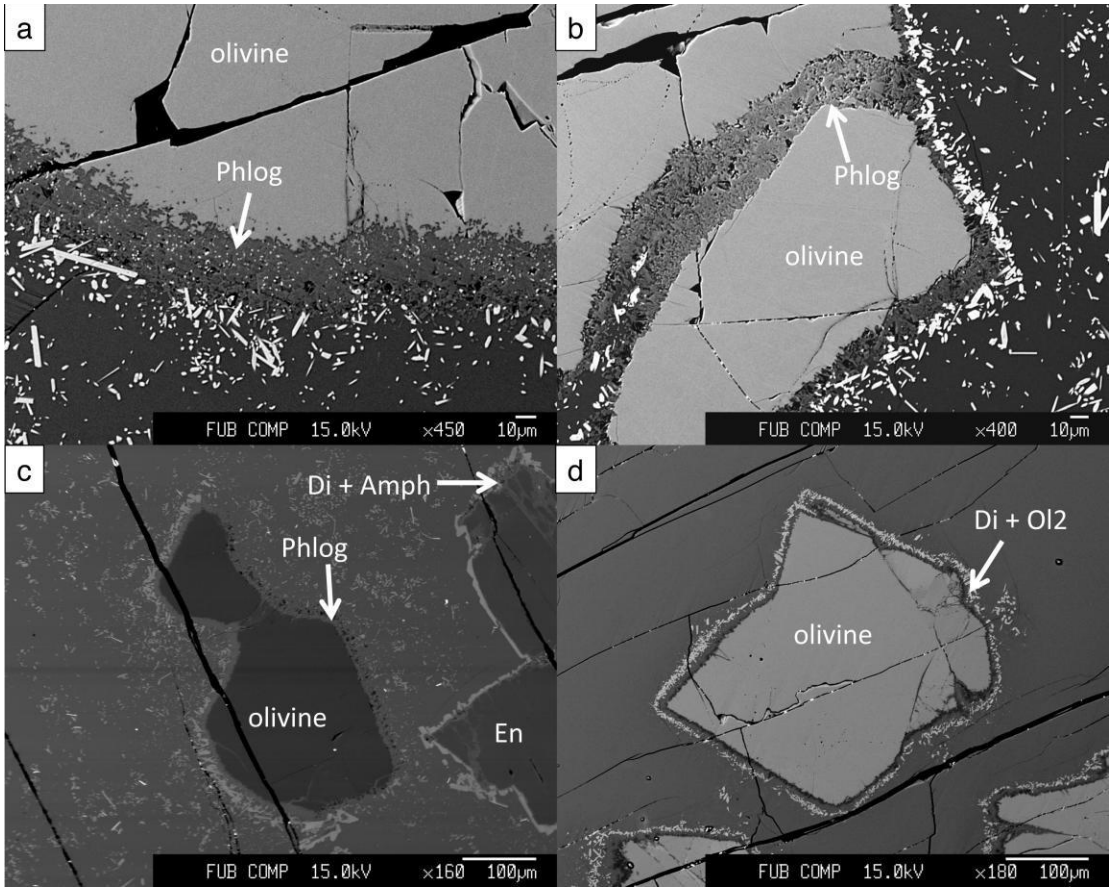

Figure 3.1. BSE images of reactions between olivine and melt. Mineral abbreviations are; Di = diopside, phlog = phlogopite, amph = amphibole, En = synthetic enstatite, Ol2 = secondary rim olivine. **A** – sample SC33 with a thick rim of phlogopite with an inconsistent diopside halo. Small pores and small diopside crystals are visible in the phlogopite reaction that has a highly convoluted interface with olivine. The polished section cuts this interface at an angle leading to pockets of phlogopite within the olivine at a distance away from the observable interface. **B** – also sample SC33. The halo of diopside is thicker and more consistent at this location. Note the lack of diopside within a thick vein going through the host olivine and the higher Fe content (brighter contrast) of the phlogopite rim further away from the melt. **C** – sample En46 contains both a forsterite and an enstatite crystal due to the starting material containing both phases. **D** – image from sample SC31 showing a rim of secondary Mg-rich olivine with a thin diopside halo and the near complete absence of liquidus phases.

Liquidus phases are unevenly distributed in the melt of the samples. They often grow in large (100-200 µm) crystal clots, surrounded by crystal free or poor regions (Figure 3.1c and Figure 3.2a). In some cases they form a ring of crystals that are orientated towards the center of the clot (Figure 3.2a). No free fluid bubbles formed within the melt in any of the experiments despite the high bulk H_2O in some samples. This means that the melt did not become fluid saturated, and is in agreement with studies of that show high water solubility in phonolites even at low pressures (Schmidt and Behrens, 2008; Carroll and Blank, 1997).

The stability of different liquidus phases can be compared to the only two studies where the high-pressure phase relations of phonolite have been reported; melt composition DG-1 from Draper and Green (1997) and Hay and Wendlandt (1995). Feldspar can form at both pressures tested as long as the temperatures are low and bulk H_2O is low. Results for the stability of feldspar are consistent with

those in Hay and Wendlandt (1995), where the water contents required to suppress feldspar reduce slightly with increasing temperature from around 5wt.% H_2O at 900°C to near dry conditions at 1000-1100°C. Diopside can form up to temperatures of around 1000°C. This was also observed in Draper and Green (1997) but is up to 50°C higher than in Hay and Wendlandt (1995). This could be due to differences in the compositions of starting glasses such as SiO_2 that is around 6 wt.% higher in both this study and in Draper and Green (1997).

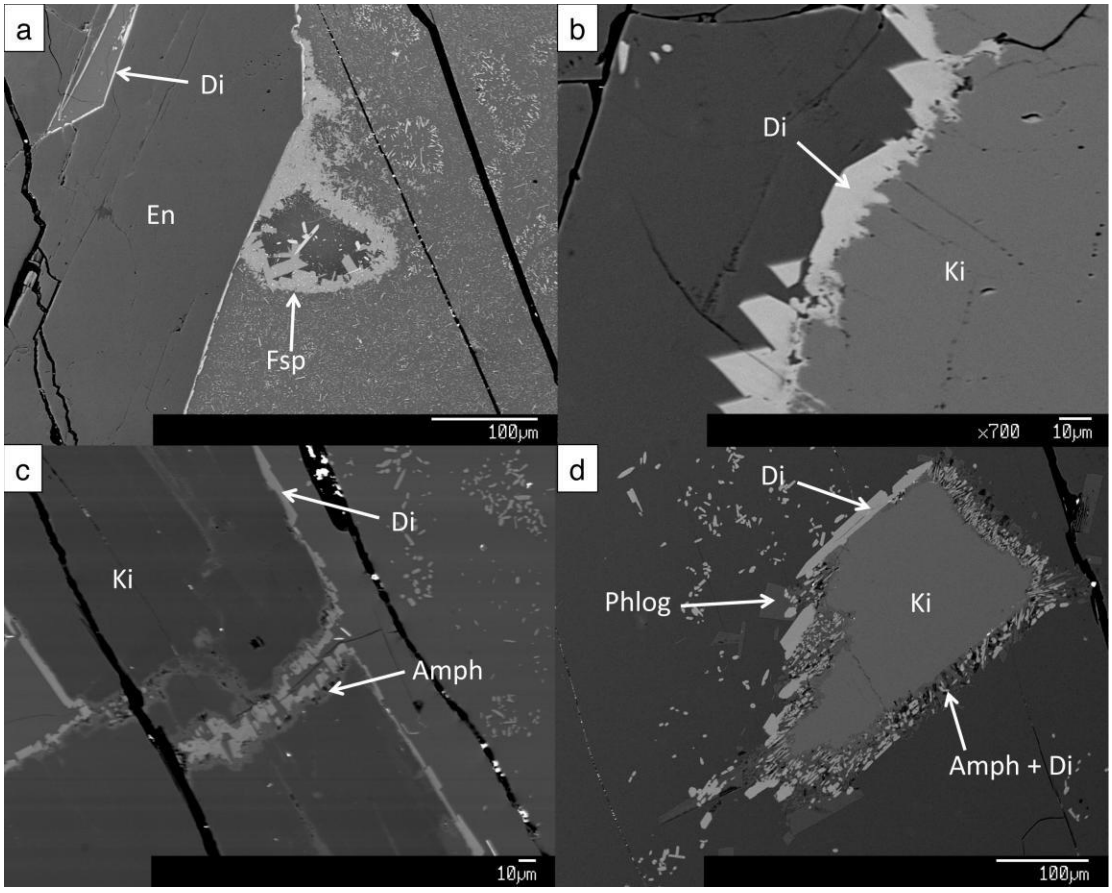

Figure 3.2. BSE images of reaction between orthopyroxene and melt. Mineral abbreviations are the same as in Figure 1 with Ki = Kilosa orthopyroxene. **A** – sample En40 shows a thin rim of diopside forming around enstatite, with no amphibole formation. Crystal clots of either alkali feldspar + diopside or just diopside are visible in the glass. **B** – sample Ki44. **C** – sample En46. **D** – Ki 47.

Reaction rim assemblages

The reaction rim assemblages formed in each experiment are shown in Table 3.2 and in Figure 3.1 and 3.2. There were no differences in reaction rim formation over the pressure range tested and there were no differences between natural and synthetic xenocrysts of olivine or orthopyroxene. Rim formation was strongly influenced by the bulk water content of the sample and the temperature.

Olivine

At low temperatures (900°C) and low bulk H_2O (<4 wt.%), olivine does not react with phonolite melt. Sharp crystal edges are present and there is little indication of dissolution. As temperatures and H_2O contents are increased olivine begins to react with the phonolite close to the point at which feldspar disappears as a liquidus phase. The rim assemblage is most commonly a phlogopite inner rim surrounded by diopside outer rims. These textures are extremely similar to those of the natural examples (Grant et al., 2013). BSE images of reaction rims are shown in Figure 3.1. Phlogopite grain sizes in the rims are typically <10 µm but are often much smaller. Diopside in the outer rims are larger (>10-20 µm) and are comparable to diopside formed in the matrix. Grain sizes do not vary significantly across reaction rims. Phlogopite is only present in the inner rims, with some small diopside grains also forming in the inner rims. Outer rims only contain diopside + interstitial glass. Outer rims are inconsistent, sometimes nearly absent and diopside is an abundant liquidus phase. Texturally, the diopside appears to be preferentially nucleating in a halo around phlogopite rims rather than being part of an outer rim. Olivine – phlogopite interfaces are always convoluted and highly irregular at the micron to submicron scale. This is a common feature observed in mineral replacement reactions (for example, Coombs and Gardner, 2004; Putnis, 2009). All phlogopite inner rims contain black patches (<10%). Some of the black patches could originate from plucking during polishing but the majority appears to be a primary texture, and is therefore likely to be fluid filled pores. In most rims these are rounded to oblong in shape and are <2 µm in size (Figure 3.1 a-c). In some reaction rims these appear to be elongated and channel-like with orientations perpendicular to the olivine interface and are similar to the fluid channel textures observed during serpentinization (Boudier et al., 2010), although this is not a particularly common feature. Pores can also be concentrated near to the olivine interface (Figure 3.1b). Large cracks are present in the olivines. These are filled with phlogopite and diopside "veins" with thicknesses that range from 1-40 µm. The modal percentage of diopside in the veins decreases with vein width.

In sample experiments (SC22) at 1000˚C, some olivines reacted to form thin rims (~6 µm) of secondary olivine surrounded by melt and then a thin halo of diopside (Figure 3.1d). The olivine is typically <5 µm in size. This is consistent with the phase relations of Draper and Green (1997), where olivine becomes a stable liquidus phase at 1000˚C instead of clinopyroxene and phlogopite. Olivine-phlogopite interface are irregular and convoluted.

Orthopyroxene

Orthopyroxene reacts to form several types of reaction rims (Table 3.2), including single diopside rims, double rims of amphibole + diopside and rims of amphibole + diopside + phlogopite. Single diopside rims formed when the bulk water contents were low (<4 wt.%) at temperatures of 900-950ºC, and at high temperatures (1000ºC). The interface between orthopyroxene and diopside is typically regular and straight, with few embayments and lobate intrusions into the host orthopyroxene at 1000ºC (Figure 3.2b). Texturally these are similar to the natural examples (Grant et al., 2013) and to epitaxial rim growth of diopside on orthopyroxene (Tarney, 1969). Diopside rim grains are elongated at interfaces parallel to the long direction in host orthopyroxenes but display a saw-toothed texture at interfaces

perpendicular to the long direction. This was also noted in the natural reaction rims at Heldburg, where the saw toothed rim textures were always present at (001) orthopyroxene surfaces.

At contents of H_2O in the melt, localized inner rim growth of amphibole forms at the orthopyroxene – diopside interface (Figure 3.2d) and is most commonly associated with saw-toothed diopside. The amphibole is fine grained (<1 µm) and contains pore spaces (1-3 µm). Orthopyroxene – amphibole interfaces are always highly irregular and convoluted. In some cases amphibole inner rims protrude as small veins (diopside absent) for several 10s of µm into the host orthopyroxene. The amphibole – diopside interface is often regular, possibly marking the original orthopyroxene – diopside (or melt) interface. At very high water contents and in experiments with longer run durations, some phlogopite forms locally at the outer rims, as well as being present as a liquidus phase.

Spinel

Some San Carlos olivine contained small chrome spinel inclusions. In one sample (SC22), a spinel inclusion was exposed to the melt and formed a reaction rim of phlogopite and locally associated Cr-rich clinopyroxene. We do not go into detail on this type of reaction rim as there is only one example but the identification of this rim type fits well with the natural observations of phlogopite rims around Cr-spinel (Grant et al., 2013).

Chemistry

Olivine and orthopyroxene

Natural olivine and orthopyroxene single crystals show no internal compositional variation after reaction. There is no evidence of Mg-Fe interdiffusion at the rim of reacting xenocrysts, and is consistent with the natural examples (Grant et al, 2013). This means that the rates of rim growth exceed that of Mg-Fe interdiffusion in olivine and orthopyroxene.

Glass

Glass analyses all have low totals. It is not thought that this is due to Na_2O volatilization by the microprobe. Anhydrous starting material glass samples and hydrous experimental glass were analysed with varying beam widths and showed minimal alkali loss above 10-12 µm. Low totals simply reflect high volatile (water) contents. All glass analyses were renormalized to 100 and then averaged (Table 3.3.). Bulk water contents may also increase during the experiment as the matrix crystallization is dominated by nominally anhydrous phases of feldspar or diopside. Glass analyses are relatively consistent in composition within a given sample and little spatial variation is observed. There are no clear indications of melt boundary layers formed by slow diffusion in the melt. Measuring this was problematic due to large amounts of phenocrysts within the matrix and no reliable data for this was collected. It was also not possible to analyse glasses at all in some samples because the density of phenocryst phases was too high and glass spaces too small to be analysed by wide beam widths.

Sample	P/T/H_2O	Phase	SiO_2	Al_2O_3	FeO	MgO	CaO	Na_2O	K_2O	Total
En41	14.7/900/9.7	Di (10)	55.83	1.68	-	18.64	22.25	0.94	0.13	99.47
		Phlog (1)	45.89	13.40	-	27.72	0.10	0.14	7.47	94.72
		Amph (2)	55.87	1.98	-	25.76	5.35	4.20	3.44	96.60
En46	10.7/950/5.7	Di (19)	55.55	1.75	-	18.39	22.35	0.98	0.18	99.21
		Glass (3)	64.65	18.84	-	1.08	0.46	7.71	7.24	100.00
		Amph (5)	55.95	1.79	-	25.34	7.31	4.32	2.42	97.13
		Phlog (1)	42.65	12.77	-	30.17	b.d.l.	0.29	10.00	95.88
Ki39	10.7/900/12.4	Di (12)	55.96	1.32	0.17	18.05	23.88	0.71	0.14	100.23
		Glass (4)	64.43	18.86	b.d.l.	0.66	0.61	8.31	7.04	100.00
		Amph (10)	54.06	3.08	1.31	26.26	5.39	2.91	3.40	96.40
		Phlog (4)	42.82	12.85	0.22	27.73	0.02	0.43	9.92	93.99
Ki42	14.7/900/6.5	Di (2)	55.55	3.80	b.d.l.	16.78	20.86	1.87	0.14	99.01
		Glass (4)	62.54	20.09	b.d.l.	0.79	0.54	8.14	7.80	100.00
		Amph (1)	50.32	7.71	0.91	25.91	2.71	2.53	6.06	96.16
Fo30	10.7/950/7.7	Di (6)	56.18	2.66	-	17.24	22.55	1.11	0.33	100.06
		Phlog (7)	43.02	12.83	-	27.80	0.11	0.49	9.33	93.57
		Glass (10)	62.27	20.16	-	1.07	0.76	8.49	7.22	100.00
Fo32	14.7/1000/4.7	Di (7)	56.66	5.01	-	16.31	19.24	2.39	0.37	99.98
		Phlog (4)	44.76	12.73	-	26.91	0.13	0.66	9.44	94.62
		Glass (16)	61.89	18.55	-	2.50	1.90	8.22	6.89	100.00
SC22	14.7/950/8.1	Di (6)	57.23	4.76	0.39	14.99	20.55	1.92	0.38	100.22
		Phlog (2)	43.75	12.59	0.70	26.48	0.09	0.44	9.34	93.39
		Glass (8)	62.81	20.21	b.d.l.	0.92	0.60	8.35	7.00	100.00
SC31	14.7/1000/4.2	Di (5)	57.45	5.40	0.47	15.79	18.25	2.45	0.34	100.16
		Phlog (3)	47.35	13.42	0.46	26.41	0.13	1.14	8.34	97.25
		Glass (14)	62.01	19.19	b.d.l.	2.08	1.53	8.36	6.78	100.00
SC33	10.7/950/3.8	Di (13)	56.24	2.19	0.31	17.71	22.46	1.05	0.14	100.09
		Phlog (5)	44.21	11.54	0.82	29.23	0.42	0.70	8.55	95.46
		Glass (13)	62.10	20.24	b.d.l.	1.30	0.58	8.45	7.26	100.00

Table 3.3. Selected averages (in wt.%) of EPMA data for selected samples. Numbers in brackets in the phase column indicate number of analyses used for the averages. B.d.l. indicates an element that was below the detection limit within the error of the data and a hyphen indicates an element that was not measured. Glass data is renormalized to 100.00.

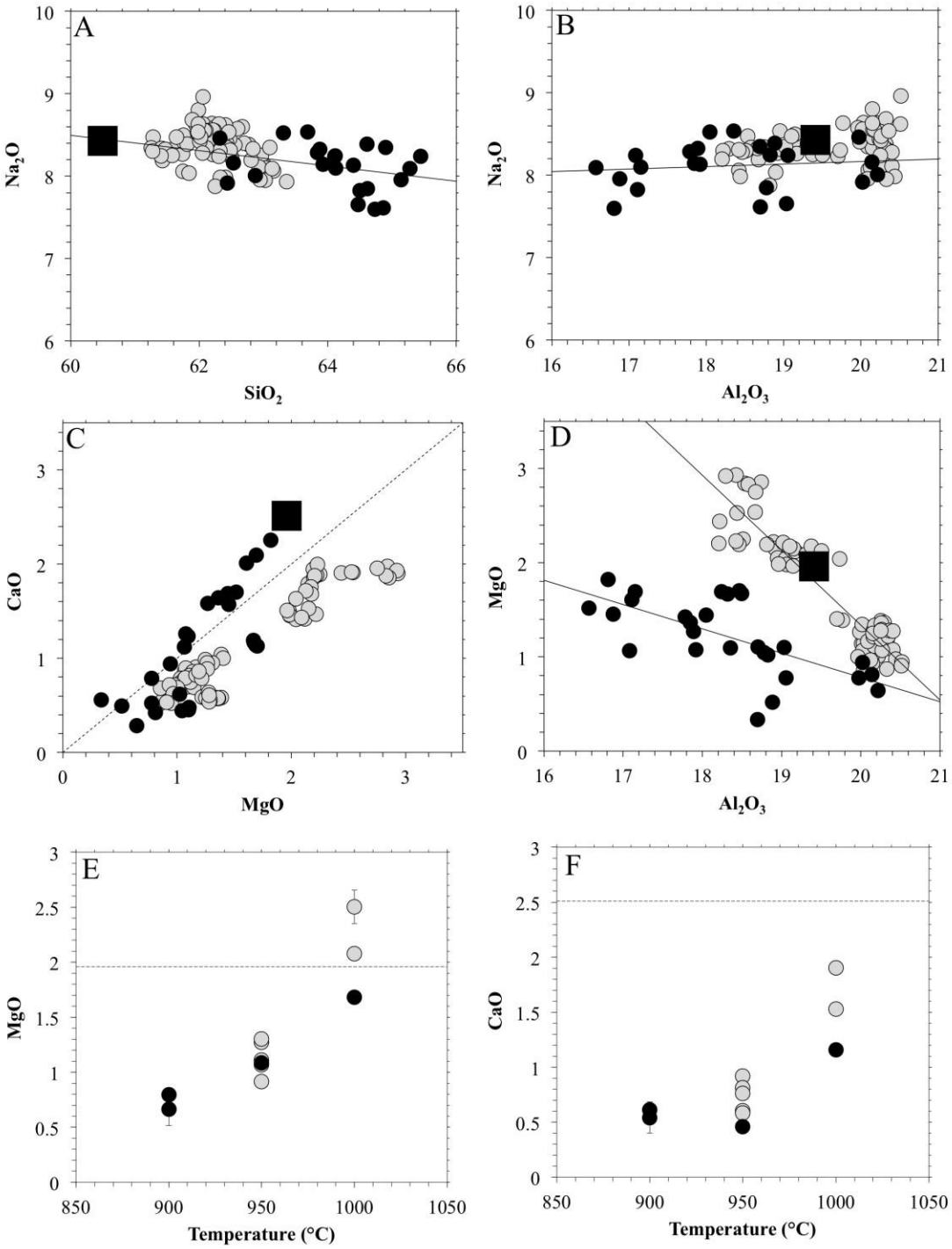

Figure 3.3. Variations in glass compositions. All glass data has been renormalized to 100.00. Black square = original glass composition, black circles = olivine reaction experiments, grey circles = orthopyroxene reaction experiments. Trend line in C is a 1:1 ratio between MgO and CaO. Dashed lines in E and F are indicate the original MgO and CaO content of the starting material glass PHG2.All chemical values in wt.%.

Glass compositions do not change dramatically during the experiments but some consistent trends are shown in Figure 3.3. The concentrations of K_2O and Na_2O stay fairly constant. Most experiments show some increase in SiO_2 (+ 1-3 wt.%) and a small increase or decrease in Al_2O_3 (± 2 wt.%) relative to the starting glass. Across all experiments there is a consistent trend of decreasing

MgO and CaO with temperature down to ~0.4 wt.% at 900°C due to diopside crystallization. The experiments at 1000°C show a small increase in MgO but still decrease slightly in CaO due to an increase in the dissolution of xenocrysts relative to diopside crystallization.

Phlogopite

The concentrations of MgO, CaO and Al_2O_3 at 950°C and 1000°C are generally consistent and rim phlogopite varies little between samples (the error bars are small). At 900°C the MgO and CaO concentrations increase and the Al_2O_3 decreases. The variation in phlogopite compositions at this temperature also vary much more, giving larger error bars. This is particularly noticeable for CaO. The high variability of rim phlogopite at 900°C does not correlate with the bulk water content of the melt, the Fe content of the host olivine or the run duration. The CaO contents of rim phlogopite at high temperatures, 950-1000°C, are more consistent with the CaO concentrations of phlogopites that occur as phenocrysts in enstatite bearing experiments. Even at temperatures of 900°C the phenocryst phlogopite are typically low in CaO (average of all experiments at 900°C is 0.06 wt.%). These are assumed to be in equilibrium with the surrounding melt and would give a $kD_{Ca}^{phlog/melt}$ of around 0.1. This is consistent with experimental results from Hay and Wendlandt (1995), who produced phlogopites with low CaO of 0.06 wt.% at similarly high pressures and are also consistent with other experiments on phonolites at lower P-T conditions (Berndt et al., 2001; Andújar and Scaillet, 2012).

Amphibole

Amphiboles in reactions are anthophyllite to gedrite in composition (Leake et al., 1997). They vary across the reaction rim being more Si rich at the orthopyroxene interface and becoming more Al and K rich towards the diopside outer rim interface. The exchange of Si for Al (charged balanced by K) over the amphibole rim occurs on a near 1:1 ratio indicating direct substitution and is the same for all measured amphiboles. Compositional variations for rim amphibole are best observed in line scans, see Figure 3.4 for an example. Due to amphibole rims generally being very thin (<5µm) line scans were not feasible except for in Ki39, which contained the most water (12.4 wt.%).

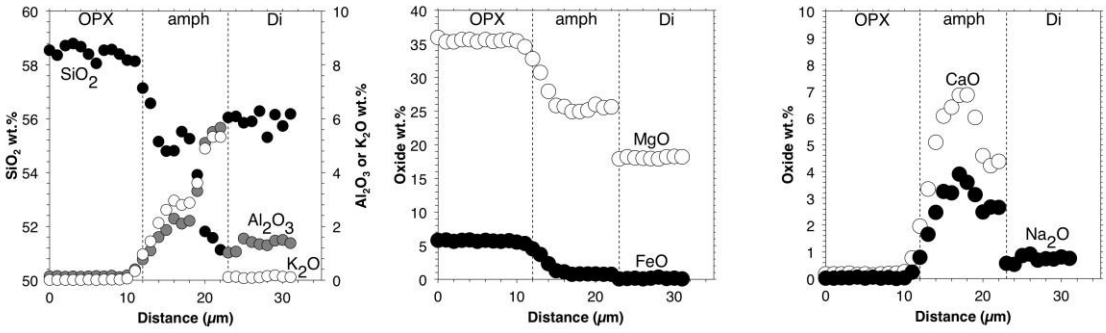

Figure 3.4. Line scan across orthopyroxene – amphibole – diopside rim sequence from sample Ki39. Dashed lines indicate the approximated location of each interface. Due to a focused beam used in the line scan, volatilization of alkalis was high and the glass data points were removed from the line scan images.

Rim olivine

Reaction rims of secondary olivine formed in samples SC31 (and SC32) is compositionally different to that of the host San Carlos olivine, being depleted in FeO and NiO, and enriched in Al_2O_3, CaO, K_2O, and Na_2O. The concentrations of Al_2O_3, K_2O and Na_2O are strikingly high. The rim olivine is stoichiometric and the measured $D^{ol/melt}{}_{Ca}$ are within the calculated values from the model given in Libourel (1999). However, measured partition coefficients for Al_2O_3, K_2O and Na_2O are significantly higher than the ranges given within the literature. For example, partition coefficients for Al and Na are at least twice and up to an order of magnitude greater than reported in Grant and Wood (2010). Rim olivine K_2O and Na_2O fall along mixing line between host San Carlos and the melt. Therefore, these analyses are likely to be contaminated by glass. As the analyses were taken on the largest olivine rim grains available, the exact composition of rim olivine cannot be accurately determined.

Diopside

All matrix clinopyroxene and all clinopyroxene formed in rims around olivine and orthopyroxene are diopsides. There are no significant differences between matrix and rim diopsides within a given sample. However within a sample there is some variation in Na_2O and Al_2O_3 (i.e. jadeite), which increase linearly with each other and correlate negatively with SiO_2, MgO and CaO (i.e. diopside component). The variations within a single sample could be due to changing liquid compositions as the melt becomes progressively depleted in MgO and CaO as more diopside crystallizes. For these reasons it is more convenient to observe compositional variations with temperature, pressure and bulk water content by taking average diopside compositions (matrix and rim) for each sample. The jadeite component increases and the diopside component decreases with increasing pressure. This observation is well documented because the jadeite component has a lower molar volume (Blundy et al., 1995) and this is the basis for several clinopyroxene-liquid geobarometers (Putirka, 2008). The trends with temperature are unclear. For experiments at 1.0 GPa there does not appear to be any obvious change in jadeite or diopside with temperature, but for samples at 1.4 GPa jadeite increases and diopside decreases with temperature. The bulk H_2O in the sample does appear to affect the diopside compositions at 1.0 GPa. There is only a slight decrease in jadeite and increase in diopside with increasing water content. At 1.4 GPa this is much more pronounced. It is possible that the effects of H_2O on clinopyroxene compositions are greater with increasing pressure. This data highlights the need for any clinopyroxene-melt barometer to take into account the H_2O content of the melt (for example equation 32C in Putirka, 2008; Masotta et al., 2013).

The decrease in jadeite component in clinopyroxene with increasing bulk water contents (Figure 3.5) could be related to the incorporation of hydrous species. High melt water contents could lead to higher amounts of H^+ or OH^- in clinopyroxene. Although there is limited data, and none for phonolite melts, the partition coefficient for H_2O in clinopyroxene is about 0.01 or greater (Wade et al., 2013). If this is the case, clinopyroxenes in the most water rich melts could contain up to 1200ppm H_2O. There are two main mechanisms by which H^+ is incorporated into clinopyroxene; a coupled substitution with Al^{IV}, or by creating metal cation vacancies (O'Leary et al., 2010). There are only very minor amounts of Al^{IV} (according to calculations of stoichiometry) and there is no clear correlation

with the bulk water content of the sample. Therefore, it is possible that cation vacancies are created by H^+ incorporation and this reduces the amounts of jadeite in clinopyroxene. However, this does not fit well with the diopside content, which increases with bulk H_2O. Furthermore, data from Purwin et al. (2009) suggest that Na should increase with H^+ in diopside and Sundvall and Stalder (2011) reported no significant correlation between diopside compositions and water contents.

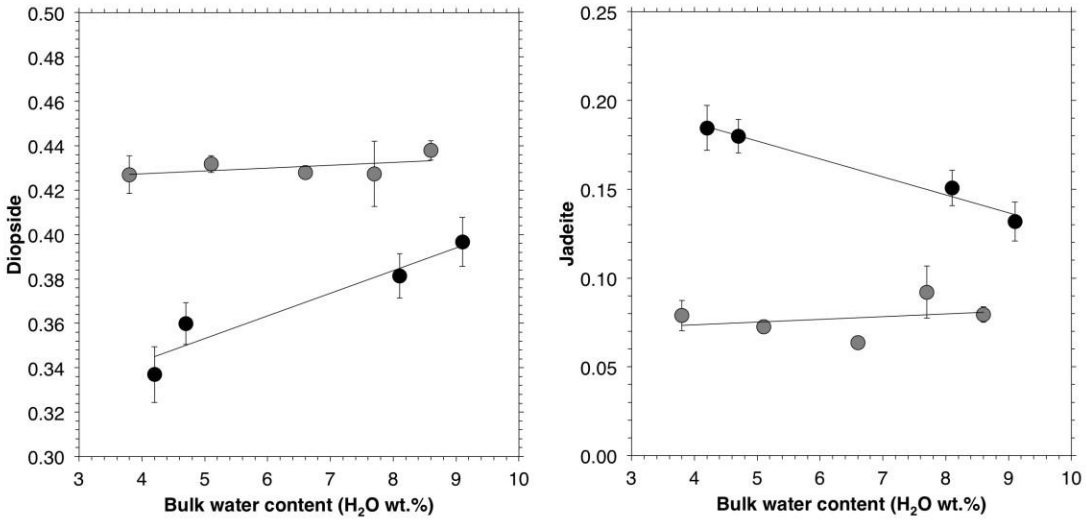

Figure 3.5. Average diopside compositions in forsterite or San Carlos bearing samples with bulk water content. Grey circles = 1.07 GPa, black circles = 1.47 GPa.

3.6 DISCUSSION

Rim forming conditions and the effects of temperature and H_2O

The simple experiments conducted here produce the phlogopite + diopside rims on olivine and either single rims of diopside or double rims of amphibole + diopside around orthopyroxene. Phlogopite is only present in samples containing orthopyroxene and forms near outer rims of diopside. These generally have the same mineralogy of the reaction rims formed in the Heldburg Phonolite. However, our experiments did not produce double rims of amphibole + phlogopite on orthopyroxene that are common in the natural samples. The reasons for this are discussed in the following section. The reaction rims are the same at both pressures (1.0-1.4 GPa) and do not depend on the host xenocryst composition (synthetic or natural). Low bulk H_2O contents, below around 3.8 wt.% do not produce reaction rims due to the crystallization of alkali feldspar. Alkali feldspar will also be stable at temperatures below 900ºC over a wider range of H_2O and pressures (Hay and Wendlandt, 1995). At around 1000ºC and 1.0 GPa secondary olivine rims form on olivine. This is consistent with olivine being a stable liquidus phase at these P-T conditions (Draper and Green, 1997). Inner rims of amphibole that form at the expense of orthopyroxene do not appear to form at these conditions. This therefore places a narrow temperature range in which the natural rims could have formed: 900-1000ºC (although possibly even narrower at 900-950ºC). These temperature ranges are consistent with the likely crystallization temperatures for the phenocrysts of amphibole and clinopyroxene at Heldburg (Grant et al., 2013). Reaction rim formation, over the pressure range tested here does not vary

significantly, and these reactions can probably occur over a range of pressures that correspond to the upper mantle (1-1.5 GPa) and the lower crust (0.5-1.0 GPa). In summary, amphibole and phlogopite rims around orthopyroxene and olivine can only form within a relatively narrow temperature (900-990ºC) and melt H_2O (>3.5 wt.%) conditions. This therefore places some constraints on the conditions of rim formation in the Heldburg Phonolite that are consistent with previous data from phenocryst a geothermometry (Grant et al., 2013).

Double rim formation

Grant et al. (2013) noted that the outer rims of diopside around both olivine and orthopyroxene and the outer rims of phlogopite on orthopyroxene are halos and not outer rims, formed from the melt and not by a direct reaction with the host xenocryst. This is supported by the experimental results. Diopside outer rims on olivine contain interstitial glass, are sometimes absent, have very similar compositions to matrix diopside and do not form in micro-veins within host olivines. These observations strongly suggest that the diopside outer rims form as an halo or overgrowth by preferential nucleation around phlogopite rims around olivine. Instantaneous enrichment of the melt, at the reaction interface, in MgO, (by dissolving olivine – see Figure 3.3) and CaO (by removal of K_2O, Al_2O_3) during the formation of phlogopite locally enhances the stability of diopside. Linear interfaces between diopside and orthopyroxene indicate minimal dissolution and are consistent with textures of epitaxial growth of clinopyroxene rims on orthopyroxene as described by Tarney (1969). The outer rim layers in double rims therefore crystallize from the melt and their mineralogy will be principally controlled by the melt composition. As diopside crystallizes the melt becomes depleted in CaO (see Figure 3.3), this explains the appearance of phlogopite in orthopyroxene reaction experiments that had longer run durations (higher bulk H_2O is also important). Furthermore, a test experiment using Ca-free melt (Grant et al., see Chapter 4) with the same composition as PHG2 formed phlogopite single rims on orthopyroxene, liquidus phlogopite and diopside was absent. As the CaO content of the natural phonolite at Heldburg is low, this component becomes depleted quickly by crystallization of diopside (as shown by the experiments here) and changes the mineralogy of outer rims. The experiments demonstrate that small spatial variations in CaO within the Heldburg Phonolite during intrusion would be sufficient to result in differences in the mineralogy of the outer rims; i.e. diopside or phlogopite outer rims on orthopyroxene and variable amounts of diopside outer rims on olivine.

Melt fractionation during reaction

At high melt to wall rock fractions (in our experiments and the Heldburg Phonolite) the fractionation of the melt is primarily controlled by the crystallization of liquidus phases. This therefore causes a loss of Ca and Mg from the melt and an increase in Si and alkalis. However, during metasomatic reactions in the upper mantle the ratio of melt to wall rock will be much lower. The evolution of the melt composition (starting from phonolite) will vary depending on the phases that crystallize, which vary on the temperature, water content of the melt, vein width and primary mineralogy of the wall rock peridotite. This therefore poses an array of different reaction scenarios resulting in a range of melt

compositions and vein assemblages. We therefore summarize several possible outcomes for the interaction of phonolite melt with wall rock peridotite.

At lower temperatures (<900ºC) and nearly dry conditions there will be little reaction with wall rock olivine and orthopyroxene. The melt will predominantly crystallize alkali feldspar and diopside with other minor phases in a similar assemblage to that of the groundmass observed at Heldburg. Residual melts will therefore be similar to groundmass glasses in the natural samples that are distinctly Si-Al-Na rich (Grant et al., 2013). At high temperatures (>1000ºC) olivine and orthopyroxene (+ clinopyroxene) maybe be stable phases, depending on the pressure (Draper and Green, 1997). Phonolites may therefore be able to percolate through the upper mantle without significant reaction (in terms of modal metasomatism) with peridotite wall rocks.

At 900-1000ºC with high melt water contents, the relative amounts of diopside, phlogopite and amphibole will depend on the vein width and mineralogy of the peridotite wall rock (olivine / orthopyroxene), which will vary spatially. Narrow veins are likely to be devoid of diopside and involve near iso-volumetric replacement of orthopyroxene and olivine by amphibole and phlogopite respectively. Mass balance equations (Table 3.4) show that the reaction with olivine releases Mg and Fe into the melt and consumes Al, K, Si and minor Ca and Na. The reaction of orthopyroxene to form amphibole will release Si, Mg and Fe and will consume Ca, Na, K and minor amounts of Al. Residual melts from reactions with orthopyroxene will be Si, Al and Na enriched (see also Grant et al., 2013), whereas residual melts from olivine reactions may have similar compositions except for increasing Mg with olivine dissolution. In wider veins, growth of diopside or phlogopite will remove Mg and Ca from the melt as well as further K. The residual melts will therefore be Si-Al-Na enriched with compositions that may plot in the trachyte field. Enrichment in Si and loss of alkalis (by loss of K) may take the residual towards trachyte compositions. This may explain the range of glass compositions from basanite-phonolite-trachyte compositions during melt infiltration and reaction with peridotite discussed by Wulff-Pedersen et al. (1996; 1999).

	Ki39	**Ki42**	**SC22**	**SC31**	**SC33**	**Peridotite**
SiO_2	-24.7	-60.2	56.5	72.7	49.4	28.9
TiO_2	-0.3	-0.3	0.0	0.0	0.0	-0.1
Cr2O3	0.0	0.0	-0.2	-0.2	-0.2	-0.1
Al_2O_3	30.2	77.8	132.8	136.1	118.1	106.5
FeOtot	-31.8	-34.7	-54.0	-55.9	-53.3	-48.1
MgO	-108.1	-114.7	-249.6	-263.8	-223.8	-205.4
CaO	48.6	23.2	-0.1	0.2	2.9	11.5
Na_2O	48.6	41.8	7.7	19.1	11.8	22.6
K_2O	37.6	67.0	106.8	91.8	95.0	84.2

Table 3.4. Mass balance calculations for olivine to phlogopite and orthopyroxene to amphibole reactions using the same method as Grant et al. (2013). The mass balance assumes iso-volumetric replacement of olivine or orthopyroxene with no halo of diopside (i.e. vein reaction). All values are in mmol/cm^3. Peridotite column uses the averages of the two reactions with orthopyroxene and three with olivine and a bulk mass balance of 30% orthopyroxene and 70% olivine is calculated. Minus values indicate a loss of component from olivine or orthopyroxene to the melt.

Formation of phonolites and highly evolved alkali rich melts in the upper mantle

Phonolite melts could be produced at high pressures by several possible methods. Irving and Green (2008) demonstrated that fractional crystallization of basanite would lead to nepheline mugearites and finally to phonolitic liquids at upper mantle conditions by the early crystallization of olivine + amphibole + clinopyroxene and then to clinopyroxene + phlogopite. Similarly, percolative fractional crystallization (PFC) models of alkali rich basaltic melts and basanites lead to the formation of SiO_2, Al_2O_3 and alkali rich residual melts observed as glasses in mantle xenoliths (Bodinier et al., 1990; Wulff-Pedersen et al., 1996; Xu et al., 1996; Wulff-Pedersen et al., 1999; Zajacz et al., 2007; Pilet et al., 2010; Miller et al., 2012). The most enriched melts have phonolitic compositions according to the TAS classification (LeBas et al., 1986) and follow a differentiation trend close to that of typical basanite – phonolite lineages.

Partial melting of peridotite tends to produce increasingly Si, Al and alkali rich compositions with decreasing melt fraction (also by temperature) at low pressures (0.7-1.5 GPa) and low H_2O conditions (Baker et al., 1995; Falloon et al., 1997; Hirschmann et al., 1998; Chalot-Prat et al., 2010). The reported melt compositions range from basalt to trachy-andesite / trachyte and are less enriched in alkalis and more SiO_2 saturated. Partial melting is perhaps unlikely to form phonolite melts in the mantle, however, there is also some evidence to suggest that phonolite can be produced directly by low degree partial melts (0.9-1.6 wt.%) of K-doped lherzolite compositions at conditions of 1.3 GPa and 1200ºC (personal communication with Didier LaPorte, 2013). The Heldburg Phonolite and other spinel lherzolite xenolith bearing phonolites are unlikely to be direct partial melts of the mantle due to their Mg numbers being too low (Irving and Price, 1981).

The most likely origin of high-pressure phonolites is fractionation from basanitic melts either in veins by PFC or within a large magma chamber. Phonolites formed by PFC will become trapped in the mantle but they will have significant implications for alkali metasomatism in the upper mantle. Fractionation in a lower crust – upper mantle magma chamber without loss of more evolved melts to shallower pressures is possibly rare and provides an explanation as to why there are so few spinel lherzolite, high-pressure phonolites.

Implications for the origins of alkali basalts

In this section, we discuss our results in the context of alkali metasomatism and the formation of hydrous metasomatic vein assemblages. There are many ideas for the formation of continental alkalic melts such as melting of pyroxenite (e.g. Hirschmann et al., 2003), enriched mantle or deeply subducted oceanic crust (e.g. Spandler et al., 2010). Some recent models for the generation of intraplate alkalic magmas suggest melting of pre-metasomatised, hydrous vein bearing mantle rocks (Pilet et al. 2010; 2011). Such a model consists of three main stages.

1. The first stage involves partial melting of H_2O or CO_2 bearing mantle at pressures of around 2-3.5GPa. This forms *Ne*-normaitve basaltic liquids (Hirose, 1997; Hirschmann et al., 2003).
2. As these melts percolate through the upper mantle they cool and crystallize, resulting in the fractionation of the melt phase towards more evolved compositions. This process is generally referred to as percolative fractional crystallization (PFC) or reactive percolative fractionation

and forms metasomatic veins in a continuum between anhydrous (clinopyroxene + garnet ± olivine ± orthopyroxene) and hydrous (amphibole + clinopyroxene ± phlogopite ± orthopyroxene) compositions.

3. The final stage involves melting of hydrous vein assemblages, along with the surrounding cryptically metasomatised wall rock. This produces melts that have trace element signatures similar to intraplate alkalic magmas (Pilet et al., 2011).

The composition of the melt that forms the hydrous veins is poorly constrained but it must be a relatively evolved liquid, rich in alkalis and H_2O. This melt must also be a differentiated product of the basanite parent melt. Experimental studies have been conducted on the reactions between olivine and orthopyroxene with basanites. This leads to the consumption of orthopyroxene and the crystallization of rims consisting of olivine and Ti-augite (Shaw et al., 1998; Shaw, 1999; Klügel, 2001). Clinopyroxene and olivine rims also form on orthopyroxene in more differentiated melts such mugearites and phonotephrites (Shaw et al., 1998). Therefore, it does not seem likely that a basanite, mugearite or phono-tephrite will form hydrous vein assemblages of diopside + phlogopite + amphibole. The latter stage of differentiation from nepheline mugearite to phonolite will involve diopside + phlogopite + amphibole at upper mantle conditions (Irving and Price, 2008). These are also the main liquidus phases of the Heldburg Phonolite (Grant et al., 2013) and that of the reaction rims in this study. Therefore, a phonolite (or similarly evolved) melt is a likely candidate for the parent melt of hydrous metasomatic veins. Witt-Eickschen et al. (1998) also suggested that phonolites or trachytes could form hydrous (amphibole) dominated veins in the mantle, if Sr and Nd ratios are primitive enough to be consistent with observed vein compositions. The Heldburg Phonolite notably has more primitive Sr and Nd ratios than other phonolites (Wedepohl et al., 1994).

Pilet et al. (2010) experimentally modelled a percolative fractionation process along the liquid line of descent and formed highly alkalic residual liquids with up to 15.5wt.% $Na_2O + K_2O$, and SiO_2 no greater than 45.3 wt.%. Higher SiO_2 could be produced by amphibole fractionation if the initial melt is more enriched in SiO_2. This could be achieved by greater amounts of olivine fractionation during the early stages of percolation. Alternatively, higher SiO_2 contents could be produced by the interaction of basanite melts with peridotites by forming olivine at the expense of orthopyroxene, as experimental studies show. Other examples of reactive percolative fractionation produce distinctly more SiO_2 enriched residual melts (Bodinier et al., 1990; Witt-Eickschen et al., 1996; Zajacz et al., 2007; Szabó et al., 2009; Miller et al., 2012), suggesting that the contribution of reacting wall rock must be considered.

Trace elements

Trace element compositions of the Heldburg Phonolite, other high-pressure phonolites (Irving and Price, 1981), phonolite glasses formed by PFC and other phonolites worldwide are compared in Figure 3.6. The Heldburg Phonolite and other high-pressure phonolites have similar trace element abundances (Figure 3.6A). These are also strikingly similar to the trace element composition of the residual melt (L2) during vein fractionation in the model of Pilet et al. (2011), although L2 is slightly less enriched (Figure 3.6A). The Heldburg Phonolite is also very similar in trace element composition to the most

extreme melts (that plot in the phonolite field of the TAS diagram) formed by PFC from SiO_2 undersaturated alkali melt (Zajacz et al., 2007) or a more evolved hydrous alkalic melt (Szabó et al., 2009) reacting with peridotite in the upper mantle (Figure 3.6B). High-pressure phonolites are also different to most (low-pressure) phonolites based upon the absence of Sr and Eu anomalies associated with feldspar fractionation (Irving and Price, 1981). From this data it appears that there are significant similarities in trace element characteristics between high-pressure phonolites, phonolite glasses formed by PFC and the predicted residual melts that form hydrous mantle veins. However, there is limited data available in the literature to compare a wider range of elements and locations. Further trace element analysis is required to fully understand these relationships.

As Grant et al. (2013) showed, the diffusion controlled, reactive replacement of orthopyroxene by amphibole results in the chemical characteristics of the host orthopyroxene being preserved in the amphibole rims. Phenocryst amphibole and rim amphibole were chemically distinct. Therefore, vein minerals formed by replacement of primary phases may have different major and trace element compositions compared to those that crystallize directly from the melt. The amount of reaction with the wall rock and the mobility of trace elements during replacement reactions during metasomatism will affect the trace element composition of metasomatic veins.

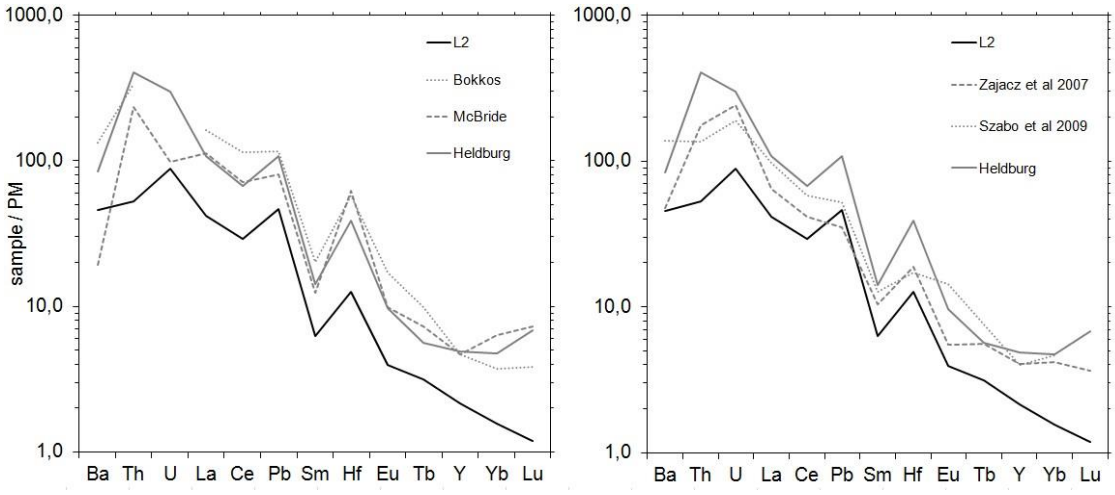

Figure 3.6. Trace element compositions normalized to primitive mantle (PM) from McDonough and Sun (1995). Left panel – trace element compositons of high-pressure phonolites from Bokkos, McBride and Heldburg (Irving and Price, 1981) and residual melt, L2, formed during percolative fractional crystallization in the model of Pilet et al. (2011). Right panel – Comparison between Heldburg and L2 with phonolite glasses in mantle xenoliths from Zajacz et al. (2007) and Szabó et al. (2009).

3.7 CONCLUSIONS

Fractionation of basanitic magmas at upper mantle depths either within high-pressure magma chambers or by percolative fractional crystallization models can lead to the formation of phonolites. The reaction of phonolite with peridotite wall rocks will lead to the consumption of olivine and orthopyroxene forming a metasomatic assemblage dominated by amphibole + phlogopite + diopside. No other melt compositions have been shown to metasomatise the mantle in this way. Therefore phonolite melts are

the likely parent melts of hydrous metasomatic veins composed of diopside + phlogopite + amphibole. This is strongly supported by observations of natural reaction rims at Heldburg, the experiments presented here, major element trends of glasses in mantle xenoliths formed by percolative fractional crystallization of silica undersaturated basaltic melts and trace element characteristics of high-pressure phonolites, xenolith glasses and residual melts in fractionation models.

Chapter 4

Experimental study of phlogopite reaction rim formation on olivine in phonolite melts: the nature of hydrated interfaces and their effects on mantle metasomatism.

Submitted as;

Grant, T.B., Milke, R., Wunder, B., Wirth, R., Rhede, D. (2014). Experimental study of phlogopite reaction rim formation on olivine in phonolite melts: the nature of hydrated interfaces and their effects on mantle metasomatism. *Sumbitted to American Mineralogist, currently under review at time of thesis print.*

4.1 ABSTRACT

Experiments are conducted to reproduce reaction rims of phlogopite ± diopside around olivine that have been observed within a wide range of potassic melts, including phonolite. Phlogopite is also a common secondary phase formed at the expense of olivine during metasomatic events involving K_2O and H_2O rich fluids or melts. Piston cylinder experiments where olivine single crystals were reacted with synthetic phonolite at 10.7-14.7kbar and 950-1000ºC recreate the mineralogy and textures documented in natural samples. Rim growth is parabolic with time, indicating a diffusion-controlled reaction. Fast diffusion in the melt and varying compositions across the phlogopite reaction rims suggest that diffusion through the rims is rate limiting. Reaction rates dramatically increase with temperature as well as the bulk water content of the sample charge. Transmission electron microscopy shows the presence of isolated pores and open grain boundaries. These are interpreted to represent the formation of an intergranular fluid during peak run conditions despite the bulk melt being fluid undersaturated. The majority of this fluid is probably atomically bound within the grain boundary structure. Increasing the bulk water contents in the samples appears to increase the amounts of intergranular fluid and this correlates well with increasing rim growth rates. Fluid can increase the rates of rim growth by lowering the activation energy for diffusion and by increasing the solubility of diffusing species in the grain boundary region. The measured rim growth rates at different conditions are then used to estimate residence times of reacting olivine crystals in natural systems. Development of an intergranular fluid during metasomatic reactions could also explain some aspects of cryptic metasomatism.

4.2 INTRODUCTION

Phlogopite bearing peridotite rocks have been identified in a number of locations; the Ivrea Zone, Southern Alps (Zanetti et al., 1999; Grieco et al., 2001), the Horoman peridotite complex (Arai and Takahashi, 1989), Lherz (Bodinier et al., 2004). Additionally, phlogopite bearing peridotite xenoliths are observed (Aoki, 1975; Lloyd et al., 1991; Wulff-Pedersen et al., 1996; Stiefenhofer et al., 1997). The phlogopite, along with other phases, is often secondary and forms at the expense of primary peridotite phases such as olivine during metasomatic events involving K_2O and H_2O rich melts or fluids. Clear evidence of replacement of olivine by phlogopite was described in the Horoman peridotite complex (Arai and Takahashi, 1989). The origin and composition of the fluids or melts involved in these reactions are not always well constrained. Slab derived melts or fluids (Sudo and Tatsumi, 1990; Zanetti et al., 1999; Prouteau et al., 2001, Wunder and Melzer, 2003), partial melting of pre-metasomatised mantle (Grieco et al., 2001; Thibault et al., 1992) and fluids released from fractionating alkali basaltic melts (Arai and Takahashi, 1989) have been suggested as potential sources. The range in pressures and temperatures of phlogopite formation are also potentially very large. Xenolith examples from Bultfontein Floors (Aoki, 1975) are thought to originate from 170-100km compared with much shallower conditions in the Horoman peridotite complex (Arai and Takahashi, 1989) and the Ivrea Zone (Grieco et al., 2001). The stability field of phlogopite has been shown to extend deep into the mantle (Trønnes, 2002) making it an important reservoir for volatiles, alkalis and trace elements. Phlogopite, may also be an important phase in the genesis and alkali budget of arc magmas (Sudo and

Tatsumi, 1990), intraplate magmas (Pilet et al., 2011) and ultrapotassic melts (Foley, 1992) during partial melting of metasomatised mantle. Therefore, the mechanisms by which phlogopite forms at the expense of upper mantle minerals is of particular interest.

In addition to this, there are numerous examples of where olivine xenocrysts have reacted to form phlogopite ± diopside reaction rims when in contact with K_2O and H_2O rich melts such as; lamprophyre (Foley et al., 2002; Semiz et al., 2012), Lamproite (Carmichael, 1967; Çoban and Flower, 2006), Kimberlite (Neal and Taylor, 1989), Minettes (Davis and Smith, 1993), nephelinite – leucitite (Lloyd et al., 2002) as well as phonolite (Henderson et al., 2012, Grant et al., 2013). These are very small-scale analogues of metasomatic reactions and in all these cases olivine cores clearly show reacted textures indicative of dissolution and replacement by phlogopite. Phase relationships of potassic melts show a change in liquidus phases from olivine + liquid to phlogopite ± diopside + liquid during cooling (Luth, 1967; Arima and Edgar, 1983; Draper and Green, 1997).

In this paper we experimentally react olivine single crystals with synthetic phonolite melt to form phlogopite ± diopside reaction rims. This simple experimental setup recreates the textures and mineralogy observed in naturally occurring rims formed between olivine and phonolite (Henderson et al., 2012; Grant et al., 2013) and other similar melts. The dissolution of olivine and precipitation of phlogopite is driven by a combination of diffusion and interface kinetics, where the slower of the two is rate-limiting (see Dohmen and Chakraborty, 2003 for a detailed discussion). We find that the rate limiting process is grain boundary diffusion through the phlogopite reaction rims. The influence of pressure, temperature and bulk H_2O content of the melt on reaction rim growth rates is also discussed. Rim growth rates are then used to estimate residence times of olivine xenocrysts in the Heldburg Phonolite described by Grant et al. (2013).

Due to diffusion along grain boundaries being rate limiting, the structural properties of grain boundaries are analyzed using transmission electron microscopy (TEM). It has been shown in many metamorphic systems that the properties of the grain boundaries and the presence of intergranular fluid dramatically affects the transport rates of chemical components during mineral replacement reactions (Liu et al., 1997; Yund, 1997; Harlov and Milke, 2002; Putnis, 2002; Keller et al., 2008; Putnis, 2009; Carlson, 2010; Gardés et al., 2012; Milke et al., 2013) and can effect microstructural development (Joachim et al., 2012). This is because hydrous fluid increases the solubility of components, lowers the activation energies of diffusing species and reduces interfacial energies for dissolution and precipitation (Rubie, 1986). Grain boundaries are also fast pathways for diffusion (Dohmen and Milke, 2010) and reservoirs for incompatible elements (Wirth, 1996; Hiraga et al., 2002; Hiraga et al., 2003; Hiraga et al., 2004; Hiraga and Kohlstedt; 2007, Pinilla et al., 2012). During metasomatic reactions the exchange of elements between wall rock peridotite and the metasomatizing agent will be mediated by the grain boundaries of the secondary phases in the reaction zone. We show that there is evidence of an intergranular fluid during our experiments. The amounts of fluid appear to increase with bulk water content of the experiment, which is also strongly correlated with increasing rim growth rates. This data gives a vital insight into the reaction rim forming processes and the influence of intergranular fluids during metasomatism. The formation and properties of intergranular fluid during metasomatism are then discussed. Intergranular fluids formed during the reaction could provide a medium for rapid

chemical exchange of fluid soluble incompatible elements between the melt and the wall rock. This therefore provides a simple mechanism for cryptic metasomatism and could remove the necessity for some more complex multistage models of metasomatism.

	PHG2 glass (N=13)	PHG3 glass (N=28)	San Carlos olivine (N=40)
SiO_2	60.50 (0.31)	60.09 (0.67)	39.43 (0.30)
TiO_2	-	-	-
Cr2O3	-	-	-
Al_2O_3	19.39 (0.27)	19.57 (0.60)	0.04 (0.02)
FeOtot	-	-	8.47 (0.19)
NiO	-	-	0.38 (0.02)
MgO	1.95 (0.06)	1.98 (0.05)	52.07 (0.30)
CaO	2.51 (0.03)	-	0.11 (0.01)
Na_2O	8.43 (0.18)	6.84 (0.29)	-
K_2O	7.12 (0.08)	8.67 (0.08)	-
Total	99.94	97.18	100.55

4.1. Starting material compositions. No data is given for the synthetic olivine as it is pure forsterite.

4.3 EXPERIMENTAL METHODS

Starting materials

Two Fe-free synthetic phonolite glasses were prepared (PHG2 and PHG3). The compositions of these two glasses are given in Table 4.1. Oxide and carbonate forms of each component were accurately weighed, crushed in an agate pestle and mortar in ethanol, and then placed into a platinum crucible. The mixture was then heated in a box furnace at 1600ºC for >24 hrs to create a homogenous melt. The melt was then quenched in water to form a glass, removed and checked for homogeneity before being crushed and used in experiments. PHG3 is a Ca-free glass, which was used in experiments to avoid liquidus diopside that formed in experiments using PHG2 (see later). Both starting material glasses were reasonably homogenous (see Table 4.1), experienced little alkali loss during heating and quenching rates were fast enough to inhibit micro-crystals.

We used synthetic pure forsterite from a single crystal synthesized by IKZ Berlin and a single crystal of San Carlos olivine. Fragments of each were then crushed dry using a metal pestle and mortar separated under size intervals of >500 μm, 250-500 μm and <250 μm and the median size grouping was used for experiments. Olivine grains were then added to the crushed glasses of PHG2 or PHG3 in ratios of 84:16 wt.% (glass : forsterite / San Carlos). The composition of the San Carlos olivine is given in Table 4.1.

Platinum capsules with lengths of about 6mm, widths of 3 mm, and wall thicknesses of 0.3 mm were used for all experiments. One end was crimped and then welded using a PUK3 arc welder. Double distilled water was then added via micro-syringe, and then followed by the forsterite-glass (or San Carlos-glass) mixture in proportions to give the desired bulk water contents. The top of the capsule was then welded, weighed and then placed in a 100ºC oven for around an hour and then weighed again to check for any weight loss and the quality of the welded seal. Samples that showed no weight loss

were then used. Capsules were also cleaned and weighed after the experiments to check for any weight loss. No samples showed any loss of weight after the experiments, indicating that no volatiles were lost at peak run conditions. Sample names, bulk water contents, estimated melt water contents (based on an assumed 84:16 ratio), and run conditions (P-T-t) are given in Table 4.2. Three sets of time series experiments were conducted with three different bulk water contents of 3.9-4.2 wt.% (low water), 5.6-6.5 wt.% (medium water) and 7.2-8.0 wt.% (high water).

Sample	Temperature (ºC)	Pressure (Kbar)	Bulk water (H_2O wt.%)	Melt water	Duration (hrs)	Rim thickness (µm)
Time series						
TSF2	950	10.7	6.5	7.7	168.0	21.3 (3.9)
TSF3	950	10.7	5.6	6.7	74.0	13.8 (3.5)
TSF4	950	10.7	5.7	6.8	3.0	1.7 (1.5)
TSF6	950	10.7	5.7	6.8	26.0	7.9 (3.4)
TSF7	950	10.7	3.9	4.6	26.0	2.8 (1.1)
TSF11	950	10.7	4.2	5.0	72.5	5.3 (2.2)
TSF14	950	10.7	4.2	5.0	5.3	1.6 (0.5)
TSF8	950	10.7	7.2	8.6	26.0	25.0 (4.2)
TSF12	950	10.7	8.0	9.5	72.5	34.0 (5.4)
TSF13	950	10.7	7.8	9.3	5.3	11.8 (2.8)
Single experiments						
Fo25	950	14.7	9.1	10.6	3.0	14.1 (1.5)
Fo28	950	10.7	8.6	10.0	3.0	10.7 (1.5)
Fo30	950	10.7	7.7	9.0	3.0	10.2 (2.0)
SC31	1000	14.7	4.2	4.9	3.8	9.8
Fo32	1000	14.7	4.7	5.5	3.8	9.8
SC33	950	10.7	3.8	4.4	24.0	6.6 (1.4)

Table 4.2. Experimental run conditions, including measured rim thicknesses. All time series experiments use Ca-free glass (PHG3), and all "Single experiments" use Ca-bearing glass (PHG2).

Piston cylinder apparatus

All experiments were conducted using a Johannes type piston cylinder (see Johannes et al, 1971; and Johannes, 1973). The sample charge consisted of; a drilled natural CaF_2 holder for two capsules and the Ni/Ni-Cr thermocouple that measured the temperature at the middle of the capsules, this was surrounded by a graphite sleeve (oven), and then encased in a 1 inch wide drilled natural CaF_2 outer part. Friction effects were accounted for due to the use of natural CaF_2 pieces (Harlov and Milke, 2002). Loading of pressure was done first and then the temperature was increased to the peak conditions. Pressure stayed constant to within 0.2 Kbar and the measured thermocouple temperature to within 2-3°C during the experiments. However there could be small thermal gradients across the samples, and the ΔT across the sample is unlikely to be more than 20ºC (Schilling and Wunder, 2004). Samples were quenched at a rate of around 20°C/s. Run conditions for all experiments are given in Table 4.2. We conducted two sets of experiments; single series experiments tested a wider range of

different temperatures, pressure, water content, duration and olivine composition, and time series experiments where all parameters were kept constant except for the run duration.

4.4 ANALYTICAL METHODS

Electron microprobe (EMP)

An initial assessment of all samples was conducted using the JEOL JXA-8200 (Superprobe) at FU Berlin, Geocampus. Back-scattered electron (BSE) images were taken as well as microprobe analysis of reaction rims and host olivines. Some data was collected for glasses using wide beams of 15 µm to limit loss of alkalis compared to fully focused beams for all other phases. All analyses were taken with accelerating voltages of 15 kV, 20 nA beam current and counting times of 10s on peak and background. The same analytical conditions but with focused beams of 1µm were used to take a series of line scans on SC31.

Analyses of glasses were taken using a JEOL (Hyperprobe) JXA-8500F with a thermal field emission cathode (FEG) at GFZ Potsdam. The analysis of glass posed a significant problem considering the high alkali content (>14 wt.%), high volatile contents and the presence of small crystals of phlogopite throughout the glass. In order to measure profiles through glasses away from reaction rims with the maximum spatial resolution (i.e. distance between each point) whilst minimizing migration of alkalis required specific conditions of; 5 nA beam current, an accelerating voltage of 6 kV, short counting times of 10s on peak and background with a defocused beam of 5µm. Standards included; Jadeite (Si and Na), periclase (Mg), orthoclase (Al and K).

Rim thickness measurements

Using the BSE images from the microprobe, rim thicknesses were measured. For each sample several rims were measured, giving >20-30 data points of rim thickness. These were then averaged to give the estimated rim thickness for each sample. Due to the uncertainty in the orientation of the reaction rim with respect to the polished surface, some rims could be cut at a low angle, making their thicknesses appear larger than they actually are. This means that the observed thickness is always slightly larger than the actual rim thickness (Liu et al., 1997). For this reason, the best locations for thickness measurements were where the rims were generally thinner. Rim thicknesses are comparable from different experiments as long as the same method of measuring rim thickness is always used.

Transmission electron microscope (TEM)

TEM foils were prepared using the focused ion beam (FIB) techniques described by Wirth (2004). Two foils were cut on sample TSF2, one perpendicular to and crossing the olivine-phlogopite interface (foil #3259), and one cut parallel to the olivine interface through the phlogopite rim (foil #3281). One foil was cut from sample TSF6 that was perpendicular to and crossed the olivine –phlogopite interface. Two further foils (#3518 and #3520) were then cut in sample TSF 8, both were perpendicular to the olivine interfaces. TEM and HRTEM images were taken using the FEI Tecnai G2 F20 X-Twin transmission electron microscope at GFZ Potsdam. EDX analyses were acquired using the EDX detector.

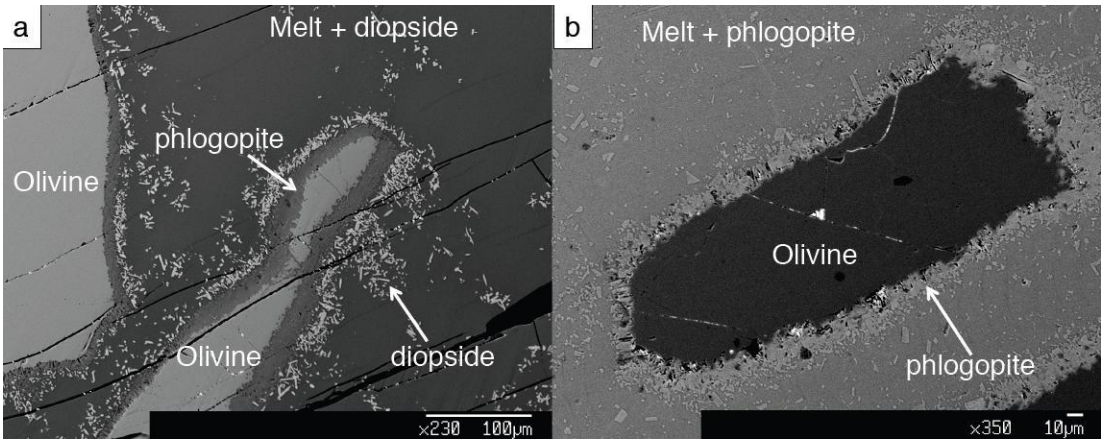

Figure 4.1. Back scattered electron (BSE) images of run products. Panel a – image taken of SC32 showing double rims of phlogopite + diopside. Diopside is also a liquidus phase in this experiment. Note the interstitial glass and discontinuous thickness of the diopside outer rim. Inner phlogopite rims are fairly consistent and include small amounts of porosity. Convoluted olivine – phlogopite interphases are clearly observable. Panel b – image from TSF6 demonstrating that single rims of phlogopite form in Ca-free melt. Phlogopite is also an abundant liquidus phase.

4.5 RESULTS

Reaction rim assemblages and textures

In all experiments the olivine (Forsterite or San Carlos) reacted with the melt. The Ca-bearing melt (PHG2) produced inner rims of phlogopite and outer rims of diopside (Figure 4.1a) with diopside also occurring as a liquidus phase. The Ca-free (PHG3) experiments produced phlogopite rims only (Figure 4.1b). These rim assemblages are consistent with those observed in natural examples (Grant et al., 2013). Reaction rims could not be formed at water contents lower than around 4 wt.% bulk H_2O. One Ca-bearing experiment at 1000°C produced rims of more Mg-rich olivine around olivine in part of the capsule, but phlogopite-diopside double rims in the rest of the capsule. This reflects a small thermal gradient across the samples, where at 1000°C olivine is stable in the melt, and is consistent with the phase relationships of Draper and Green (1997). At just below 1000°C phlogopite rims are stable, consistent with the experiments at 950°C. In the Ca-free melt single rims of phlogopite grew around olivine crystals and no diopside formed. Phlogopite was a liquidus phase in these experiments.

Representative BSE images of the reaction rims are shown in Figure 4.1. Olivine shows classic dissolution textures of convoluted and lobate crystal edges in contact with the phlogopite reaction rim and small amounts of porosity. These features are commonly observed in reaction rims (for example, Coombs and Gardner, 2004). Rim grain sizes vary but are mostly 5-15 µm. Grain sizes tend to increase with increasing run duration. All rims contain some small black patches that are likely to be pores, as well as in some cases they could be due to plucking of rim phases during polishing. Diopside in Ca-bearing experiments does not always form a consistent rim around phlogopite inner rims and diopside crystals are separated by melt. Diopside forming around phlogopite rims appears to a local effect of preferential nucleation as Grant et al. (2013) suggest.

Despite the high water contents used in the experiments the melts did not become saturated with fluid. One experiment (TSF12) did show some vesicles, but as several experiments at higher bulk H_2O did not show the same features, this could have just been caused during quenching. There is also little evidence of crystal settling in the experiments. High water contents are known to be soluble in phonolite melts even at low-pressure conditions (Carroll and Blank, 1997; Schmidt and Behrens, 2008).

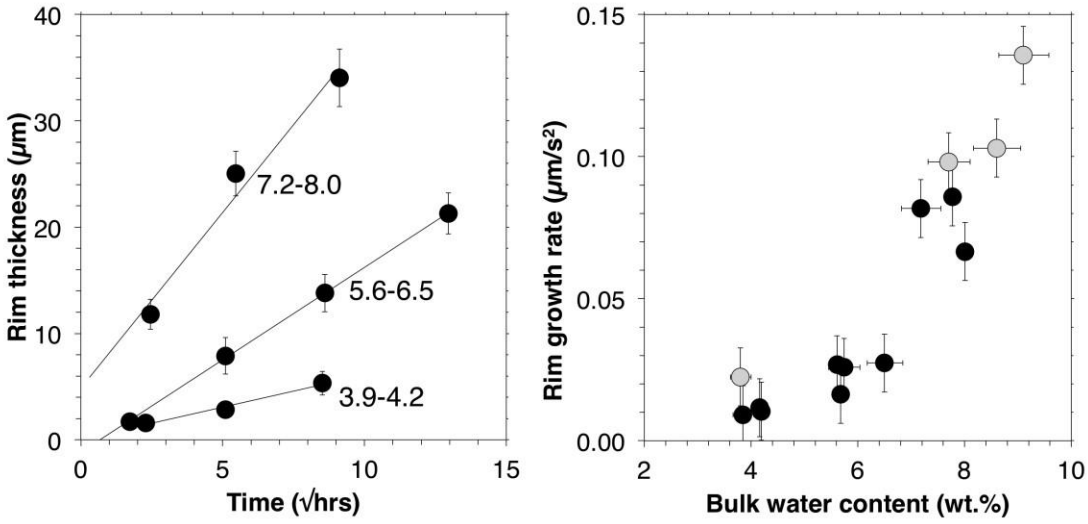

Figure 4.2. Rim growth rates. Left panel shows the variation in rim thickness with time for time series experiments (Ca-free melt). The ranges in bulk water content are given for each set of time series experiments. Error bars are the standard deviation of rim thickness for each experiment. Right panel shows the increase in rim growth rates with bulk water content of the sample at 950ºC. Black squares are the time series experiments and the grey circles are single experiments with Ca-bearing melt. Rim growth rates for single experiments were calculated based on the assumption of parabolic rim growth with time. Error bars for rim growth rates are the error propagation of growth rate calculations using an average variation of measured rim thicknesses of 3µm. Error bars for the bulk water content corresponds to the likely maximum variations in the amount of olivine from 10-20% of the bulk in the sample.

Reaction rates

Measured rim thicknesses for the time series experiments in Ca-free melt were plotted against the square root of time (Figure 4.2a). For all three different water contents rim growth is parabolic with time, indicating a diffusion-controlled reaction. As the water content increases so does the growth rate; at ~4 wt.% H_2O growth rates of around $1.0x10^{-15}$ m^2/s are observed, at ~5.7 wt% H_2O – $1.1x10^{-14}$ m^2/s and at ~8 wt.% H_2O growth rates are $1.3x10^{-13}$ m^2/s. By doubling the bulk water contents, the rim growth rates have increased by more than two orders of magnitude.

To further explore the effects of water on the rim growth rates we looked at the experiments in Ca-bearing melt. For each sample the rim thickness was measured in the same way as before (only measuring the phlogopite inner rims) and it was assumed that parabolic rim growth occurred in all experiments. The estimated rim growth rate was then calculated for each sample that was conducted at 950ºC to be comparable with the time series experiments. The results of this are shown in Figure 4.2b.

The Ca-bearing and Ca-free melt experiments are consistent with each other despite differences in melt composition, and therefore phase relations, host olivine composition (San Carlos or forsterite), and pressure (10 or 14 kbar). The bulk H_2O content and temperature have a large impact on the rates of rim growth whereas small differences in melt composition, pressure and olivine composition do not.

From Figure 4.2b two possible trends can be observed. There could be a simple exponential increase in growth rates with increasing bulk water content. Alternatively, there appears to be a break in slope at around 7 wt.% H_2O. This would mean that there are two regimes, one at 4-7 wt.% H_2O and one >7 wt.% H_2O, with both having linear increases in growth rates with bulk water content. A sharp jump in reaction rates between "dry" and fluid saturated grain boundaries was observed by Gardes et al (2012) in the system olivine-enstatite-quartz and was also predicted in Rubie (1986). TEM analyses of samples from with 6 wt.% H_2O and 8 wt.% H_2O (either side of the possible break in slope) are compared below.

TEM results

Phlogopite-phlogopite grain boundaries

For experiments at around 6 wt.% H_2O the majority of grain boundaries do not appear to have any open space or non-crystalline material between phlogopite crystals. HRTEM imaging shows that the lattice fringes of adjacent phlogopite crystals touch (Figure 4.3c). This means that the grain boundaries are closed, at least to the scale of ~1 nm, although a very thin fluid film cannot be ruled out. Some grain boundaries appear to have open cavities that are linear and follow crystal edges (Figure 4.3a). During quenching, phlogopite will undergo a net decrease in volume (Tutti et al., 2000; Comodi et al., 2004), and this could cause some grain boundaries to open. Opening of grain boundaries by anisotropic thermal contraction has been observed in quartz (Kruhl et al., 2013). Despite this it is still possible that some grain boundaries were open or partially open at peak conditions. There are also grain boundaries that contain small micro-pores (<400 nm) (Figure 4.3b). These pores are oblong to elongate and curved but are separated by regions of grain boundaries where lattice fringes touch. There is no obvious connectivity between micro-pores along the grain boundaries at scales visible by HRTEM.

At higher H_2O contents of around 8 wt.% there appears to be a higher density of open linear, to slightly curved, grain boundaries around (greater or equal to) 10 nm wide. These can terminate at crystal edges or taper out along a grain boundary. Pores are present at most grain boundaries and these can be up to 100 nm (Figure 4.3d) or very small nm sized pores along a grain boundary (Figure 4.3e). The pores in the latter case are much closer together than those seen in experiments with less water (Figure 4.3b).

For all analyzed TEM foils, rim phlogopites do not appear to be orientated in one crystallographic direction and show random orientations throughout the reaction rims.

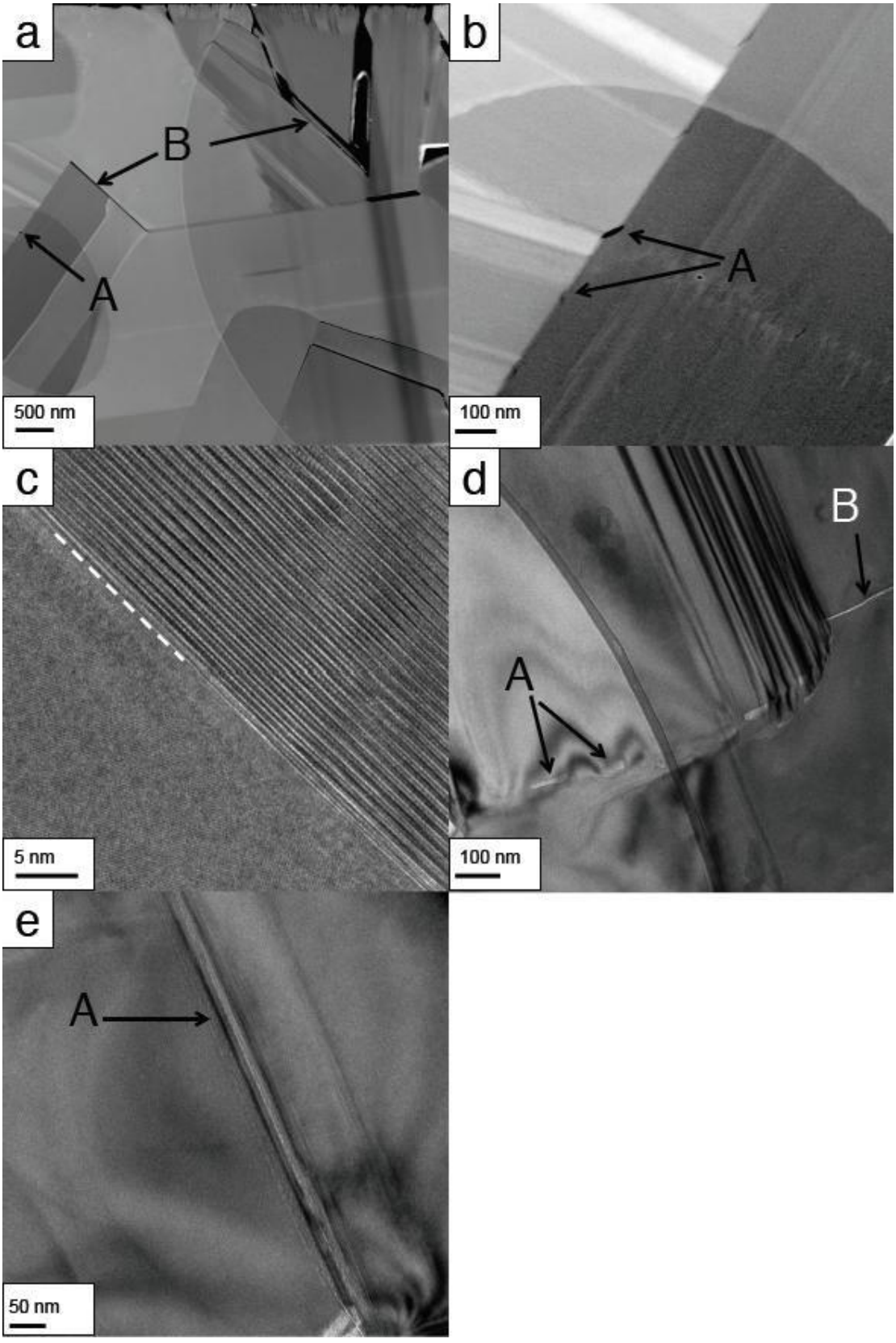

Figure 4.3. HAADF, TEM bright field and HREM images of phlogopite-phlogopite grain boundaries. The images only contain phlogopite. Images a-c are from sample TSF2 and d-e TSF8. a) HAADF image: a pore along a grain boundary, B = open grain boundary. Panel b is a higher magnification of the HAADF image of the grain boundary with the highlighted pore in panel a. Panel c is a HREM lattice fringe image of a phlogopite-phlogopite grain

boundary. Lattice fringes are touching. Panel d is a TEM bright-field image showing a grain boundary decorated by isolated pores typically around 100nm in size. Panel e is a TEM bright-field image showing a grain boundary decorated by small (<20nm) pores that are very closely spaced.

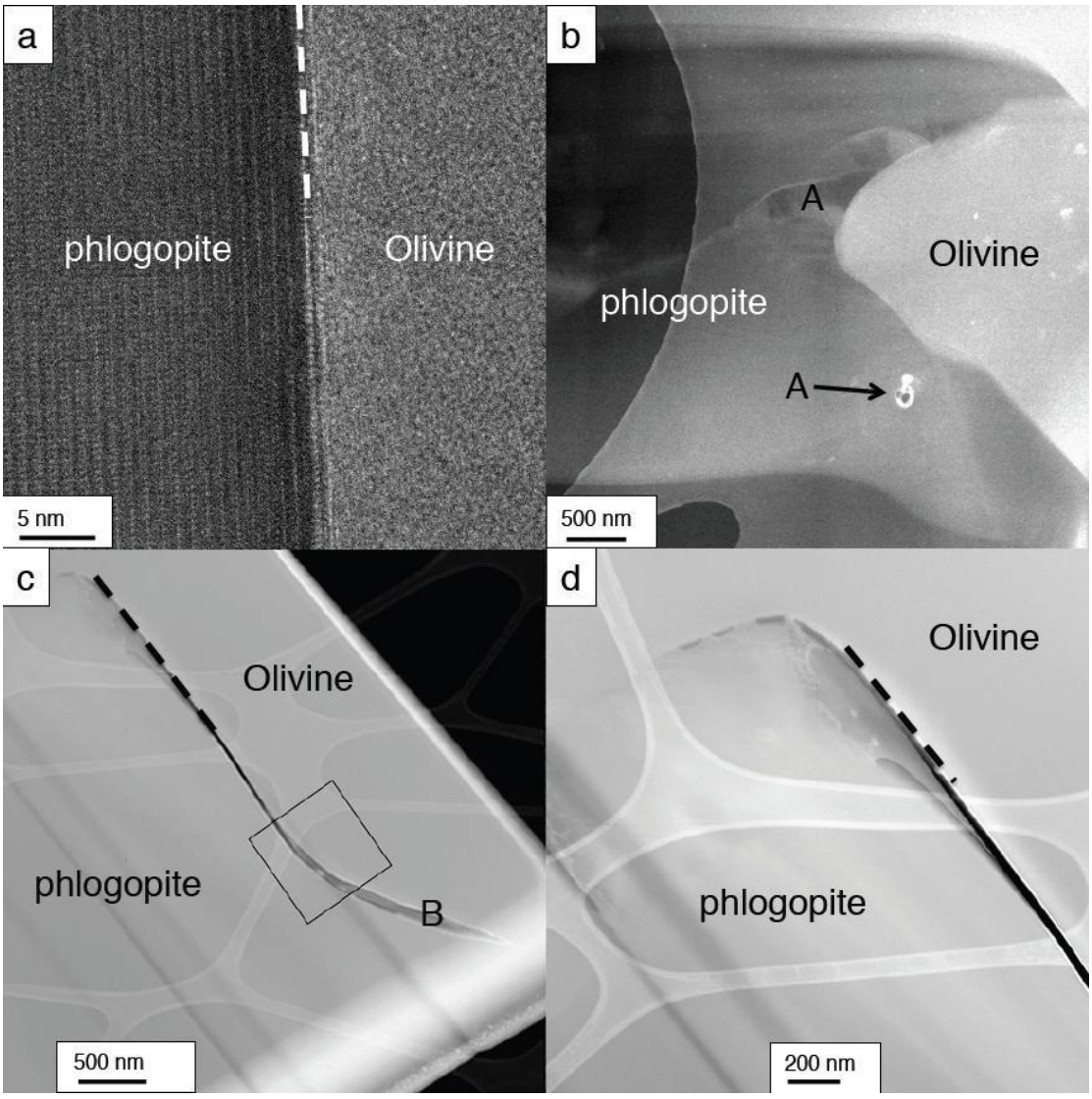

Figure 4.4. TEM images of olivine – phlogopite interphase boundaries. A and B have the same meanings as in Figure 4.3 and dashed lines indicate the location of the interphase boundary. Panel a, a HREM lattice fringe image is taken from sample TSF6 and shows a closed interphase boundary where the lattice fringes of phlogopite and olivine are touching. Panel b, a HAADF image, is from sample TSF2 and shows a micro-pore at the olivine interface. Facets in the olivine surface are visible at these resolutions. Panel c (HAADF image) is from sample TSF8 and shows a completely open grain boundary between olivine and phlogopite. The image is around 4.5µm across. Black square shows the location of the images taken by HRTEM in Figure 4.5. Panel d (HAADF image) shows a higher magnification image of the open grain boundary that tapers out and closes towards the top left of the image.

Phlogopite-olivine interphase boundaries

At intermediate water contents (6 wt.%), olivine-phlogopite interphase boundaries are typically closed with few pores and often the lattice fringes of olivine and phlogopite touch (Figure 4.4a). Open pore

cavities are present in some locations (Figure 4.4b). Although only a small section of the olivine interface was captured by the TEM foil the presence of pores was not limited to being at the head of finger like projections, as shown by Milke et al. (2013) for quartz-orthopyroxene interphase boundaries, into olivine but can occur anywhere along the rim. This does not go against their mechanism but shows that other processes might also be involved. Olivine surfaces appear rounded at large magnifications but at low magnifications crystal facets in the dissolving olivine are created (Figure 4.4). The irregular shape of the interface suggests that the dissolution of olivine is not necessarily faster at different crystal planes or orientations. There is also no correlation between the orientations of phlogopite with that of the host olivine.

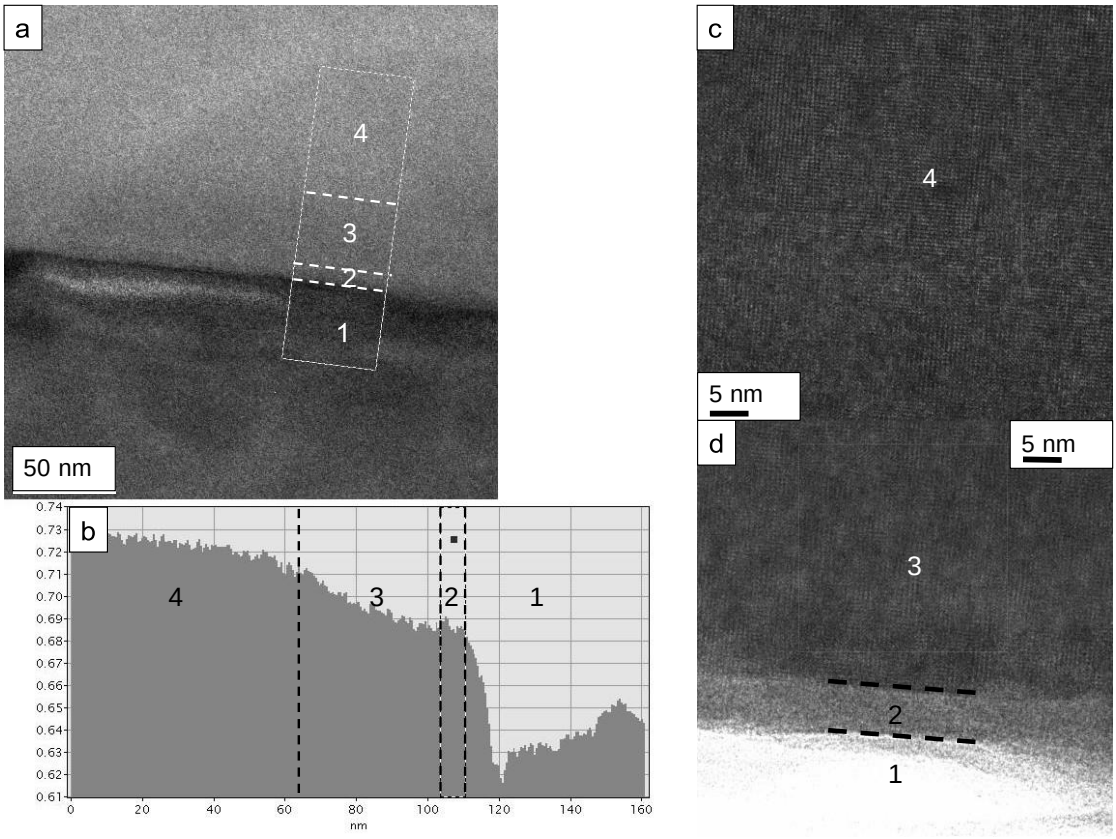

Figure 4.5. HRTEM imaging of the interface region shown in panel c in Figure 4.4. The Si-jump ratio grey-scale map in panel a with light grey indicating high Si concentration and dark grey lower Si concentration. An intensity line scan in panel b shows four main regions across the interface, denoted by numbers 1-4 in each panel. 1 corresponds to the interface region, 2 is a thin 8-10nm amorphous Si-rich surface layer (ASSL) similar to those observed by Hellmann et al. (2012), 3 is a distorted olivine and shows a mottled texture in panel d, and region 4 is un-distorted olivine. The y-axis in panel b is in arbitrary units.

At higher water contents the olivine-phlogopite interphase boundaries are clearly open (Figure 4.4c-d). The space between olivine and the phlogopite rim is between 40-50 nm wide. HRTEM shows that there are several zones of different material at this interphase boundary (Figure 4.5) and that the layer sequence is consistent at the olivine interface throughout the foil. Adjacent to the phlogopite is an open cavity that was most likely filled with fluid. An amorphous Si-rich surface layer (ASSL) is observed at the olivine interface. This is around 8 nm thick and is consistent with the ASSL observed

on olivine by Daval et al. (2011) and other phases (Hellmann et al., 2012, Daval et al., 2013). The first 40 nm of the olivine crystal at the interface is highly distorted and typically has a regular and nearly linear interface with the ASSL. Daval et al. (2011) also noted that olivine adjacent to interfacial regions can be distorted. The distorted olivine region is apparently depleted in Si relative to the undistorted olivine region. However this could simply reflect a lower density of the distorted region. The boundary between distorted and undistorted olivine is irregular. Due to the small sizes of the layers it was not possible to obtain quantitative data on the composition of the ASSL or the olivine at the interface to compare the distorted olivine to the undistorted olivine. Despite this, qualitative EDX measurements do not show a change in stoichiometry in the distorted olivine from normal olivine within the error of the analyses, suggesting stoichiometric dissolution.

Melt pockets

No melt films were observed in any of the TEM foils but melt pockets were observed (Figure 4.6). These melt pockets are not common and do not appear to be connected by melt films along the grain boundaries, indicating low wetting properties. The melt pockets can vary in size from 1 µm to several nm. In one case we see an area of amorphous material in association with a fluid cavity, indicating that fluid and melt can be closely linked (Figure 4.6).

We took some semi-quantitative EDX measurements of melt pockets and found that their compositions showed enrichments in both Si and Al with minor K and Mg. This would be the expected composition of the bulk melt if isolated and then fractionated phlogopite (high fractionation factor), except for the absence of Na. Due to short counting times it is unlikely that all the Na would have been volatilized even though there was some beam damage after the analyses, which also reflects the hydrous nature of the melts. The Na could have been fractionated into the phlogopite but seeing as the Na content of phlogopites is very low this also seems unlikely too. Alternatively, Na could be partitioned into any fluid present and be highly mobile through the reaction rims.

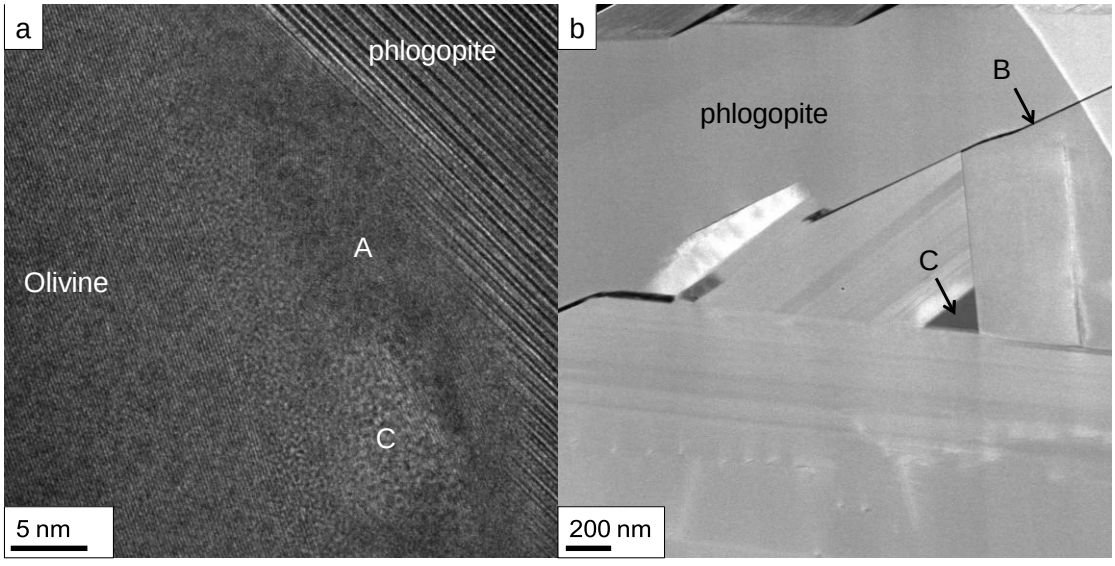

Figure 4.6. HRTEM and HAADF images of melt pockets. Both images are form sample TSF2. The right hand panel image is about 1.25µm wide. Note the partially open grain boundaries. In the HREM image the non-

crystalline material is characterized by the absence of lattice fringes as seen in olivine and phlogopite. A and B labels are the same as in Figure 4.3 and 4.4. C = amorphous material. When analyzed the amorphous material was very Si and Al rich with very small amounts of K and Mg.

Chemistry

Melt profiles

Two samples (TSF4 and TSF6) with intermediate bulk H_2O contents were tested to see if there were any concentration profiles in the melt (Figure 4.7). For each sample, 4 line scans were taken parallel to each other. The locations of the line scans were taken in regions of glass that were free of other olivines to avoid the possibility that profiles from nearby reactions overlap. Step sizes of 5 µm were used to avoid further loss of alkalis by damaging an area of glass by multiple analyses. This was a noticeable problem when step sizes were lower. Due to the presence of crystals within the glass, mixed analyses were common. This was especially problematic for TSF4, and is why the MgO profile is much more irregular than for TSF6. Data points with anomalously low SiO_2, and higher MgO than the majority of glass analyses were then removed from the data set, but there are still many which could represent small fractions of phlogopite in the analyses. For each sample, all four line scans were then compiled together into a single profile. The results of this are shown in Figure 4.7. The error bars for Na_2O and K_2O are large because of the short counting times needed to reduce loss of alkalis.

All elements (Si, Al, Na and K) except for Mg have very similar concentrations as the starting material glass within the error bars of the analyses. This is the same for both samples. Magnesium contents in the glasses (<1 wt.%) are significantly lower than the starting material (1.9 wt.%, taking into account the water content of the melt). All elements show homogenous distribution throughout the line scans within the error of the analyses. The closest point to the reaction rims has the same composition as the melt >300µm away from the rims. Calculating the differentiation in the melt with different amounts of phlogopite can produce the same melt compositions and the depletion in MgO with around 2-3% phlogopite formation.

The low totals of the analyses (around 92%) reflect the high level of volatiles in the melt and are consistent with the amounts of water added, just under 7wt.% by melt (5.7 wt.% by bulk of the sample). Note that the water content should increase slightly as phlogopite crystallizes.

Reaction rim profiles

One sample (SC31) was chosen for a detailed analysis of the distribution of elements throughout the phlogopite reaction rims. This sample was a good choice for this study because the reaction rims were large and due to the presence of Fe, Ni and Ca, this sample allowed to observe a wider range of elements during reaction. Six line scans were taken from the olivine through the rim and into the melt. Melt analyses were then removed as the focused beams caused significant damage. The presence of small diopside crystals in the rims caused a large number of mixed analyses. These were easily spotted by higher CaO contents in the rim phlogopite data. We placed a cut off point and removed all phlogopite data points with >0.15 wt.% CaO. All line scans were then collated together into one single profile for each element. The results of the rim profiles are given in Figure 4.8.

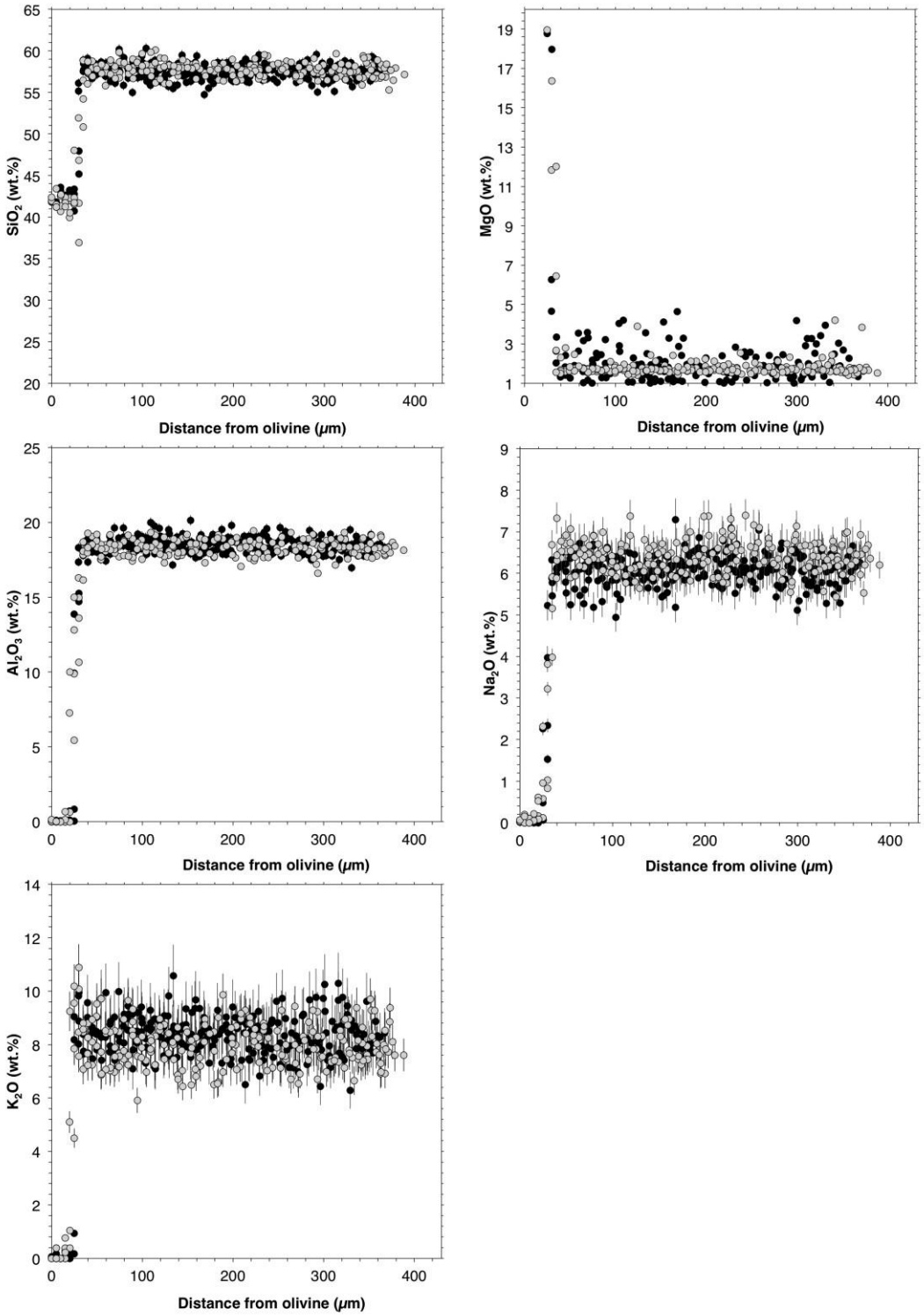

Figure 4.7. Line scans taken in samples TSF4 and TSF6 using the FEG probe at the GFZ Potsdam. All line scans go from the olivine, through the phlogopite reaction rim and extend through the glass. Error bars correspond to the standard deviation from the FEG-probe data. See the analytical methods section for how this data was collected.

The profiles for SiO_2 show a constant concentration in the olivine right up to the reaction interface and then a step jump at the rim. The inner rim is then constant in SiO_2 compositon for several microns and then becomes very irregular towards the outer rim. The distribution of K_2O is constantly low in the

olivine and then increases over several microns, corresponding to mixed analyses across the olivine-rim interface. Throughout the rim K_2O is relatively constant. Both FeO and MgO show very homogenous concentrations in the host olivine right up to the rim interface. The rims are slightly enriched in both components in the inner rims near the olivine and become depleted towards the melt. For Na_2O and CaO, the overall contents are very low in both olivine and the reaction rims and the short counting times mean that their analyses carry large errors. This makes it difficult to observe any real trends in these components, however they do not appear to vary across the reaction rims significantly. The profile for Al_2O_3 shows a consistent and strong variation throughout the phlogopite rim, being higher in concentration near the melt interface compared to near the olivine interface. Finally, for NiO, despite the low overall abundances, there does appear to be a consistent trend of decreasing NiO with distance from the olivine.

The inner most phlogopite is enriched in Mg by around 0.028 (atomic fraction) and depleted by around 0.012 in Al and 0.14 in Si compared to the phlogopite at the melt interface. The exchange between Si and Mg does charge balance, but the addition of Al does not. There is slightly less K and Na as well as Ca, Fe and Ni at the melt interface that could balance the additional Al. In general terms, the melt interface phlogopite appears to contain more octahedral Al and tetrahedral Si with less octahedral Mg (Ca, Fe^{2+} and Ni) compared to the olivine interface phlogopite.

4.6 DISCUSSION

Reaction mechanisms

Diffusion mechanism

The results of the time series experiments show that the rim thicknesses show a linear relationship with the square root of time, i.e. parabolic rim growth. This is a strong indication that rim growth rates are controlled, or rate limited, by a diffusion process. It is therefore important to discuss where diffusion is rate limiting. There are several possible phases through which diffusion could be rate limiting; the melt, the polycrystalline reaction rims (phlogopite) or through the host olivine.

We see no evidence of any concentration profiles in major elements forming in the host olivines, which remain homogenous throughout the reaction. Therefore the reaction process must outpace volume diffusion of elements within olivine. Element profiles through the glass do not show any signs of concentration profiles as well. The melt is homogenous over distance >300 µm and right up to the reaction rim interface, within the resolution of the analyses. For phlogopite to continually form there must be a supply of elements from the melt. The step profiles imply that diffusion in the melt must be fast. Most elements in the glass remain similar to the host melt, whereas MgO shows significant depletion. The homogenous depletion of MgO throughout the melt could only have formed if the diffusion rates in the melt were fast. Secondly, although there is little data on element diffusion rates in phonolites, diffusion rates in wet rhyolite melts for Na (from Zhang et al., 2010) are fast enough to equilibrate over the time and length scales of the experiments. Furthermore, the diffusion of elements in the melt will be related to the viscosity of the melt. Adding water will reduce the viscosity and therefore the diffusion rates, but this effect is most pronounced at low water contents, where OH^-

acts as a network modifier, and then reduces at higher water contents. This is inconsistent with the exponential increase in reaction rates with increasing water contents.

It is therefore most likely that the mobility of components through the reaction rims limits the rates of reaction. Concentration profiles through the reaction rims shows that they are not homogenous in concentration and are not well equilibrated. Diffusion through polycrystalline materials is most likely to be concentrated along grain boundaries (Dohmen and Milke 2010).

Dissolution / interface mechanism

At high bulk water contents the olivine-phlogopite interphase boundary is completely open. At the olivine interphase we see remarkably similar structures (ASSL) to those observed during dissolution of olivine at completely different P-T conditions (90°C and 25 MPa) (Daval et al., 2013). Even though the conditions are very different it is reasonable to assume that olivine dissolves in the exact same way regardless of P-T. These results also appear to support the universal dissolution mechanism proposed by Hellmann et al. (2012). The same features are not observed in locations where the interphase boundary has been mechanically opened during polishing and quenching. Therefore, the open cavity observed in TEM must have been filled with fluid at peak run conditions.

The distorted region observed here and in Daval et al. (2013) has not been observed in other phases (Hellmann et al., 2012). Weakening of the olivine lattice as Si, O or Mg is removed during dissolution could explain the distortions. Alternatively incorporation of protons could also distort the lattice. If the dissolution of olivine and the formation of distorted region is non-stoichiometric this could provide support for leaching models. Due to difficulties in measuring such a small volume of material with a high degree of accuracy we cannot unequivocally answer this question. However, several EDX measurements were taken of the distorted region and the non-distorted region. No significant stoichiometric differences (Si/Mg) were observed within the error of the analyses. This suggests that if dissolution is non-stoichiometric at all it is minimal.

A key point is that despite the interface mechanism being observed here, rim forming components must still pass through the reaction rim to reach the interface and we interpret rim growth in this case to be limited by grain boundary diffusion.

Presence of intergranular fluid

The TEM data must be treated with some caution, as any fluid present during peak run conditions will be transient and dynamic (Billa et al., 2013). There are also several ways in which the rim structure can be modified during quenching and polishing that can introduce cavities. Despite this there does appear to be a clear difference between experiments at low water (6 wt.%) and high water (8 wt.%) concentrations where in the latter foils there appears to be a greater abundance of pores and open interphase boundaries. These features correlate well with increasing growth rates with increasing bulk H_2O. We interpret these features as representing a small but potentially significant increase in the amount of fluid present along the grain and interphase boundaries in our experiments. Several important questions remain; how can a fluid form along the grain boundaries when the melt, which is a semi-infinite reservoir of fluid relative to volume of grain boundaries, in the system remains

undersaturated with fluid? How do the properties of the grain boundaries change with increasing fluid? How does this relate to the observed trend shown in Figure 4.1b?

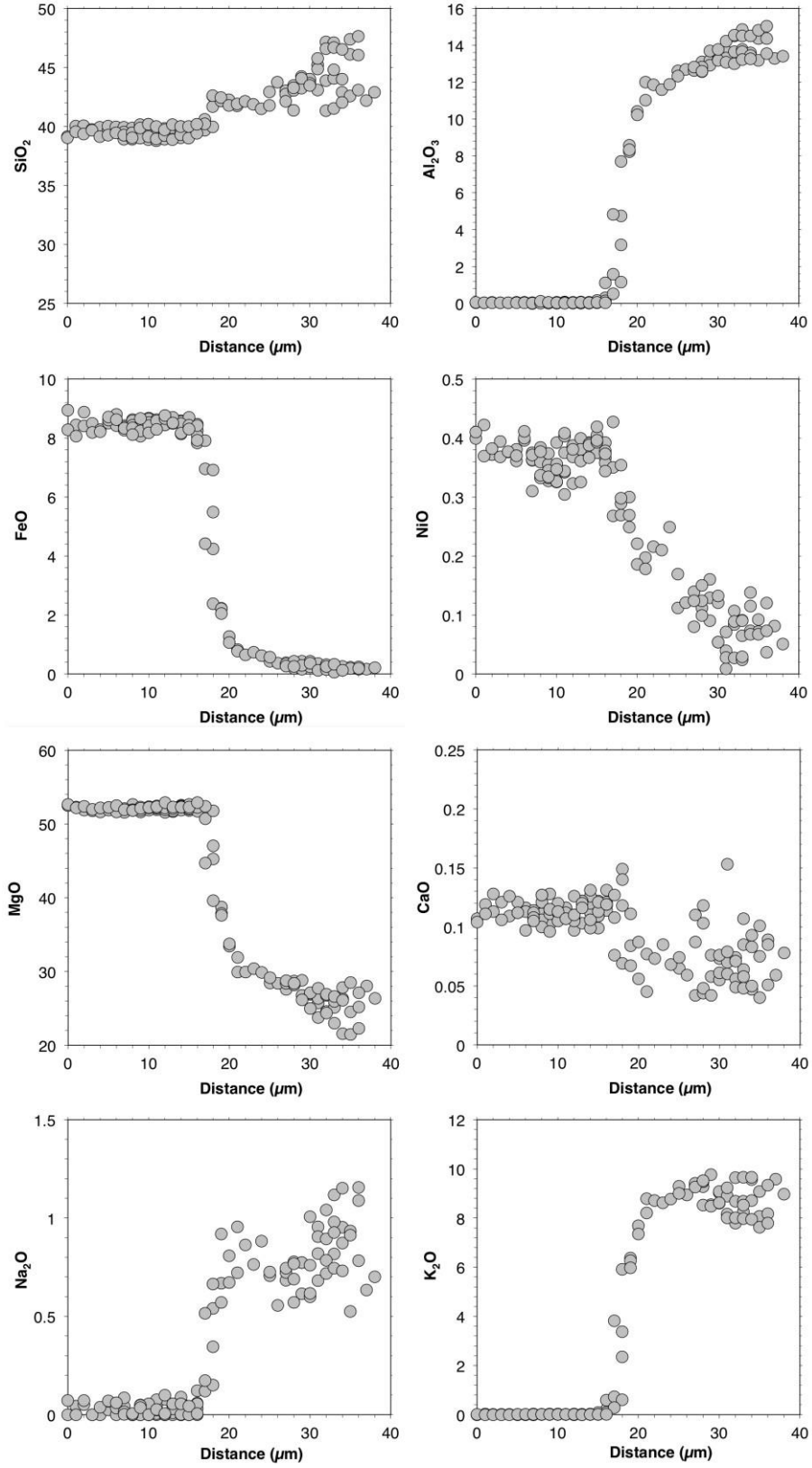

Figure 4.8. Line scans through phlogopite reaction rims from SC33. Y-axes in wt.%.

How does inter granular fluid form?

As the melt remains undersaturated with fluid, it is perhaps surprising that fluid can form at grain (and interphase) boundaries. However, the grain boundaries must be treated as a separate phase within the system and like any other phase they have their own set of physical and chemical properties. Grain boundaries have a limited number of structural sites in which hydrous species can be atomically bound, and this is dependent on structural properties derived from the adjacent mineralogy, the degree of mis-orientation between adjacent grains (Dohmen and Milke, 2010) and anisoptropic interfacial energies (as discussed in Farver and Yund, 1999). Beyond this limit the grain boundaries will become saturated and a fluid phase will form. From the experiments it is evident that the saturation of grain and interphase boundaries occurs at lower H_2O than the melt. Two driving forces perpetuate this. Firstly, a distribution coefficient for hydrous species between all phases means that increasing H_2O in the melt increases the amount of H_2O in the grain and interphase boundaries. Secondly there is a large chemical potential gradient across the reaction rims between nominally dry olivine and hydrous melt. Additionally, once a fluid phase if formed along a grain boundary there will be a concentration gradient in solute species from the dissolving olivine interface to the melt interface. An attempt to regain osmotic equilibrium (Rutter and Elliot, 1976) may further force fluid into the grain boundaries towards the olivine interface.

Inter-granular fluid regimes

It has been shown in several other chemical systems that there are distinct types or regimes of fluid bearing grain boundaries (Rubie, 1986; Carlson, 2010; Milke et al., 2009; Gardes et al., 2012). Regimes discussed in the literature are; "dry", fluid undersaturated and fluid saturated grain boundaries. Some of these regimes are identifiable in the experiments shown here and the possibility of a fourth regime, confined fluid film, is discussed. The chemical and physical properties of grain boundaries, specifically the diffusion rates of components, vary between regimes. It is important to not only view grain boundaries as a separate phase in the system but also to consider that going from one fluid regime to the next is analogous to a phase change. This view has been used in the material science literature where regimes defined by changing properties of grain boundaries with different amounts of impurities are referred to as complexions (Dillon et al., 2007). Crossing one of these phase boundaries results in relatively sudden changes in the properties of the grain boundary, such as the diffusion rates of chemical components.

1. Dry grain boundaries – In the absence of any hydrous species at all, the grain boundaries will be dry. Such a scenario is highly unlikely in nature and certainly not present in these experiments. The lattice structures of adjacent grains touch and the activation energy for diffusion is high due to the strength of Si-O and M-O (M= metal cation) bonds that form the grain boundary network.
2. Fluid undersaturated - Like any other chemical impurity, hydrous species such as H^+ or OH^- can be atomically bound with the grain boundaries. The incorporation of these species breaks Si-O bonds and creates weaker H-O bonds thereby lowering the activation energies for diffusion. The grain boundary is undersaturated if not all of the potential sites for hydrous

species are occupied and it is clear that increasing amounts of hydrous species should continually increase the diffusion rates within this regime. Estimates of the thicknesses of mineral surface-fluid complexes on orthoclase; 2.69Å (Fenter et al., 2000) and mica; 2.5Å (Beach, 1982) have been given. This means that the thickness of an atomically bound fluid film will be in the order of 0.6 nm. Such a layer may be too small to be observed by HRTEM.

3. Confined fluid – once the grain boundaries become saturated, secondary layers of hydrated complexes, that are not directly bound to the mineral surfaces, begin to form. However this fluid film is still very thin and it will not have the properties of a free or bulk fluid. Confined fluid films are affected by surface forces imposed by the adjacent minerals that change the structural and dynamical properties of thin fluid films compared to a bulk fluid (Hess, 1994). Thin fluid films may well have quasi-crystalline properties (Hess, 1994). Molecular dynamics and x-ray spectra show that a fluid film within mica grain boundaries undergoes a sudden jump in diffusion rates of water by two orders of magnitude at a thickness of 0.6 nm followed by a plateau in diffusion rates at greater thicknesses (Leng and Cummings, 2006). However the results of Kersit and Lui (2009) suggest that a thin film of fluid may not have the properties of a bulk fluid until it reaches around 5 nm in thickness, or even several tens to hundreds of angstroms (Hess, 1994) Confined fluids therefore have thickness greater and faster diffusion than that of surface-fluid complexes but are thinner and have diffusion rates slower than free fluids. Sudden jumps in diffusion rates with increasing fluid have been noted by Milke et al. (2009) and Gardes et al. (2012) in the Fo-En-Qz system. Furthermore, at higher pressures and temperatures the structural properties of a confined fluid may well be different to the studies outlined above (Manning, 2013). Additionally, solvated ions may have important consequences on the densities of intergranular fluids.
4. Free fluid – Beyond the confined fluid regime, fluid films behave much like a free or bulk fluid phase but the effects on component diffusion rates through the polycrystalline rim depends on the connectivity of fluid. At low connectivity, i.e. for single and isolated (no free fluid connections) pores, diffusion is only increased locally. Even at low connectivity, the fluid will act as an effective medium for transport, dissolution and precipitation for mineral reactions to proceed (Putnis et al., 2009).

It is highly likely that one single rim can express several different regimes over time and space. Porosity and fluid along grain boundaries are not static but dynamic and may change their locations and amounts as the system attempts to reach equilibrium. This has been noted in other systems; for example recrystallization of alkali feldspars (Norberg et al., 2013). Additionally, thermodynamic calculations suggest that thin fluid films are unlikely to be stable at low angle grain boundaries compared to high angle ones and will be generally thicker (more stable) at interphase boundaries compared to grain boundaries (Hess, 1994). This is consistent with our TEM data that shows some locations appear to be saturated and others do not. Therefore we must take into account a more generalized view of the reaction rim as a whole. The regimes discussed above can explain the increase in reaction rim growth rates with increasing bulk fluid.

It is obvious from our results that the system is not in the 'dry' regime. It is also clear that in some cases, even if locally, there is some free fluid present. The amounts of observable free fluid also increase with bulk water content, but the TEM data suggest that the connectivity of this fluid appears to be limited. Observations of where the lattice fringes of adjacent grains are touching rule out fluid films that are greater than around > 1 nm. At this thickness the fluid could fall within the range of atomically bound fluid species or a confined fluid phase. Therefore, the majority of the reaction rims at lower water contents of 6 wt.% are dominated by confined or atomically bound fluid along grain boundaries. This connects localized regions of free fluid that are dynamic throughout time and space. Increasing the bulk water content to around 8 wt.% increases the amount of water within the grain boundaries. This leads to a larger amount of free fluid, thereby increasing its connectivity with some areas of confined or atomically bound fluid. The interphase boundary changes dramatically and the presence of free fluid here enhances the transfer of elements from the dissolving olivine interface to the precipitating phlogopite interface. This could be why there appears to be a sudden jump in reaction rates in Figure 4.2b. Beyond this jump, reaction rates still increase due to increasing free fluid connectivity.

	Olivine interface	**Olivine interface**	**Mid-rim**	**Mid-rim**	**Melt interface**	**Melt interface**	**Melt interface**
SiO_2	42.24 (17)	41.77 (17)	43.01 (17)	43.48 (17)	46.06 (18)	42.88 (17)	43.09 (17)
Al_2O_3	10.41 (9)	10.23 (9)	12.77 (9)	13.09 (10)	14.36 (10)	13.44 (10)	13.55 (10)
FeO	1.27 (10)	1.07 (11)	0.38 (7)	0.19 (7)	0.16 (7)	0.25 (7)	0.19 (7)
NiO	0.22 (3)	0.19 (3)	0.08 (3)	0.11 (3)	-	0.12 (2)	0.07 (3)
MgO	33.44 (16)	33.73 (16)	27.56 (15)	28.21 (15)	25.17 (14)	27.83 (15)	27.11 (15)
CaO	0.06 (1)	0.09 (1)	0.04 (1)	0.04 (1)	0.09 (1)	0.05 (1)	0.05 (1)
Na_2O	0.67 (7)	0.81 (7)	0.68 (7)	0.78 (7)	0.78 (7)	0.73 (7)	1.16 (8)
K_2O	7.68 (4)	7.35 (4)	9.33 (5)	9.28 (5)	8.18 (4)	9.56 (5)	9.34 (5)
Total	96.04	95.22	93.84	95.22	94.84	94.86	94.59
X (μm)	20	20	27	28	36	34	36

Table 4.3. Phlogopite compositions. X (μm) refers to the distance along the rim line scan shown in Figure 4.8. Errors in brackets are to 2 decimal places.

Diffusion modeling and element mobilities

As discussed above, the reaction rims are extremely dynamic, heterogeneous and will vary in their diffusion properties over very small length time scales. This makes modeling the diffusion rates of elements in this system particularly difficult. We attempt a simple method of calculating effective diffusion coefficients across the phlogopite reaction rim formed in sample SC33 (950ºC), giving semi-quantitative values. The aim is to identify the likely rate-limiting component.

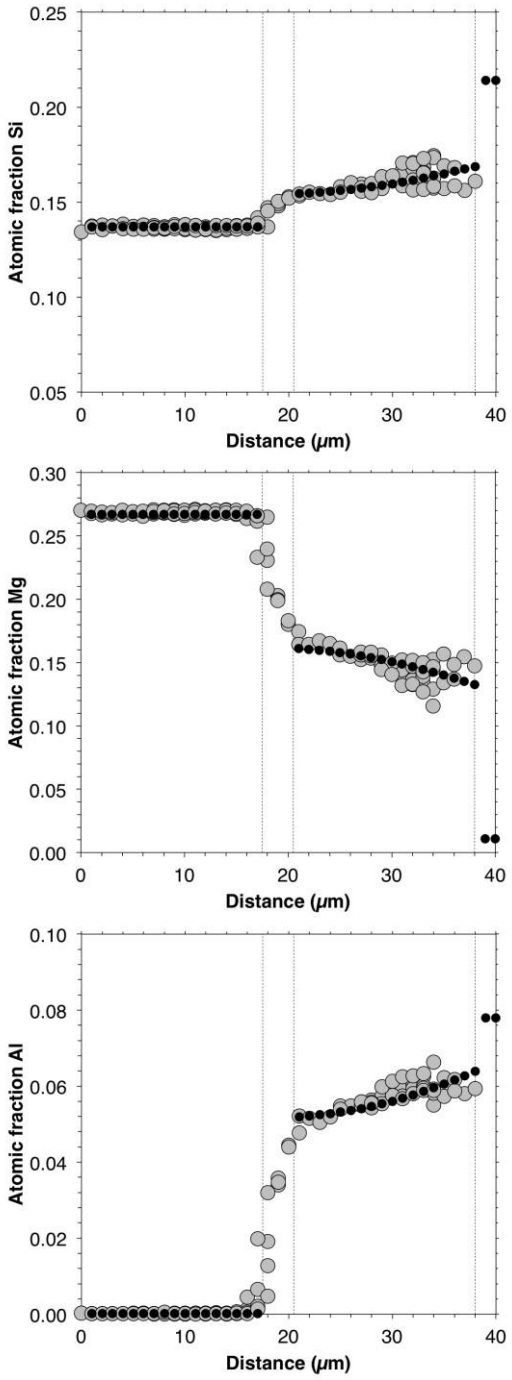

Figure 4.9. Line scans across a reaction from SC33. Grey circles are the measured data, and black circles are the calculated and fitted profile using the moving interface diffusion model of Ganguly (2002) in equation 4.1.

The system involves six components; SiO_2, MgO, Al_2O_3, K_2O, Na_2O and H_2O. The latter three components are most likely to diffuse the fastest and are homogenous throughout the reaction rim (H_2O presumed to be). The line scans show that SiO_2, MgO, and Al_2O_3 vary across the reaction rim and these components are likely to diffuse much more slowly. The simple diffusion model uses the equation for diffusion with a moving interface from Ganguly (2002), see equation 4.1. We assume that the original olivine-melt interface was at the current location of the phlogopite-melt interface, implying one directional rim growth. A second assumption is that the composition of the newly formed

phlogopite at the olivine interface is the same as that of the inner most phlogopite measured in the rim line scan (Figure 4.9). Diffusional exchange of elements then occurs between the melt and the olivine through the reaction rim along the grain boundaries. This leads to the phlogopite at the melt interface becoming more enriched in melt elements such as Al and the phlogopite at the olivine interface being enriched in Mg, as is observed in the rim line scans.

– —= — —= (4.1)

The results from these calculations give estimate diffusion rates of around 3.5-4.0 $x10^{-15}$ m^2/s for Al, Si and Mg. These diffusion rates are a factor of five slower than the estimated rim growth rate for this sample (8.4 $x10^{-14}$). Within the error of the calculations, all three elements have virtually the same diffusion coefficient. It is therefore difficult to determine the rate-limiting component within the error of the data and calculations.

4.7 IMPLICATIONS

Residence times

Reaction rims can be used to provide estimates of residence times of phenocrysts or xenocrysts in their host magma (Rutherford, 2008). Therefore, the reaction rates calculated here can be used to estimate residence times of olivine xenocrysts from the Heldburg Phonolite (Grant et al., 2013). The natural phlogopite rim thicknesses are typically around 20-30 µm. Using the measured growth rate for each experiment in this study, the estimated time that a rim of 25 µm would take to grow is calculated. This is a rough estimate of the residence times at different conditions and the results are shown in Figure 4.10. At the highest bulk H_2O the estimated residence time would be around several hours, whereas at the lowest bulk H_2O the estimated residence times would be up to around 100 days. It is more likely that the water content in the melt at Heldburg were towards the lower end of this scale, giving residence times of several weeks to a few months for the natural reaction rims. This data fits well with previous estimates given within Grant et al. (2013). We also show the difference of temperature with two experiments at 1000°C. It is clear that the water content of the melt will have an important effect, as well as temperature on the rim growth rates and constraining both parameters will be important if reaction rims of this kind are to be used as a way of calculating residence times. It is also potentially possible to calculate the melt water contents based on H_2O partitioning between clinopyroxene and melt (Wade et al., 2008; O'Leary et al., 2010), although data for phonolite melts are lacking.

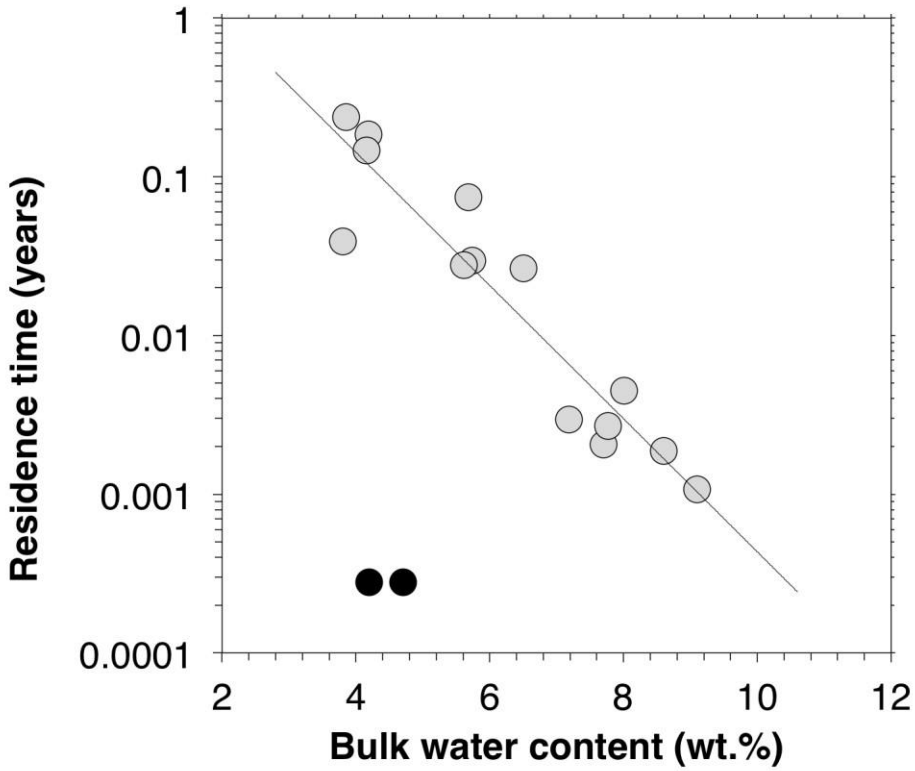

Figure 4.10. Using the calculated rim growth rates from each experiment the predicted time to produce a rim with a thickness of 100µm is estimated. This equates to an estimate residence time of the olivine xenocrysts found within the Heldburg Phonolite (Grant et al, 2013) that have rim thicknesses that are typically <100µm. Grey circles are for experiments at 950ºC and black circles for two experiments at 1000ºC.

In systems where the rim growth was rate limited by diffusion in the melt, these results may still apply. If convection or any kind of mechanical movement of xenocryst relative to the melt takes place, and this is highly likely during eruption, then melt boundary layers could be eroded. This means that diffusion through the rim itself will have a more direct effect on rim growth rates in a dynamic system rather than a static experimental setting.

A final consideration is that reaction rims can become self limiting (Klügel, 2001). This is because increasing rim thicknesses increases the diffusion distance, which in turn reduces the flux per unit time. At some distance the flux reduces to a negligible amount and the rim growth essentially stops. However, this may not happen if the diffusion rates, relative to the potential maximum diffusion distance (radius of the initial xenocryst), are large. Xenocrysts with slow rim growth (low temperature or water content) are more likely to be preserved whereas small crystals experiencing rapid rim growth rates can be completely replaced.

Cryptic metasomatism

Our experiments clearly show that a fluid phase can form along the grain boundaries during reaction even when the melt remains undersaturated with fluid. During metasomatic reactions between a melt and wall rock peridotite it is very possible that small amounts of fluid can form along the grain boundaries. Even at low water contents (ppm) and low connectivity, this could have significant impacts

on the grain boundary diffusion rates (Gardes et al., 2012), enhancing chemical exchange between melt and wall rock. Sommer et al. (2008) showed that fluid could become concentrated at grain boundaries and dislocation structures. They also suggested that this could provide an efficient pathway for the element exchange during cryptic metasomtism. Similar ideas of chemical fractionation along grain boundaries have also been discussed by Hiraga et al. (2004), Frezzotti et al. (2010) and in terms of the chemical communication of melt inclusions in olivine with their host melts (Bakker and Jansen, 1994; Massare et al., 2002; Portnyagin et al., 2008). An inter-granular thin fluid film, even if only at very low fractions, could mobilize trace elements segregated at grain boundaries (Hiraga et al., 2004). Flow of a small amount of fluid through a relatively large volume of rock could therefore become enriched or further enriched in trace elements. Pervasive fluids can also control the exchange of trace elements during metasomatism (Keppler, 1996). A lowering of activation energies for diffusion and increasing incompatible element solubility by atomically bound water at grain boundaries (Rubie, 1986) will reduce the effects of a leakage flux to the adjacent solid phases that can retard grain boundary diffusion over large length scales (Dohmen and Milke, 2010). In summary, grain boundary fluid does not need to be pervasive or interconnected to have significant implications for the transport rates and chemical exchange during metasomatism.

Several authors discuss the possibility of a percolating low-density liquid or fluid (Berkesi et al., 2012) in the mantle. Fluids generated during slab dehydration are generally thought to be dilute (Manning, 2004), although some authors suggest the presence of more solute rich fluids in the mantle (McInnes et al., 2001; Scambelluri and Phillpot, 2001). Fluids can transport high amounts of compatible and incompatible elements over large distances during channelized flow (Zack and John, 2007). We suggest that during metasomatic reactions compatible elements will become fixed in the reaction zone, whereas the incompatible elements will be transported further into the adjacent wall rock. This is a chromatographic or kinetic fractionation process (Bodinier et al., 2004; Milke et al., 2011). These models show that modal and cryptic metasomatic processes can occur simultaneously, thus removing the necessity for more complicated multi-stage metasomatic models. One example of this is the development of apatites and LREE trace element enrichments at distances of many cm away from metasomatic veins via chromatographic fractionation of percolating melt through the surrounding wall rock (Bodinier et al., 2004). These authors suggest that this was caused by a melt possibly of Carbonatitic composition, however a fluid or dense fluid is also possible.

Chapter 5

Conclusions and outlook

This work aimed to explore if phonolites can exist in the upper mantle and how phonolite melt reacts with upper mantle phases such as olivine and orthopyroxene. The results of this have significant implications for the role of more evolved melts in their contribution to metasomatic vein formation and chemical exchange in the mantle. The main conclusions and key results are summarized in the following paragraphs.

Origin of the Heldburg Phonolite

The results and discussion in Chapter 2 are consistent with a high-pressure lower crust to upper mantle origin for the Heldburg Phonolite and support the model proposed by Irving and Price (1981). Thermo-barometric calculations of amphibole and clinopyroxene phenocrysts suggest pressures of 0.5-0.9 GPa, which is close to the crust-mantle boundary. It is therefore likely that the Heldburg Phonolite sampled the spinel lherzolite and gabbro-norite xenoliths directly from the wall rocks that it passed through during intrusion. However it also possible that a mixing event between a xenolith free phonolite and a xenolith-bearing primary melt at the crust mantle boundary occurred in a similar model to that of Downes (1989). The geobarometric calculations (0.5-0.9 GPa) places qualitative estimates for the origin of the Heldburg Phonolite and shows that in some cases phonolite melt can be produced at much higher pressures than normal phonolites. High-pressure fractionation models such as that of Irving and Green (2008) provide an adequate explanation to how high pressure phonolites can form.

Reactions between olivine and orthopyroxene with phonolite melt

The natural examples show that olivine reacts to form a rim of phlogopite with and a halo of diopside, and orthopyroxene reacts to form a rim of amphibole with overgrowths of either diopside or phlogopite. Experiments reproduce the mineralogy and textures of the natural reaction rims and show that the overgrowths are dependent on the melt composition, forming diopside only when CaO is high enough and phlogopite when CaO becomes depleted. The experiments also show that the reaction rims only form within a narrow set of conditions of temperature (900-1000ºC) and melt water content (>3.8 wt.%). The reactions were reproducible across the range of pressures tested (10-15 kbar) and it is likely that in the natural samples reaction rim formation may have persisted to lower pressures. These constraints on the conditions of rim formation are consistent with pressure, temperature and melt water content estimates from phenocryst assemblages and thermo-barometric calculations from the natural samples.

Formation and origin of hydrous metasomatic veins

It is clear from the natural samples and experiments that a phonolite melt will react with upper mantle peridotite to form a metasomatic assemblage dominated by phlogopite + amphibole + diopside at the expense of olivine, orthopyroxene and spinel. Similar hydrous metasomatic veins are commonly found within mantle xenoliths, yet the major element composition of the melt that forms these veins is poorly constrained (Witt-Eickschen et al., 1998; Szabó et al., 2009; Pilet et al., 2010; Pilet et al., 2011). No other melt compositions have been shown to directly form veins with this mineralogy by reactions with peridotite phases. It is therefore likely that the melts that form hydrous metasomatic veins are highly evolved alkali melts with phonolitic or near phonolite major element compositions. Phonolite melts will be the expected residual melts during PFC processes as *ne*-normative basalts ascend into colder shallower mantle in a model similar to that of Pilet et al. (2011). The most extreme melts formed during PFC are often as evolved as phonolites (Wulff-Pedersen et al., 1996; Xu et al., 1996; Wullf-Pedersen et al., 1999; Zajacz et al., 2007; Miller et al., 2012). Trace element modeling (Pilet et al., 2011) and compositions of evolved PFC glasses (Zajacz et al., 2007; Szabó et al., 2009) are remarkably similar to the trace element compositions of high pressure phonolites (Irving and Price, 1981). Therefore, there is strong evidence to suggest that PFC produces phonolites, which then forms hydrous metasomatic veins consisting of phlogopite + amphibole + diopside.

Kinetics of phlogopite rim formation on olivine

Time series experiments showed that the increase in phlogopite rim thickness on olivine is parabolic with time, indicating that the reaction is diffusion-controlled. The absence of concentration profiles in the melt and host olivines indicates that diffusion in the melt is extremely fast and diffusion within olivine is extremely slow. Concentration profiles across reaction rims suggest that the reaction is rate limited by diffusion through the rim via grain boundaries. Reaction rim growth rates were significantly affected by the bulk water content of the melt and temperature. Estimates of residence times from the reaction rates, determined by the experiments, range from several days (at 950°C with ~8 wt.% H_2O), to ~100 days (at 950°C and ~4 wt. % H_2O). The water contents of the Heldburg Phonolite were likely to be closer to 4 wt.% H_2O, therefore giving a residence times of olivine xenocrysts in the Heldburg Phonolite of several weeks to several months.

Role of intergranular fluid during metasomatic reactions

Phlogopite rim growth rates increase significantly with the bulk water content of the melt. The reactions are controlled by diffusion along phlogopite-phlogopite grain boundaries and phlogopite-olivine interphase boundaries. Therefore the increase in bulk melt water contents must affect the rates of diffusion by changing the chemical and physical properties of grain and interphase boundaries. TEM analyses showed that there was strong textural evidence of intergranular fluid present along grain and interphase boundaries at peak conditions despite the bulk melt being undersaturated in fluid. The amounts of this intergranular fluid also appear to increase with bulk melt water content. This is consistent with observations from other systems (e.g. Gardés et al., 2012; Milke et al., 2013). Several different intergranular fluid regimes have been identified previously. These include; dry, fluid

undersaturated and fluid saturated grain boundaries (Rubie, 1986; Carlson, 2010; Gardés et al., 2012). In this work the fluid saturated regime is split into two further regimes; confined fluid and free fluid. Although saturated with fluid the physical properties of fluid in grain boundaries depends on the thickness of the fluid film. A sudden jump in diffusion rates is expected when a fluid is no longer confined by the adjacent mineralogy and behaves like a free fluid phase.

Intergranular fluid will increase the diffusion rates of components along grain and interphase boundaries, which will lead to higher reaction rates. Fluid may also act as a medium for rapid chemical exchange allowing fractionation of fluid soluble components from the metasomatising silicate melt, thereby providing a possible mechanism for cryptic metasomatism.

Outlook

The use of doped olivine or orthopyroxene crystals has been shown to be a simple method for understanding how different chemical species behave during reactions (Milke et al., 2011). Further work within this system would benefit from a systematic determination of trace element behaviour during metasomatic reactions between alkali melts and upper mantle phases. This may also help to understand how elements are fractionated during metasomatism aiding trace element modeling during percolative fractional crystallization. The lack of trace element data from mantle xenolith glasses and high pressure xenolith bearing phonolites makes it difficult to assess the strength of the correlations given in Chapter 3. Further work should aim to establish if these correlations are robust in a wider set of samples.

The experiments presented here only used water as the sole volatile species. It would be of particular interest to observe how other volatile species such as Cl, F and CO_2 might affect these reactions and the ability for phonolites to metasomatise the mantle. Some preliminary work was carried out using 0.5 mol NaF_2 solution. This did not show any significant changes to the rim mineralogy, or rates of rim growth, however additional experiments would be necessary to be certain of this. It is clear that intergranular fluid has a large role to play during metasomatic reactions. The role of other volatiles in the properties of intergranular fluids should also be investigated in future works.

Bibliography

Ablay, G.J., Carroll, M.R., Palmer, M.R., Marti, J., Sparks, R.S.J. (1998). Basanite-phonolite lineages of the Teide-Pico Viejo volcanic complex, Tenerife, Canary Islands. *Journal of Petrology*, **39**, 905-936.

Abratis, M., Mädler, J., Hautmann, S., Leyk, H. J., Meyer, R., Lippolt, H. J., Viereck-Götte, L. (2007). Two distinct Miocene age ranges of basaltic rocks from the Rhön and Heldburg areas (Germany) based on $^{40}Ar/^{39}Ar$ step heating data. *Chemie der Erde-Geochemistry*, **67**, 133-150.

Andújar, J., Costa, F., Martí, J., Wolff, J.A., Carroll, M.R. (2008). Experimental constraints on pre-eruptive conditions of phonolitic magma from the caldera-forming El Abrigo eruption, Tenerife (Canary Islands). *Chemical Geology*, **257,** 173-191.

Andújar, J., Scaillet, B. (2012). Experimental constraints on parameters controlling the difference in the eruptive dynamics of phonolitic magmas: the case of Tenerife, (Canary Islands). *Journal of Petrology*, **53**, 1777-1806.

Aoki, K. (1975) Origin of phlogopite and potassic richterite bearing peridotite xenoliths from South Africa. *Contributions to Mineralogy and Petrology*, **53**, 145-156.

Arai, S., Takahashi, N. (1989) Formation and compositional variation of phlogopites in the Horoman peridotite complex, Hokkaido, northern Japan: implications for origin and fractionation of metasomatic fluids in the upper mantle. *Contributions to Mineralogy and Petrology*, **101**, 165-175.

Arai, S., Takada, S., Michibayashi, K., Kida, M. (2004). Petrology of peridotite xenoliths from Iraya Volcano, Philippines, and its implication for dynamic mantle-wedge processes. *Journal of Petrology*, **45**, 369-389.

Arima, M., Edgar, A.D. (1983) High pressure experimental studies on a katunigte and their bearing on the genesis of some potassium-rich magmas of the west branch of the African rift. *Journal of Petrology*, **24**, 166-187.

Baker, M.B., Wyllie, P.J. (1990). Liquid immiscibility in a nephelinite-carbonatite system at 25 kbar and implications for carbonatite origin. *Nature*, **346**, 168-170.

Baker, I.A., Gamble, J.A., Graham, I.J. (1994). The age, geology, and geochemistry of the Tapuaenuku Igneous Complex, Marlborough, New Zealand. *New Zealand Journal of Geology and Geophysics*, **37,** 249-268.

Baker, M.B., Hirschmann, M.M., Ghiorso, M.S., Stolper, E.M. (1995). Compositions of near-solidus peridotite melts from experiments and thermodynamic calculations. *Nature*, **375**, 308-311.

Bakker, R.J., Jansen, J.B.H. (1994) A mechanism for preferential H_2O leakage from fluid inclusions in quartz, based on TEM observations. *Contributions to Mineralogy and Petrology*, **116**, 7-20.

Ban, M., Witt-Eickschen, G., Klein, M., Seck, H.A. (2005). The origin of glasses in hydrous mantle xenoliths from the West Eifel, Germany: incongruent break down of amphibole. *Contributions to Mineralogy and Petrology*, **148**, 511-523.

Beach, A. (1982) Deformation in some cover thrust sheets from the external French Alps. *Journal of Structural Geology*, **4**, 137-149.

Berkesi, M., Guzmics, T., Szabó, C., Dubessy, J., Bodnar, R.J., Hidas, K., Ratter, K. (2012) The role of CO_2-rich fluids in trace element transport and metasomatism in the lithospheric mantle beneath the Central Pannonian Basin, Hungary, based on fluid inclusions in mantle xenoliths. *Earth and Planetary Science Letters*, **331-332**, 8-20.

Berner, R.A. (1978). Rate control of mineral dissolution under earth surface conditions. *American Journal of Science,* **278**, 1235-1252.

Berndt, J., Holtz, F., Koepke, J. (2001). Experimental constraints on storage conditions in the chemically zoned phonolitic magma chamber of the Laacher See volcano. *Contributions to Mineralogy and Petrology*, **140**, 469-486.

Billa, M.A., Timms, N.E., Toy, V.A., Hart, R.D., Prior, D.J. (2013) Grain boundary dissolution porosity in quartzfeldspathic ultramylonites: implications for permeability enhancement and weakening of mid-crustal shear zones. *Journal of Structural Geology*, **53**, 2-14.

Blundy, J.D., Falloon, T.J., Wood, B.J., Dalton, J.A. (1995). Sodium partitioning between clinopyroxene and silicate melts. *Journal of Geophysical Research,* **100**, 15501-15515.

Bodinier, J. L., Vasseur, G., Vernieres, J., Dupuy, C., Fabries, J. (1990). Mechanisms of mantle metasomatism: geochemical evidence from the Lherz orogenic peridotite. *Journal of Petrology*, **31**, 597-628.

Bodinier, J-L., Menzies, M.A., Shimizu, N., Frey, F.A., McPherson, E. (2004). Silicate, hydrous and carbonate metasomatism at Lherz, France: contemporaneous derivatives of silicate melt-harzburgite reaction. *Journal of Petrology,* **45**, 299-320.

Boudier, F., Baronnet, A., Mainprice, D. (2010). Serpentine mineral replacement of natural olivine and their seismic implications: oceanic lizardite versus subduction-related antigorite. *Journal of Petrology*, **51**. 495-512.

Boyd, F.R., England, J.L. (1960). Apparatus for phase-equilibrium measurements at pressures up to 50 kilobars and temperatures up to 1750°C. *Journal of Geophysical Research,* **65**, 741-748.

Brearly, M., Scarfe, C.M. (1986). Dissolution rates of upper mantle minerals in an alkali basalt at high pressure: an experimental study and implications for ultramafic xenolith survival. *Journal of Petrology*, **27**, 1157-1182.

Brey, G.P., Köhler, T. (1990). Geothermobarometry in four-phase lherzolites II. New thermometers, and practical assessment of existing thermometers. *Journal of Petrology,* **31**, 1353-1378.

Carlson, W. D. (2010). Dependence of reaction kinetics on H2O activity as inferred from rates of intergranular diffusion of aluminium. *Journal of Metamorphic Geology*, **28**, 735-752.

Carmichael, I.S.E. (1967). The mineralogy and petrology of the volcanic rocks from the Leucite Hills, Wyoming. *Contributions to Mineralogy and Petrology*, **15**, 24-66.

Carroll, M.R., Blank, J.G. (1997) The solubility of H_2O in phonolite melts. *American Mineralogist*, **82**, 549-556.

Chalot-Prat, F., Falloon, T.J., Green, D.H., Hibberson, W.O. (2010). An experimental study of liquid compositions in equilibrium with plagioclase + spinel lherzolite at low pressures (0.75 GPa). *Journal of Petrology,* **51,** 2349-2376.

Çoban, H., Flower, M.F.J. (2006) Mineral phase compositionsin silica-undersaturated 'leucite' lamproites from the Bucak area, Isparta, SW Turkey. *Lithos*, **89**, 275-299.

Coltorti, M., Bonadiman, C., Hinton, R.W., Siena, F., Upton, B.G.J. (1999). Carbonate metasomatism of the oceanic upper mantle: evidence from clinopyroxenes and glasses in ultramafic xenoliths of Grand Comore, Indian Ocean. *Journal of Petrology*, **40**, 133-165.

Coltorti, M., Beccaluva, L., Bonadiman, C., Salvini, L., Siena, F. (2000). Glasses in mantle xenoliths as geochemical indicators of metasomatic agents. *Earth and Planetary Science Letters*, **183**, 303-320.

Comodi, P., Fumagalli, P., Montagnoli, M., Zanazzi, P.F. (2004) A single-crystal study on the pressure behavior of phlogopite and petrological implications. *American Mineralogist*, **89**, 647-653.

Coombs, M.L., Gardner, J.E. (2004). Raction rim growth on olivine in silicic melts: implications for magma mixing. *American Mineralogist*, **89**, 748-758.

Dalton, J. A., Presnall, D.C. (1998). The continuum of primary carbonatitic-kimberlitic melt compositions in equilibrium with lherzolite: data from the system CaO-MgO-Al_2O_3-SiO_2-CO_2 at 6 GPa. *Journal of Petrology*, **39**, 1953-1964.

Dautria, J.M., Girod, M., Rahaman, O. (1983). The upper mantle beneath eastern Nigeria: inferences from ultramafic xenoliths in Jos and Biu volcanics. *Journal of African Earth Sciences*, **1**, 331-338.

Daval, D., Sissman, O., Menguy, N., Saldi, G., Guyot, F., Martinez, I., Corvisier, J., Garcia, B., Machouk, I., Knauss, K.G., Hellmann, R. (2011) Influence of amorphous silica layer formation on the dissolution rate of olivine at 90ºC and elevated pCO_2. *Chemical Geology*, **284**, 193-209.

Daval, D., Hellmann, R., Saldi, G.D., Wirth, R., Knauss, K.G. (2013) Linking nm-scale measurements of the anisotropy of silicate surface reactivity to macroscopic dissolution rate laws: new insights based on diopside. *Geochimica et Cosmochimica Acta*, **107**, 121-134.

Davis, L.L., Smith, D. (1993). Ni-rich olivine in minettes from Two Buttes, Colorado: a connection between potassic melts from the mantle and low Ni partition coefficients. Geochimica et Cosmochimica Acta, 57, 123-129.

Dawson, J. B., Smith, J. V. (1988). Metasomatised and veined upper-mantle xenoliths from Pello Hill, Tanzania: evidence for anomalously-light mantle beneath the Tanzanian sector of the East African Rift Valley. *Contributions to Mineralogy and Petrology*, **100**, 510-527.

Dillon, S.J., Tang, M., Carter, C.W., Harmer, M.P. (2007) Complexion: a new concept for kinetic engineering in material science. *Acta Materialia*, **55**, 6208-6218.

Dohmen, R., Chakraborty, S. (2003). Mechanism and kinetics of element and isotopic exchange mediated by a fluid phase. *American Mineralogist*, **88**, 1251-1270.

Dohmen, R., Chakraborty, S. (2007). Fe-Mg diffusion in olivine II: point defect chemistry, change of diffusion mechanisms and a model for calculation of diffusion coefficients in natural olivine. *Physics and Chemistry of Minerals*, **34**, 409-430.

Dohmen, R., Milke, R. (2010). Diffusion in polycrystalline materials: grain boundaries, mathematical models, and experimental data. *Reviews in Mineralogy and Geochemistry*, **72**, 921-970.

Downes, H. (1989). Magma mixing in undersaturated alkaline volcanics, Cantal, Massif Central, France. *Mineralogical Magazine*, **53**, 43-53.

Downes, H., Macdonald, R., Upton, B.G.J., Cox, K.G., Bodinier, J-L., Mason, P.R.D., James, D., Hill, P.G., Hearn, B.C. Jr. (2004). Ultramfic xenoliths from the Bearpaw Mountains, Montana, USA: evidence for multiple metasomatic events in the lithospheric mantle beneath the Wyoming craton. *Journal of Petrology*, **45**, 1631-1662.

Draper, D.S., Green, T.H. (1997). P-T phase relations of silicic, alkaline, aluminous mantle-xenolith glasses under anhydrous and C-O-H fluid saturated conditions. *Journal of Petrology*, **38**, 1187-1224.

Drury, M. R., Gerald, F., John, D. (1996). Grain boundary melt films in an experimentally deformed olivine-orthopyroxene rock: Implications for melt distribution in upper mantle rocks. *Geophysical Research Letters*, **23**, 701-704.

Falloon, T.J., Green, D.H., O'Neill, H.St.C., Hibberson, W.O. (1997). Experimental tests of low degree peridotite partial melt compositions: implications for the nature of anhydrous near-solidus peridotite melts at 1GPa. *Earth and Planetary Science Letters*, **152**, 149-162.

Farver, J.R., Yund, R.A. (1999) Oxygen bulk diffusion measurements in and TEM characterization of a natural ultramylonite: implication for fluid transport in mica-bearing rocks. *Journal of Metamorphic Geology*, **17**, 669-683.

Fenter, P., Teng, H., Geissbühler, P., Hanchar, J.M., Nagy, K.L., Sturchio, N.C. (2000) Atomic-scale structure of the orthoclase (001)-water interface measures with high-resolution X-ray reflectivity. *Geochimica et Cosmochimica Acta*, **64**, 3663-3673.

Foley, S. (1992) Vein-plus-wall-rock melting mechanisms in the lithosphere and the origin of potassic alkaline magmas. *Lithos*, **28**, 435-453.

Foley, S.F., Andronikov, A.V., Melzer, S. (2002) Petrology of ultramafic lamprophyres from the Beaker Lake area of Eastern Antarctica and their relation to the breakup of Gondwanaland. *Mineralogy and Petrology*, **74**, 361-384.

Franz, L., Wirth, R. (1997). Thin intergranular melt films and melt pockets in spinel peridotite xenoliths from the Rhön area (Germany): early stage of melt generation by grain boundary melting. *Contributions to Mineralogy and Petrology*, **129**, 268-283.

Franz, L., Seifert, W., Kramer, W. (1997). Thermal evolution of the mantle underneath the Mid-German Crystalline Rise: Evidence from mantle xenoliths from the Rhön area (Central Germany). *Mineralogy and Petrology*, **61**, 1-25.

Franz, L., Becker, K-P., Kramer, W., Herzig, P.M. (2002). Metasomatic mantle xenoliths from the Bismark Microplate (Papua New Guinea)- thermal evolution, geochemistry and extent of slab-induced metasomatism. *Journal of Petrology*, **43**, 315-343.

Freise, M., Holtz, F., Koepke, J., Scoates, J., Leyrit, H. (2003). Experimental constraints on the storage conditions of phonolites from the Kerguelen Archipelago. *Contributions to Mineralogy and Petrology*, **145**, 659-672.

Frezzotti, M.L., Andersen, T., Neumann, E-R., Simonsen, S.L. (2002). Carbonatite melt-CO_2 fluid inclusions in mantle xenoliths from Tenerife, Canary Islands: a story of trapping, immiscibility and fluid-rock interaction in the upper mantle. *Lithos*, **64**, 77-96.

Frezzotti, M.L., Ferrando, S., Peccerillo, A., Petrelli, M., Tecce, F., Perucchi, A. (2010). Chorine-rich metasomatic H_2O-CO_2 fluids in amphibole-bearing peridotites from Injibara (Lake Tana region,

Ethiopian plateau): nature and evolution of volatiles in the mantle of a region of continental flood basalts. *Geochimica et Cosmochimica Acta*, **74**, 3023-3039.

Ganguly, J. (2002) Diffusion kinetics in minerals: principals and applications to tectono-metamorphic processes. *EMU notes in Mineralogy*, **4**, 271-309.

Gardés, E., Wunder, B., Wirth, R., & Heinrich, W. (2011). Growth of multilayered polycrystalline reaction rims in the $MgO–SiO_2$ system, part I: experiments. *Contributions to Mineralogy and Petrology*, **161**, 1-12.

Gardés, E., Wunder, B., Marquardt, K., Heinrich, W. (2012). The effect of water on intergranular mass transport: new insights from diffusion-controlled reaction rims in the MgO–SiO2 system. *Contributions to Mineralogy and Petrology*, **164,** 1-16.

Giessler, W.H., Kämpf, H., Seifert, W., Dulski, P. (2007). Petrological and seismic studies of the lithosphere in the earthquake swarm region Vogtland/NW Bohemia, Central Europe. *Journal of Volcanology and Geothermal Research*, **159**, 33-69.

Grant K.J., Wood, B.J. (2010). Experimental study of the incorporation of Li, Sc, Al and other trace elements into olivine. *Geochimica et Cosmochimica Acta*, **74**, 2412-2428.

Grant, T.B., Milke, R., Pandey, S., Jahnke, H. (2013) The Heldburg Phonolite, Central Germany: reactions between phonolite and xenocrysts from the upper mantle and lower crust. *Lithos*, **182-183**, 86-101.

Green, D.H., Edgar, A.D:, Beasley, P., Kiss, E., Ware, N.G. (1974). Upper mantle source for some hawaiites, mugearites and benmoreites. *Contributions to Mineralogy and Petrology*, **48**, 33-43.

Green, D.H., Wallace, M.E. (1988). Mantle metasomatism by ephemeral carbonatite melts. *Nature*, **336,** 459-462.

Grégoire, M., Jego, S., Maury, R.C., Polve, M., Payot, B., Tamayo, R.A. Jr., Yumul, G.P.Jr. (2008). Metasomatic interactions between slab-derived melts and depleted mantle: insights from xenoliths within Monglo adakite (Luzon arc, Philippines). *Lithos*, **103**, 415-430.

Grieco, G., Ferrario, A., Von Quadt, A., Koeppel, V., Mathez, E.A. (2001). The zircon-bearing chromitites of the phlogopite peridotite of Finero (Ivrea Zone, Southern Alps): evidence and geochronology of a metasomatized mantle slab. *Journal of Petrology*, **42**, 89-101.

Harlov, D. E., Milke, R. (2002). Stability of corundum+ quartz relative to kyanite and sillimanite at high temperature and pressure. *American Mineralogist*, **87**, 424-432.

Harms, E., Gardner, J. E., Schmincke, H. U. (2004). Phase equilibria of the Lower Laacher See Tephra (East Eifel, Germany): constraints on pre-eruptive storage conditions of a phonolitic magma reservoir. *Journal of Volcanology and Geothermal Research*, **134**, 125-138.

Hay, D.E., Wendlandt, R.F. (1995). The origin of Kenya rift plateau-type flood phonolites: results of high-pressure / high-temperature experiments in the systems phonolite-H_2O and phonolite-H_2O-CO_2. *Journal of Geophysical Research*, **100**, 401-410.

Hellmann, R., Wirth, R., Daval, D., Barnes, J-P., Penisson, J-M., Tisserand, D., Epicier, T., Hervig, R.L. (2012). Unifying natural and laboratory chemical weathering with interfacial dissolution-reprecipitation: a study based on the nanometer-scale chemistry of fluid-silicate interfaces. *Chemical Geology*, **294-295**, 203-216.

Henderson, C.M.B., Richardson, F.R., Charnock, J.M. (2012). The Highwood Mountains potassic igneous province, Montana: mineral fractionation trends and magmatic processed revisited. *Mineralogical Magazine*, **76**, 1005-1051.

Hess, P.C. (1994). Thermodynamics of thin fluid films. *Journal of Geophysical Research*, **99**, 7219-7229.

Holm, P.M., Wilson, J.R., Christensen, B.P., Hansen, L., Hansen, S.L., Hein, K.M., Mortensen, A.K., Pedersen, R., Plesner, S., Runge, M.K. (2006). Sampling the Cape Verde mantle plume: evolution of melt compositions on Santo Antão, Cape Verde Islands. *Journal of Petrology*, **47**, 145-189.

Hiraga, T., Anderson, I.M., Zimmerman, M.E., Mei, S., Kohlstedt, D.L. (2002). Structure and chemistry of grain boundaries in deformed, olivine basalt and partically molten lherzolite aggregates: evidence of melt-free grain boundaries. *Contributions to Mineralogy and Petrology*, **144**, 163-175.

Hiraga, T., Anderson, I.M., Kohlstedt, D.L. (2003). Chemistry of grain boundaries in mantle rocks. *American Mineralogist*, **88**, 1015-1019.

Hiraga, T., Anderson, I.M., Kohlstedt, D.L. (2004). Grain boundaries as reservoirs of incompatible elements in the Earth's mantle. *Nature*, **427**, 699-703.

Hiraga, T., Kohlstedt, D.L. (2007). Equilibrium interface segregation n the diopside-forsterite system I: analytical techniques, thermodynamics, and segregation characteristics. *Geochimica et Cosmochimica Acta*, **71**, 1266-1280.

Hirose, K., Kushiro, I. (1993). Partial melting of dry peridotites at high pressures: determination of compositions of melts segregated from peridotite using aggregates of diamond. *Earth and Planetary Science Letters*, **114**, 477-489.

Hirose, K. (1997). Partial melt compositions of carbonated peridotite at 3 GPa and role of CO_2 in alkali-basalt generation. *Geophzysical Research Letters*, **24**, 2837-2840.

Hirschmann, M.M., Baker, M.B., Stolper, E.M. (1998). The effect of alkalis on the silica content of mantle-derived melts. *Geochimica et Cosmochemica Acta*, **62**, 883-902.

Hirschmann, M.M., Kogiso, T., Baker, M.B., Stolper, E.M. (2003). Alkalic magmas generated by partial melting of garnet pyroxenite. *Geology*, **31**, 481-484.

Huckenholz, H.G., Werner, C.D. (1990). Die Tertiäre Vulkanite der Heldburger Gangschar (Bayerisch-thüringisches Grabfeld). Beihefte zum European Journal of Mineralogy, 2, 1-45.

Irving, A.J., Green, D.H. (2008). Phase relationships of hydrous alkalic magmas at high pressures: production of nepheline hawaiitic to mugearitic liquids by amphibole-dominated fractional crystallization within the lithospheric mantle. *Journal of Petrology*, **49**, 741-756.

Irving, A.J., Price, R.C. (1981). Geochemistry and evolution of the lherzolite-bearing phonolitic lavas from Nigeria, East Germany, and New Zealand. *Geochimica et Cosmochimica Acta*, **45**, 1309-1320.

Jerram, D.A., Cheadle, J.C., Philpotts, A.R. (2003). Quantifying the building blocks of igneous rocks: are clustered crystal frameworks the foundation? *Journal of Petrology*, **44**, 2033-2051.

Joachim, B., Gardés, E., Velickov, B., Abart, R., Heinrich, W. (2012). Experimental growth of diopside + merwinite reaction rims: the effect of water on microstructure development. *American Mineralogist*, **97**, 220-230.

Johannes, W. (1973). Eine vereinfachte Piston-Zylinder-Apparatur hoher Genauigkeit. *Neues Jahrbuch Für Mineralogie* 337-351.

Johannes, W., Bell, P.M., Mao, H.K., Boettcher, A.L., Chipman, D.W., Hays, J.F., Newton, R.C., Seifert F. (1971). An interlaboratory comparison of piston-cylinder pressure calibration using the albite-breakdown reaction. *Contributions to Mineralogy and Petrology*, **32**, 24-38.

Jung, S., Pfänder, J. A., Brügmann, G., Stracke, A. (2005). Sources of primitive alkaline volcanic rocks from the Central European Volcanic Province (Rhön, Germany) inferred from Hf, Os and Pb isotopes. *Contributions to Mineralogy and Petrology*, **150**, 546-559.

Jung, S., Mezger, K., Hauff, F., Pack, A., Hoernes, S. (2013). Petrogenesis of rift-related tephrites, phonolites, amd trachytes (Central European Volcanic Province, Rhön, FRG): constraints from Sr, Nd, Pb, and O isotopes. *Chemical Geology*, **354**, 203-215.

Kelemen, P.B. (1990). Reaction between ultramafic rock and fractionating basaltic magma I. Phase relations, the origin of calc-alkaline magma series, and the formation of discordant dunite. *Journal of Petrology*, **31,** 51-98.

Kelemen, P.B., Dick, J.B., Quick, J.E. (1992). Formation of harzburgite by pervasive melt/rock reaction in the upper mantle. *Nature*, **358**, 635-640.

Kelemen, P.B., Hart, S.R., Bernstein, S. (1998). Silica enrichment in the continental upper mantle via melt/rock reaction. *Earth and Planetary Science Letters*, **164**, 387-406.

Keller, L. M., Wunder, B., Rhede, D., Wirth, R. (2008). Component mobility at 900° C and 18kbar from experimentally grown coronas in a natural gabbro. *Geochimica et Cosmochimica Acta*, **72**, 4307-4322.

Keppler, H. (1996). Constraints from partitioning exeperiments on the composition of subduction-zone fluids. *Nature*, **380**, 237-240.

Kersit, A., Liu, C. (2009). Molecular dynamics of water and ion diffusion in nanosized mineral fractures. *Environmental Science Technology*, **43**, 777-782.

Kinzler, R. J., Grove, T. L. (1992). Primary magmas of mid-ocean ridge basalts 1. Experiments and methods. *Journal of Geophysical Research: Solid Earth (1978–2012)*, **97**, 6885-6906.

Klügel, A. (1998). Reactions between mantle xenoliths and host magma beneath La Palma (Canary Islands): constraints on magma ascent rates and crustal reservoirs. *Contributions to Mineralogy and Petrology*, **131**, 237-257.

Klügel, A. (2001). Prolonged reaction between harzburgite xenoliths and silica-undersaturated melt: implications for dissolution and Fe-Mg interdiffusion rates of orthopyroxene. *Contributions to Mineralogy and Petrology*, **141,** 1-14.

Kruhl, J. H., Wirth, R., Morales, L. F. (2013). Quartz grain boundaries as fluid pathways in metamorphic rocks. *Journal of Geophysical Research*, **118,** 1957-1967.

Kushiro, I. (1996). Partial melting of a fertile mantle peridotite at high pressures: an experimental study using aggregates of diamond. *Geophysical Monograph Series*, **95**, 109-122.

Kyle, P.R., Moore, J.A., Thirlwall, M.F. (1992). Petrologic evolution of anorthoclase phonolite lavas at Mount Erebus, Ross Island, Antarctica. *Journal of Petrology*, **33**, 849-875.

Leake, B.E., Woolley, A.R., Arps, C.E.S., Birch, W.D., Gilbert, M.C., Grice, J.D., Hawthorne, F.C., Kato, A., Kisch, H.J., Krivovichev, V.G., Linthout, K., Laird, J., Mandarino, J.A., Maresch, W.V., Nickel, E.H., Rock, N.M.S., Schumacher J.C., Smith, D.C., Stephenson, N.C.N., Ungaretti, L., Whittaker, E.J.W., Youzhi, G. (1997). Nomenclature of the amphiboles: report of the subcommittee on amphiboles of the international mineralogical association, commission on new minerals and mineral names. *The Canadian Mineralogist*, **35**, 219-246.

Le Bas, M. J., Le Maitre, R. W., Streckeisen, A., Zanettin, B. (1986). A chemical classification of volcanic rocks based on the total alkali-silica diagram. *Journal of petrology*, **27**, 745-750.

Leng, Y., Cummings, P.T. (2006). Hydration structure of water confined between mica surfaces. *The Journal of Chemical Physics*, **124**, 074711.

Libourel, G. (1999). Systematics of calcium partitioning between olivine and silicate melt: implications for melt structure and calcium content of magmatic olivines. *Contributions to Mineralogy and Petrology*, **136**, 63-80.

Liu, M., Peterson, J. C., Yund, R. A. (1997). Diffusion-controlled growth of albite and pyroxene reaction rims. *Contributions to mineralogy and petrology*, **126**, 217-223.

Liu, Y., Gao, S., Hu, Z., Gao, C., Zong, K., Wang, D. (2010). Continental and oceanic crust rescycling-induced melt-peridotite interactions in the Trans-North China Orogen: U-Pb dating, Hf isotopes and trace elements in zircon from mantle xenoliths. *Journal of Petrology*, **51**, 537-571.

Lloyd, F.E., Edgar, A.D., Forsyth, D.M., Barnett, R.L. (1991). The paragenesis of upper-mantle xenoliths from the Quaternary volcanics south-east of Gees, West Eifel, Germany. *Mineralogical Magazine*, **55**, 95-112.

Lloyd, F.E., Woolley, A.R., Stoppa, F., Eby, G.N. (2002). Phlogopite-biotite parageneses from the K-mafic-carbonatite effusive magmatic association of Katwe-Kikorongo, SW Uganda. *Mineralogy and Petrology*, **74**, 299-322.

Luth, W.C. (1967). Studies in the system $KAlSiO_4$-Mg_2SiO_4-SiO_2-H_2O: inferred phase relations and petrologic application. *Journal of Petrology*, **8**, 372-416..

Manning, C. E. (2004). The chemistry of subduction-zone fluids. *Earth and Planetary Science Letters*, *223*, 1-16

Masotta, M., Mollo, S., Freda, C., Gaeta, M., Moore, G. (2013). Clinopyroxene-liquid thermometers and barometers specific to alkaline differentiated magmas. *Contributions to Mineralogy and Petrology*, **166**, 1545-1561.

Manning, C.E. (2013). Thermodynamic modeling of fluid-rock interaction at mid-crustal to upper mantle conditions. *Reviews in Mineralogy and Geochemistry*, **76**, 135-164.

Massare, D., Métrich, N., Clocchiatti, R. (2002). High-temperature experiments on silicate melt inclusions in olivine at 1 atm: inference on temperatures of homogenization and H_2O concentrations. *Chemical Geology*, **183**, 87-98.

Mayer, B., Jung, S., Romer, R. L., Stracke, A., Haase, K. M., Garbe-Schönberg, C. D. (2013). Petrogenesis of Tertiary Hornblende-bearing Lavas in the Rhön, Germany. *Journal of Petrology*, **54**, 2095-2123.

McDonough, W. F., & Sun, S. S. (1995). The composition of the Earth. *Chemical geology*, **120**, 223-253.

McInnes, B.I.A., Cameron, E.M. (1994). Carbonated, alkaline hybridizing melts from a sub-arc environment: mantle wedge samples from the Tabar-Lihir-Tanga-Feni arc, Papua New Guinea. *Earth and Planetary Science Letters*, **122**, 125-141.

McInnes, B. I., Gregoire, M., Binns, R. A., Herzig, P. M., Hannington, M. D. (2001). Hydrous metasomatism of oceanic sub-arc mantle, Lihir, Papua New Guinea: petrology and geochemistry of fluid-metasomatised mantle wedge xenoliths. *Earth and Planetary Science Letters*, **188**, 169-183.

Melluso, L., Morra, V., Riziky, H., Veloson, J., Lustrino, M., Del Gatto, L., Modeste, V. (2007). Petrogenesis of a basanite–tephrite–phonolite volcanic suite in the Bobaomby (Cap d'Ambre) peninsula, northern Madagascar. *Journal of African Earth Sciences*, **49**, 29-42.

Meyer, R., Song, X., Elkins-Tanton, L.T. (2009). Interactions between magma and the lithospheric mantle during Cenozoic rifting in the Central Europe. American Geophysical Union, Fall Meeting 2009 abs#T31C-1831.

Milke, R., Kolzer, K., Koch-Müller, M., Wunder, B. (2009). Orthopyroxene rim growth between olivine and quartz at low temperatures (750-950°C) and low water concentration. *Mineralogy and Petrology*, **97**, 223-232.

Milke, R., Abart, R., Keller, L., Rhede, D. (2011). The behavior of Mg, Fe, and Ni during the replacement of olivine by orthopyroxene: experiments relevant to mantle metasomatism. *Mineralogy and Petrology*, **103**, 1-8.

Milke, R., Neusser, G., Kolzer, K., Wunder, B. (2013). Very little water is necessary to make a dry solid silicate system wet. *Geology*, **41**, 247-250.

Miller, C., Zanetti, A., Thöni, M., Konzett, J., Klötzli, U. (2012). Mafic and silica-rich glasses in mantle xenoliths from Wau-en-Namus, Libya: textural and geochemical evidence for peridotite-melt reactions. *Lithos*, **128-131**, 11-26.

Morishita, T., Arai, S., Green, D.H. (2003a). Evolution of low-Al orthopyroxene in the Horoman Peridotite, Japan: an unusual indicator of metasomatizing fluids. *Journal of Petrology*, **44**, 1237-1246.

Morishita, T., Arai, S., Tamura, A. (2003b). Petrology of an apatite-rich layer in the Finero phlogopite-peridotite, Italian Western Alps; implications for evolution of a metasomatising agent. *Lithos*, **69**, 37-49.

Morgan, Z., Liang, Y. (2003). An experimental and numerical study of the kinetics of harzburgite reactive dissolution with applications to dunite dike formation. *Earth and Planetary Science Letters*, **214**, 59-74.

Moussallam, Y., Oppenheimer, C., Scaillet, B., Kyle, P.R. (2013). Experimental Phase-equilibrium Constraints on the Phonolite Magmatic System of Erebus Volcano, Antarctica. *Journal of Petrology*, **54**, 1285-1307.

Neal, C.R., Taylor, L.A. (1989). The petrography and composition of phlogopite micas from the Blue Ball Kimberlite, Arkansas: a record of chemical evolution during crystallization. *Mineralogy and Petrology*, **40**, 207-224.

Neumann, E. R., Wulff-Pedersen, E. (1997). The origin of highly silicic glass in mantle xenoliths from the Canary Islands. *Journal of Petrology*, **38**, 1513-1539.

Neumann, E. R., Wulff-Pedersen, E., Pearson, N. J., Spencer, E. A. (2002). Mantle xenoliths from Tenerife (Canary Islands): evidence for reactions between mantle peridotites and silicic carbonatite melts inducing Ca metasomatism. *Journal of Petrology*, **43**, 825-857.

Norberg, N., Harlov, D., Neusser, G., Wirth, R., Rhede, D., Morales, L. (2013). Experimental development of patch perthite from synthetic cryptoperthite: microstructural evolution and chemical re-equilibration. *American Mineralogist*, **98**, 1429-1441.

O'Leary, J.A., Gaetani, G.A., Hauri, E.H. (2010). The effect of tetrahedral Al^{3+} on the partitioning of water between clinopyroxene and silicate melt. *Earth and Planetary Science Letters*, **297**, 111-120.

Panter, K.S., Kyle, P.R., Smellie, J.L. (1997). Petrogenesis of a phonolite-trachyte succession at Mount Sidley, Marie Byrd Land, Antarctica. *Journal of Petrology*, **38**, 1225-1253.

Pilet, S., Ulmer, P., Villiger, S. (2010). Liquid line of descent of a basanitic liquid at 1.5Gpa: constraints on the formation of metasomatic veins. *Contributions to Mineralogy and Petrology*, **159**, 621-643.

Pilet, S., Baker, M.B., Müntener, O., Stolper, E.M. (2011). Monte Carlo simulations of metasomatic enrichemnt in the lithosphere and implications for the source of alkaline basalts. *Journal of Petrology*, **52**, 1415-1442.

Pinilla, C., Davis, S.A., Scott, T.B., Allan, N.L., Blundy, J.D. (2012). Interfacial storage of noble gases and other trace elements in magmatic systems. *Earth and Planetary Science Letters*, **319-320**, 287-294.

Portnyagin, M., Almeev, R., Matveev, S., Holtz, F. (2008). Experimental evidence for rapid water exchange between melt inclusions in olivine in olivine and host magma. *Earth and Planetary Sciences*, **272**, 541-552.

Price, R.C., Green, D.H. (1972). Lherzolite nodules in a "mafic phonolite" from North-East Otago, New Zealand. *Nature*, **235**, 133-134.

Prodehl, C., Mueller, S., Glahn, A., Gutscher, M., Haak, V. (1992). Lithospheric cross sections of the European Cenozoic rift system. *Tectonophysics*, **208**, 113-138.

Pröschold, H., Thürach, H. (1895). Erläuterungen zur geologischen Specialkarte Preussen und den Thüringischen Staaten, LX. Lieferung. Blatt Heldburg. J.H. Neumann, Berlin. 32-52.

Prouteau, G., Scaillet, B., Pichavant, M., Maury, R. (2001). Evidence for mantle metasomatism by hydrous silicic melts derived from subducted oceanic crust. *Nature*, **410**, 197-200.

Purwin, H., Stalder, R., Skogby, H. (2009). Hydrogen incorporation in Fe- and Na-doped diopsides. *European Journal of Mineralogy*, **21**, 691-704.

Putirka, K.D. (2008). Thermometers and barometers for volcanic systems. *Reviews in Mineralogy and Geochemistry*, **69,** 61-120.

Putnis, A. (2002). Mineral replacement reactions: from macroscopic observations to microscopic mechanisms. *Mineralogical Magazine*, **66**, 689-708.

Putnis, A., Putnis, C.V., (2007). The mechanism of reequilibration of solids in the presence of a fluid phase. *Journal of Solid State Chemistry*, **180**, 1783-1786.

Putnis, A. (2009). Mineral replacement reactions. *Reviews in mineralogy and geochemistry*, **70**, 87-124.

Rapp, R.P., Shimizu, N., Norman, M.D., Applegate, G.S. (1999). Reaction between slab-derived melts and peridotite in the mantle wedge: experimental constraints at 3.8 GPa. *Chemical Geology*, **160**, 335-356.

Rapp, R.P., Norman, M.D., Laporte, D., Yaxley, G.M., Martin, H., Foley, S.F. (2010). Continent formation in the Archean and chemical evolution of the cratonic lithosphere: melt-rock reaction experiments at 3-4 GPa and petrogenesis of Archean Mg-diorites (sanukitoids). *Journal of Petrology*, **51**, 1237-1266.

Rhodes, J.M., Dungan, M.A., Blanchard, D.P., Long, P.E. (1979). Magma mixing at mid-ocean ridges: evidence from basalts drilled near 22°N on the mid-Atlantic ridge. *Tectonophysics*, **55**, 35-61.

Ridolfi, F:, Renzulli, A. (2012). Calcic amphiboles in calc-alkaline, and alkaline magmas: thermobarometric and chemometric empirical equations valid up to 1,130°C and 2.2GPa. *Contributions to Mineralogy and Petrology*, **163,** 877-895.

Robinson, J.A.C., Wood, B.J., & Blundy, J.D. (1998). The beginning of melting of fertile and depleted peridotite at 1.5 GPa. *Earth and Planetary Science Letters*, **155**, 97-111.

Roden, M.F., Murthy, V.R. (1985). Mantle metasomatism. *Annual Review of Earth and Planetary Sciences*, **13**, 269-296.

Rubie, D.C. (1986). The catalysis of mineral reactions by water and restrictions on the presence of aqueous fluid during metamorphism. *Mineralogical Magazine*, **50**, 399-415.

Rutherford, M.J. (2008). Magma ascent rates. *Reviews in Mineralogy and Geochemistry*, *69*, 241-271.

Rutter, E.H., Elliot, D. (1976). The kinetics of rock deformation by pressure solution. *Philosophical Transactions of the Royal Society*, **283**, 203-219.

Scaillet, B., Pichavant, M., Cioni, R. (2008). Upward migration of Vesuvius magma chamber over the past 20,000 years. *Nature*, **455**, 216-219.

Scambelluri, M., Philippot, P. (2001). Deep fluids in subduction zones. *Lithos*, **55**, 213-227.

Schiano, P., Clocchiatti, R., Shimizu, N., Maury, R.C., Jochum, K.P., Hofmann, A.W. (1995). Hydrous, silica-rich melts in the sub-arc mantle and their relationship with erupted arc lavas. *Nature*, **377**, 595-600.

Schiano, P., Bourdon, B., Clocchiatti, R., Massare, D., Varela, M. E., Bottinga, Y. (1998). Low-degree partial melting trends recorded in upper mantle minerals. *Earth and Planetary Science Letters*, **160**, 537-550.

Schilling, F., Wunder, B. (2004). Temperature distribution in piston-cylinder assemblies: numerical simulations and laboratory experiments. *European Journal f Mineralogy*, **16**, 7-14.

Schmidt, B.C., Behrens, H. (2008). Water solubility in phonolite melts: influence of melt composition and temperature. *Chemical Geology*, **256**, 259-268.

Schmidt, G., Snow, J. (2002). Os isotopes in mantle xenoliths from the Eifel volcanic field and the Vogelsberg (Germany): age constraints on the lithospheric mantle. *Contributions to Mineralogy and Petrology*, **143**, 694-705.

Semiz, B., Çoban, H., Roden, M.F., Özpinar, Y., Flower, M.F.J., McGregor, H. (2012). Mineral composition in cognate inclusions in late Miocene-early Pliocene potassic lamprophyres with affinities to lamproites from the Denizili region, Western Anatolia, Turkey: implications for uppermost mantle processes in a back arc setting. *Lithos*, **134-135**, 253-272.

Shaw, C.S.J., Thibault, Y., Edgar, A.D., Lloyd, F.E. (1998). Mechanisms of orthopyroxene dissolution in silica-undersaturated melts at 1 atmosphere and implications for the origin of silica-rich glass in mantle xenoliths. *Contributions to Mineralogy and Petrology,* **132**, 354-370.

Shaw, C.S.J. (1999). Dissolution of orthopyroxene in basanitic magma between 0.4 and 2GPa: further implications for the origin of Si-rich alkaline glass inclusions in mantle xenoliths. *Contributions to Mineralogy and Petrology*, **135**, 11-132.

Shaw, C.S.J., Klügel, A. (2002). The pressure and temperature conditions and timing of glass formation in mantle-derived xenoliths from Baarley, West Eifel, Germany: the case for amphibole breakdown, lava infiltration and mineral-melt reaction. *Mineralogy and Petrology,* **74**, 163-187.

Shaw, C.S., Eyzaguirre, J., Fryer, B., & Gagnon, J. (2005). Regional variations in the mineralogy of metasomatic assemblages in mantle xenoliths from the West Eifel Volcanic Field, Germany. *Journal of Petrology*, **46**, 945-972.

Shaw, C.S., Heidelbach, F., Dingwell, D. B. (2006). The origin of reaction textures in mantle peridotite xenoliths from Sal Island, Cape Verde: the case for "metasomatism" by the host lava. *Contributions to Mineralogy and Petrology*, **151**, 681-697.

Shaw, C.S.J., Dingwell, D.B. (2008). Experimental peridotite-melt reaction at one atmosphere: a textural and chemical study. *Contributions to Mineralogy and Petrology,* **155**, 199-214.

Smith, D., Riter, J.C.A. (1997). Genesis and evolution of low-Al orthopyroxene in spinel peridotite xenoliths, Grand Canyon field, Arizona, USA. *Contributions to Mineralogy and Petrology*, **127**, 391-404.

Smith, D., Riter, J.C.A., Mertzman, S.A. (1999). Water-rock interactions, orthopyroxene growth, and Si-enrichment in the mantle: evidence in xenoliths from the Colorado Plateau, southwestern United States. *Earth and Planetary Science Letters,* **165**, 45-54.

Sommer, H., Regenauer-Lieb, K., Gasharova, B., Siret, D. (2008). Grain boundaries: a possible water reservoir in the Earth's mantle? *Mineralogy and Petrology*, **94**, 1-8.

Spandler, C., Yaxley, G., Green, D. H., Scott, D. (2010). Experimental phase and melting relations of metapelite in the upper mantle: implications for the petrogenesis of intraplate magmas. *Contributions to Mineralogy and Petrology*, **160**, 569-589.

Spandler, C., Pirard, C. (2013). Element recycling from subducting slabs to arc crust: a review. *Lithos,* **170-171**, 208-223.

Stiefenhofer, J., Viljoen, K.S., Marsh, J.S. (1997). Petrology and geochemistry of peridotite xenoliths from the Letlhakane kimberlites, Botswana. *Contributions to Mineralogy and Petrology*, **127**, 147-158.

Sudo, A., Tatsumi, Y. (1990). Phlogopite and K-amphibole in the upper mantle: implication for magma genesis at subduction zones. *Geophysical research letters*, **17**, 29-32.

Sundvall, R., Stalder, R. (2011). Water in upper mantle pyroxene megacrysts and xenocrysts: a survey study. *American Mineralogist*, **96**, 1215-1227.

Szabó, C., Hidas, K., Bali, E., Zajacz, Z., Kovács, I., Yang, K., Guzmics, T., Török, K. (2009). Melt–wall rock interaction in the mantle shown by silicate melt inclusions in peridotite xenoliths from the central Pannonian Basin (western Hungary). *Island Arc*, **18**, 375-400.

Tarney, J. (1969). Epitaxic relations between coexisting pyroxenes. Mineralogical Magazine, **37**, 115-122.

Thibault, Y., Edgar, A.D., Lloyd, F.E. (1992). Experimental investigation of melts from a carbonated phlogopite lherzolite: implications for metasomatism in the continental lithospheric mantle. *American Mineralogist*, **77**, 784-794.

Trønnes, R.G. (2002). Stability range and decomposition of potassic richterite and phlogopite end members at 5-15 GPa. *Mineralogy and Petrology*, **74**, 129-148.

Tutti, F., Dubrovinsky, L.S., Nygren, M. (2000). High-temperature study and thermal expansion of phlogopite. *Physics and Chemistry of Minerals*, **27**, 599-603.

Wade, J.A., Plank, T., Hauri, E.H., Kelley, K.A., Roggensack, K., Zimmer, M. (2008). Prediction of magmatic water contents via measurement of H_2O in clinopyroxene phenocrysts. *Geology*, **36**, 799-802.

Wallace, M.E., Green, D.H. (1988). An experimental determination of primary carbonatite magma composition. *Nature*, **335**, 343-346.

Wedepohl, K.H., Gohn, E., Hartmann, G. (1994). Cenozoic alkali basaltic magmas of western germany and their products of differentiation. *Contributions to Mineralogy and Petrology*, **115**, 253-278.

Wilson, M., Downes, H. (1991). Tertiary—Quaternary Extension-Related Alkaline Magmatism in Western and Central Europe. *Journal of Petrology*, **32,** 811-849.

Wirth, R. (1996). Thin amorphous films (1–2 nm) at olivine grain boundaries in mantle xenoliths from San Carlos, Arizona. *Contributions to mineralogy and petrology*, **124**, 44-54.

Wirth, R. (2004). Focused Ion Beam (FIB): a novel technology for advanced application of micro- and nanoanalysis in geosciences and applied mineralogy. *European Journal of Mineralogy*, **16**, 863-876.

Whittington, A., Richet, P., Linard, Y., Holtz, F. (2001). The viscosity of hydrous phonolites and trachytes. *Chemical Geology*, **174**, 209-223.

Witt-Eickschen, G., Kramm, U. (1997). Mantle upwelling and metasomatism beneath Central Europe: geochemical and isotopic constraints from mantle xenoliths from the Rhön (Germany). *Journal of Petrology*, **38**, 479-493.

Witt-Eickschen, G., Kaminsky, W., Kramm, U., Harte, B. (1998). The nature of young vein metasomatism in the lithosphere of the West Eifel (Germany): geochemical and isotopic constraints from composite mantle xenoliths from the Meerfelder Maar. *Journal of Petrology*, **39**, 155-185.

Wörner, G., Schmincke, H.U., Schreyer, W. (1982). Crustal xenoliths from the Quaternary Wehr volcano (East Eifel). *Neues Jahrbuch für Mineralogie-Abhandlungen*, **144**, 29-55.

Wörner, G., Schmincke, H.U. (1984). Mineralogical and chemical zonation of the Laacher See tephra sequence (East Eifel, W. Germany). *Journal of Petrology*, **25**, 805-835.

Wright, J.B. (1966). Olivine nodules in a phonolite from the East Otago Alkaline Province, New Zealand. *Nature*, **210**, 519.

Wright, J.B. (1969). Olivine nodules and related inclusions in trachyte from the Jos Plateau, Nigeria. *Mineralogical Magazine*, **37**, 370-374.

Wulff-Pedersen, E., Neumann, E. R., Jensen, B. B. (1996). The upper mantle under La Palma, Canary Islands: formation of Si− K− Na-rich melt and its importance as a metasomatic agent. *Contributions to Mineralogy and Petrology*, **125**, 113-139.

Wulff-Pedersen, E., Neumann, E-R., Vannucci, R., Bottazzi, P., Ottolini, L. (1999). Silicic melts produced by reaction between peridotite and infiltrating basaltic melts: ion probe data on glasses and minerals in veined xenoliths from La Palma, Canary Islands. *Contributions to Mienralogy and Petrology*, **137**. 59-82.

Wunder, B., Melzer, S. (2003). Experimental evidence on phlogopitic mantle metasomatism induced by phengite dehydration. *European Journal of Mineralogy*, **15**, 641-647.

Xu, Y., Mercier, J.C., Lin, C., Shi, L., Menzies, M. A., Ross, J.V., Harte, B. (1996). K-rich glass-bearing wehrlite xenoliths from Yitong, Northeastern China: petrological and chemical evidence for mantle metasomatism. *Contributions to mineralogy and petrology*, **125**, 406-420.

Yaxley, G.M., Kamenetsky, V., Green, D.H., Falloon, T.J. (1997). Glasses in mantle xenoliths from western Victoria, Australia, and their relevance to mantle processes. *Earth and Planetary Science Letters*, **148**, 433-446.

Yaxley G.M., Brey, G.P. (2004). Phase relations of carbonate-bearing eclogite assemblages from 2.5-5.5 GPa: implications for petrogenesis of carbonatites. *Contributions to Mineralogy and Petrology*, **146**, 606-619.

Yaxley, G.M., Crawford, A.J., Green, D.H. (1991). Evidence for carbonatite metasomatism in spinel peridotite xenoliths from western Victoria, Austrailia. *Earth and Planetary Science Letters*, **107**, 305-317.

Yund, R. A. (1997). Rates of grain boundary diffusion through enstatite and forsterite reaction rims. *Contributions to Mineralogy and Petrology*, **126**, 224-236.

Zack, T., John, T. (2007). An evaluation of reactive fluid flow and trace element mobility in subducting slabs. *Chemical Geology*, **239**, 199-216.

Zajacz, Z., Kovács, I., Szabó, C., Halter, W., Pettke, T. (2007). Evolution of mafic alkaline melts crystallized in the uppermost lithospheric mantle: a melt inclusion study of olivine-clinopyroxenite xenoliths, northern Hungary. *Journal of Petrology*, **48**, 853-883.

Zanetti, A., Mazzucchelli, M., Rivalenti, G., Vannucci, R. (1999). The Finero phlogopite-peridotite massif: an example of subduction-related metasomatism. *Contributions to Mineralogy and Petrology*, **134**, 107-122.

Zhang, H. (2005). Transformation of lithospheric mantle peridotite-melt reaction: a case of Sino-Korean craton. *Earth and Planetary Science Letters*, **237**, 768-780.

Zhang, Y., Ni, H. Chen, Y. (2010). Diffusion in silicate melts. *Reviews in Mineralogy and Geochemistry*, **72**, 311-408

Ziegler, P. A. (1992). European Cenozoic rift system. *Tectonophysics*, **208**, 91-111.

Acknowledgements

The work compiled in this thesis was funded by the German Research Foundation (DFG) under the FOR 741 grant with the project number of MI1205/2-2. I would like to thank the co-authors of each chapter for their hard work during our collaborations; Ralf Milke, Bernd Wunder, Sanjay Pandey, Hannes Jahnke, Richard Wirth and Dieter Rhede. Special thanks goes particularly to Ralf Milke for supervising the project and keeping me on track to finish. I am also grateful for the amphibole analysis in the Chapter 1 supplied by Sarah Incel, synthetic enstatite made by Marcin Balinski for Chapter 2 and the FIB foil preparation conducted by Anja Schreiber. This work has been strengthened by numerous discussions with Wilhelm Heinrich, Dan Harlov, Katharina Marquardt, Patrick Remmert, Luiz Morales, Timm John, Andreas Klügel, Michael Abratis, Ralf Dohmen, Etienne Médard, Didier Laporte, Bastian Joachim, Nicholas Norberg, as well as many others working at the GeoForschungsZentrum Potsdam and the Freie Universität Berlin.

Erklärung der Eigenständigkeit

Hiermit versichere ich, daß ich die vorliegende Arbeit selbständig verfaßt und keine anderen als die angegebenen Hilfmittel benutzt habe. Die Stellen der Arbeit, die anderen Werken wörtlich oder inhaltlich entnommen sind, wurden durch entsprechende Angaben der Quellen kenntlich gemacht.

Diese Arbeit hat in gleicher oder ähnlicher Form noch keiner anderen Prüfungsbehörde vorgelegen.